AN ANALYSIS OF THE TSR-LSRB INTERACTION DURING AUTOINDUCER-2 CHEMOTAXIS IN *ESCHERICHIA COLI*

A Dissertation

by

ANDREW LORAN SEELY

Submitted to the Office of Graduate and Professional Studies of
Texas A&M University
in partial fulfillment of the requirements for the degree of

DOCTOR OF PHILOSOPHY

Chair of Committee,	Michael D. Manson
Committee Members,	Gregory D. Reinhart
	Steve W. Lockless
	Arul Jayaraman
Head of Department,	Thomas McKnight

August 2017

Major Subject: Microbiology

ABSTRACT

Escherichia coli senses a variety of chemoeffectors. The Tsr chemoreceptor is known to mediate attractant response to serine. Previously, serine was the only attractant described for Tsr. Recent work suggests Tsr senses Autoinducer-2 as an attractant via a periplasmic binding protein. Autoinducer-2 is a general quorum sensing molecule recognized by Gram positive and Gram negative bacteria. In *E. coli* it is bound to LsrB during AI-2 uptake.

A testable model, based on the described interaction between MBP and the Tar chemoreceptor in *E. coli*, was generated. I first hypothesized that the shoulder regions of Tsr would associate with areas of both the amino and carboxyl domains of LsrB to elicit chemotaxis to AI-2. To test this, alanine-scanning mutations were generated in both Tsr and LsrB. Results suggest AI-2 is sensed through a direct interaction between Tsr and LsrB. I conclude residues Lys-147 and Glu-150 of Tsr and Asp-59, Asp-63 and Arg-252 of LsrB are critical for AI-2 chemotaxis.

I investigated the relationship between LsrB expression and AI-2 chemotaxis. I hypothesized altering expression of LsrB relative to chromosomal level would affect AI-2 chemotaxis. This was tested by growing cells to late phase, increasing LsrB present, and by inducing plasmid-borne LsrB. The results suggest increasing the LsrB present decreases AI-2 chemotaxis, though a clear conclusion cannot be drawn. I also explored the effect making *lsr* deletions would have on LsrB expression and AI-2 chemotaxis. I conclude there is little effect on AI-2 chemotaxis in these mutants. Lastly, I hypothe-

sized serine and AI-2 affect signaling to each other. This was tested by using Tsr variants deficient for serine chemotaxis to test AI-2 chemotaxis to establish that recognition of serine and AI-2 occurs independently at separate locations on Tsr. I introduced one ligand during log phase growth and tested chemotaxis response to the other ligand. Results indicate that serine and AI-2 bind at separate sites. However, AI-2 chemotaxis decreased when serine was present, though not vice versa. I conclude the response to serine is more robust since there are a limiting number of LsrB proteins present in the cell.

DEDICATION

I dedicate this dissertation to my wife, Ashlie Seely, for her endless patience and ceaseless motivation, and to my children, Astrid and Augustus Seely, for allowing me to fit lab time in between play times. I also dedicate this dissertation to my father and mother, Loran and Donna Seely, and to my brother, Philip Seely for their encouragement and support.

ACKNOWLEDGEMENTS

I am grateful for the opportunity to work and interact with many exceptional individuals during my tenure as a graduate student. The Manson Lab provided a host of characters that had a meaningful impact on my graduate work in one aspect or another. Dr. Gus Wright helped me develop the backbone of my research ability and critical thinking skills. He was willing to take a completely inexperienced new graduate student under his wing and had the patience to suffer through my learning curve. Fellow doctoral candidate Sneha Jani provided critical work and support during my thesis project, and to her I am eternally grateful. Drs. Bill Cohn and Louis Morgan were excellent sounding boards for ideas and theories, whether it was over a lab bench or over a beer. I would also like to thank Dr. Manjunath Hegde and the Jayaraman Lab for opening the door on this project and paving the way for further investigation. Undergraduate researchers Rachel Crowder, Attikos Hutras, Joshua Zuniga, Himanshu Patel, Paul Farrell and Colin Burns were amazingly talented and quite adept at injecting much needed levity into many situations. I owe much of my growth as a researcher to these people.

I am truly grateful to the members of my doctoral advisory committee for their guidance and patience over the course of my graduate career. The opportunity to study under Dr. Michael D. Manson, my committee chair, has been a tremendous experience, and for that I am especially grateful. He was instrumental in molding me into the scientific researcher I am today.

My deepest gratitude goes to my family, without whom I would ever have been given the opportunity to explore my scientific interests. Their encouragement and steadfast support made taking the first and subsequent steps into science possible.

CONTRIBUTORS AND FUNDING SOURCES

Contributors

This work was overseen by a dissertation committee whose members were Professor Michael Manson (advisor) of the Department of Biology, Professor Steven Lockless of the Department of Biology, Professor Gregory Reinhart of the Department of Biochemistry and Biophysics, and Professor Arul Jayaraman of the Department of Chemical Engineering.

Contributions to this work were made by Dr. Sneha Jani of the Department of Biology, Dr. Manjunath Hegde, and Dr. Kuppan Gokulan of the Department of Health and Human Services in Little Rock, Arkansas. Dr. Kuppan Gokulan developed the LsrB-Tsr binding model. Dr. Manjunath Hegde constructed some of the LsrB mutants. Dr. Sneha Jani carried out the immunoblots and AI-2 uptake assay. She also constructed the *lsr* operon deletion mutants. All remaining work for this dissertation was completed by the student, under the advisement of Michael Manson of the Department of Biology. I was assisted by undergraduate researchers Joshua Zuniga, Paul Farrell and Attikos Hutras. The plasmids carrying the Tsr binding site mutations were a kind gift from Dr. Sandy Parkinson of the University of Utah.

Funding Sources

This work was made possible through funding from the NSF and the Bartoszek Fund for Basic Biological Science.

NOMENCLATURE

Aer	Cytoplasmic redox potential receptor
AI-2	Autoinducer-2
AS	Amphipathic sequence of chemoreceptor
ATP	Adenosine 5’-triphosphate
CB	Chemotaxis buffer
DNA	Deoxyribonucleic acid
DPD	4,5-dihydroxy-2,3-pentanedione
E. coli	*Escherichia coli*
EDTA	Ethylenediaminetetraacetic acid
IPTG	Isopropyl β-D-1-thiogalactopyranoside
K_D	Equilibrium dissociation constant
kDa	Kilodalton
LB	Luria Bertani broth
LsrB	Periplasmic binding protein for AI-2 uptake
M	Molar
MBP	Maltose binding protein
MCP	Methyl-accepting chemotaxis protein
mg	Milligram
mL	Milliliters
mM	Millimolar

nM	Nanomolar
PAGE	Polyacrylamide gel electrophoresis
PCR	Polymerase chain reaction
PDB	Protein Data Bank
R-THMF	(2*R*,4*S*)-2-methyl-2,3,3,4-tetrahydroxytetrahydrofuran
SDS	Sodium dodecyl sulfate
Ser	Serine
Tap	Transmembrane peptide/thymine receptor
Tar	Transmembrane aspartate receptor
TB	Tryptone broth
TM1	Transmembrane helix one of chemoreceptor
TM2	Transmembrane helix two of chemoreceptor
Trg	Transmembrane ribose and galactose receptor
Tsr	Transmembrane serine receptor
μL	Microliters
μM	Micromolar
μg	Microgram
WT	Wild-type *Escherichia coli*

TABLE OF CONTENTS

LIST OF FIGURES

LIST OF TABLES

CHAPTER I

INTRODUCTION

Escherichia coli motility and environmental stimuli

Escherichia coli is a gram-negative bacterium of the family Enterobacteriaceae. It is rod-shaped and flagellated, measuring 2-4 μm in length and 0.7 μm in width. Its motility in liquid or semi-solid media is achieved through the use of 4-8 peritrichous flagella. When these flagella rotate counterclockwise, the flagellar filaments form a left-handed helical bundle that propels the cell forward in a run of several seconds (*1*). This run can be at speeds of up to ten times the cell body length per second (40μm/s), and either cell pole can act as leader (*2*). Cells switch from run to a very brief tumble when clockwise rotation of the flagella results in a chaotic, rapid reorientation of the cell due to dissociation of the flagellar bundle (*1*). Alternating between longer runs and shorter tumbles results in a three-dimensional random walk in a liquid environment (*3*).

The cell can modulate this run/tumble bias to respond to favorable or unfavorable environmental stimuli. Clockwise rotation of the flagellar motors is suppressed when a cell responds and moves to a favorable stimulus, allowing for a longer run in the direction of that stimulus, biasing the random walk when an attractant is present. In short, this biased random walk is comprised of the net movement up or down the attractant or repellent gradient (*3*) (Figure 1). Responding to these gradients of attractant or repellent is known as chemotaxis.

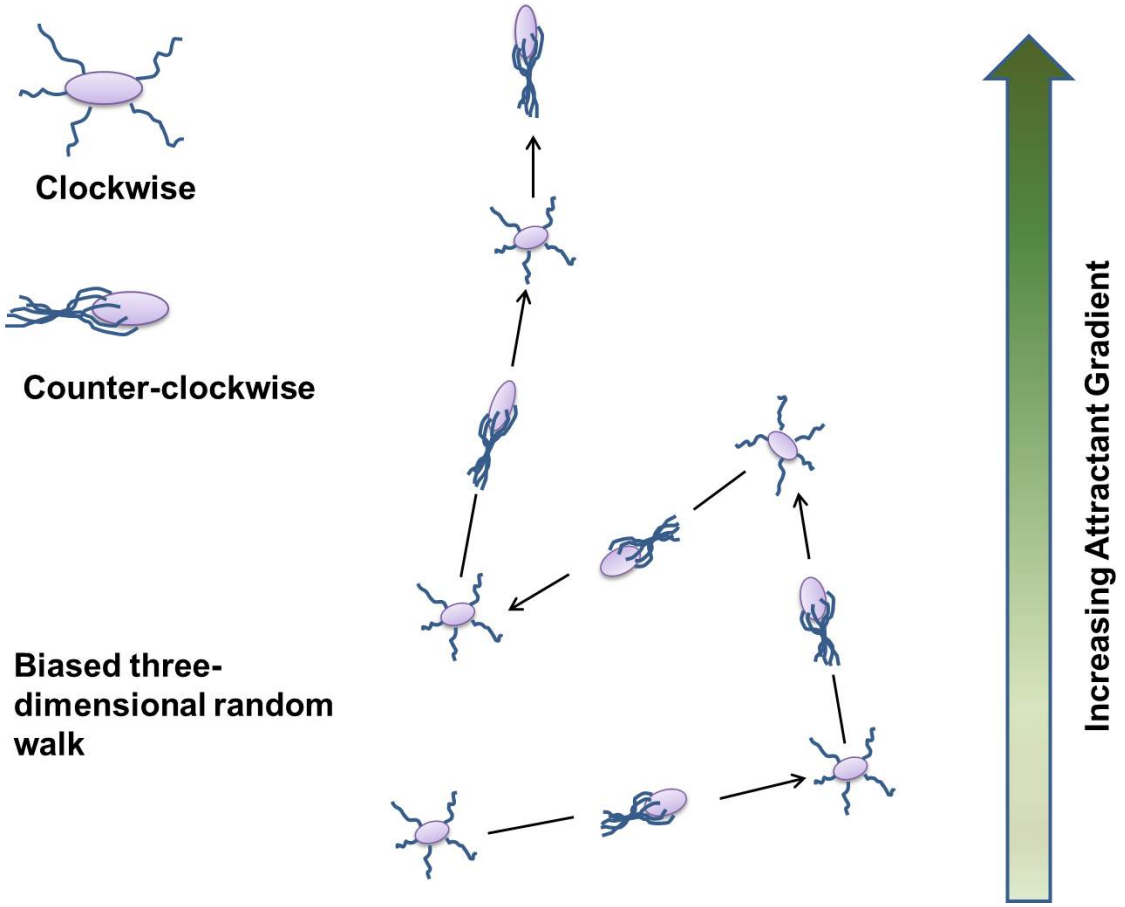

Figure 1. *E. coli* chemotaxis in an attractant gradient. Counter-clockwise flagellar rotation results in flagellar filaments forming a left-handed helical bundle, resulting in a run. Rotation clockwise dissociates the bundle and causes tumbling. Cell swims in a relatively straight-line run, interrupted by brief three-dimensional reorienting tumbles. This results in a biased three-dimensional random walk, as the cell suppresses the probability of tumbling and increases the periodicity of the runs as it migrates up the attractant gradient.

Four transmembrane methyl-accepting chemotaxis proteins (MCPs) are present in *E. coli* to mediate chemotaxis. These MCPs are located in polar clusters, typically in a large subpolar patch (*2*). They are named based on the molecules for which they are responsible for mediating response: taxis to *L*-serine and away from particular repellents (Tsr); taxis to *L*-aspartate and away from particular repellents (Tar); taxis to ribose and galactose (Trg); and taxis-associated protein for dipeptides (Tap) (*4-10*). A fifth receptor, Aer, mediates redox chemotaxis but does so in a methylation-independent manner (*11-13*). Serine and aspartate are the only substrates shown to bind directly to their specific chemoreceptors (*14, 15*). The other known substrates – maltose, ribose, galactose, glucose and dipeptides – require an initial binding to their respective periplasmic binding proteins before interacting with their specific MCPs. Additionally, some molecules are sensed as repellents by two of these chemoreceptors. Tsr senses both indole and *L*-leucine as repellents, while Tar senses nickel (Ni^{2+}) and some divalent cations such as cobalt (Co^{2+}) as repellents (*6, 14, 16, 17*).

Structure and function of *E. coli* chemoreceptors

Chemoreceptors exist in oligomeric units. Single receptor homodimers form trimers of dimers in the absence of other chemotaxis proteins, though these assemblies are stabilized by the scaffolding and kinase proteins at their cytoplasmic domain (*18-21*). These self-associated trimers of dimers localize to the poles of the cell in arrays (*22-26*) (Figure 2). These clusters contain at least a few of all four of the described chemoreceptors (Tsr, Tar, Trg and Tap) (*27*). These receptors interact in chemotaxis signaling, as

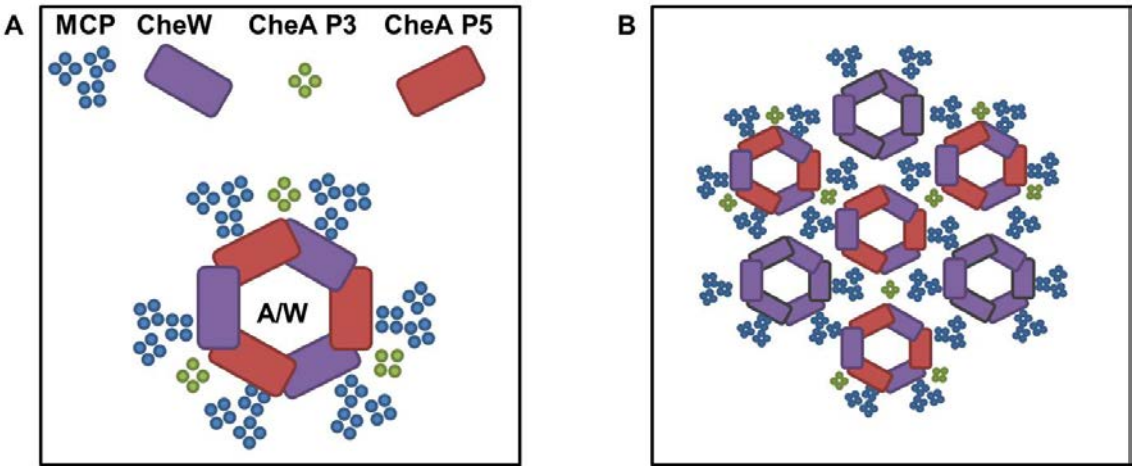

Figure 2. A patch of chemoreceptors embedded in the polar cell membrane. (a) An illustration depicting one lattice unit of chemoreceptors. The receptors are represented by blue circles, and are arranged in trimers of dimers. The CheA and CheW proteins are shown as red and purple rectangles, respectively. The P3 domain of CheA is represented by green cirlces. (b) An illustrated top view of a chemoreceptor array to show the hexagonal lattice. The cartoon illustrates the proposed assembly of an extended chemoreceptor array. CheA subunits P3 and P5, along with CheW are labeled in conjunction with the receptors to illustrate a core complex. Three core complexes are interconnected by CheA/CheW interactions to form a single lattice unit, which assembles further into larger receptor arrays (*22, 23*).

suggested by their close association in the receptor lattice (*28-30*). This is further supported by the finding that bound ligand can induce an amplified effect on signaling in receptor patches, up to 35 times more than expected of individual receptors alone (*31*). Some attractants can be sensed by *E. coli* at the sub-micromolar concentration level, and gradients can be sensed over five orders of magnitude (*32, 33*).

The amounts of Tsr and Tar, considered the major chemoreceptors, are present in approximately 3-5 fold greater abundance than Trg, Tap and Aer (*34*). The major chemoreceptors do not require the presence of another receptor in order to perform chemotaxis. This is not true of the minor chemoreceptors. Trg, Tap and Aer cannot perform chemotaxis alone, and each requires the presence of at least one of the major transducers before they can do so. Additionally, there is no requirement that a major chemoreceptor ligand be present as a prerequisite for the minor transducers to perform chemotaxis to their respective ligands (*35, 36*). These synergistic interactions serve to increase the sensitivity of the system with regard to chemoeffector concentrations (*37*).

Each of the five separate functional domains of Tsr and Tar carries out a particular function (*38, 39*) (Figure 3). Ligands or binding proteins are sensed by the periplasmic domain, a four helix bundle (α1-4). In the studied cases, small molecule ligands bind at the interface of the two subunits while binding protein-ligand complexes bind across the apex of the dimer, interacting asymmetrically with both subunits (*40-42*). Based on recent work, the AI-2 binding protein LsrB is predicted to do the latter (*43*).

The transmembrane domain of the receptor is comprised of transmembrane helix one (TM1) and transmembrane helix two (TM2). This domain's function is critical in

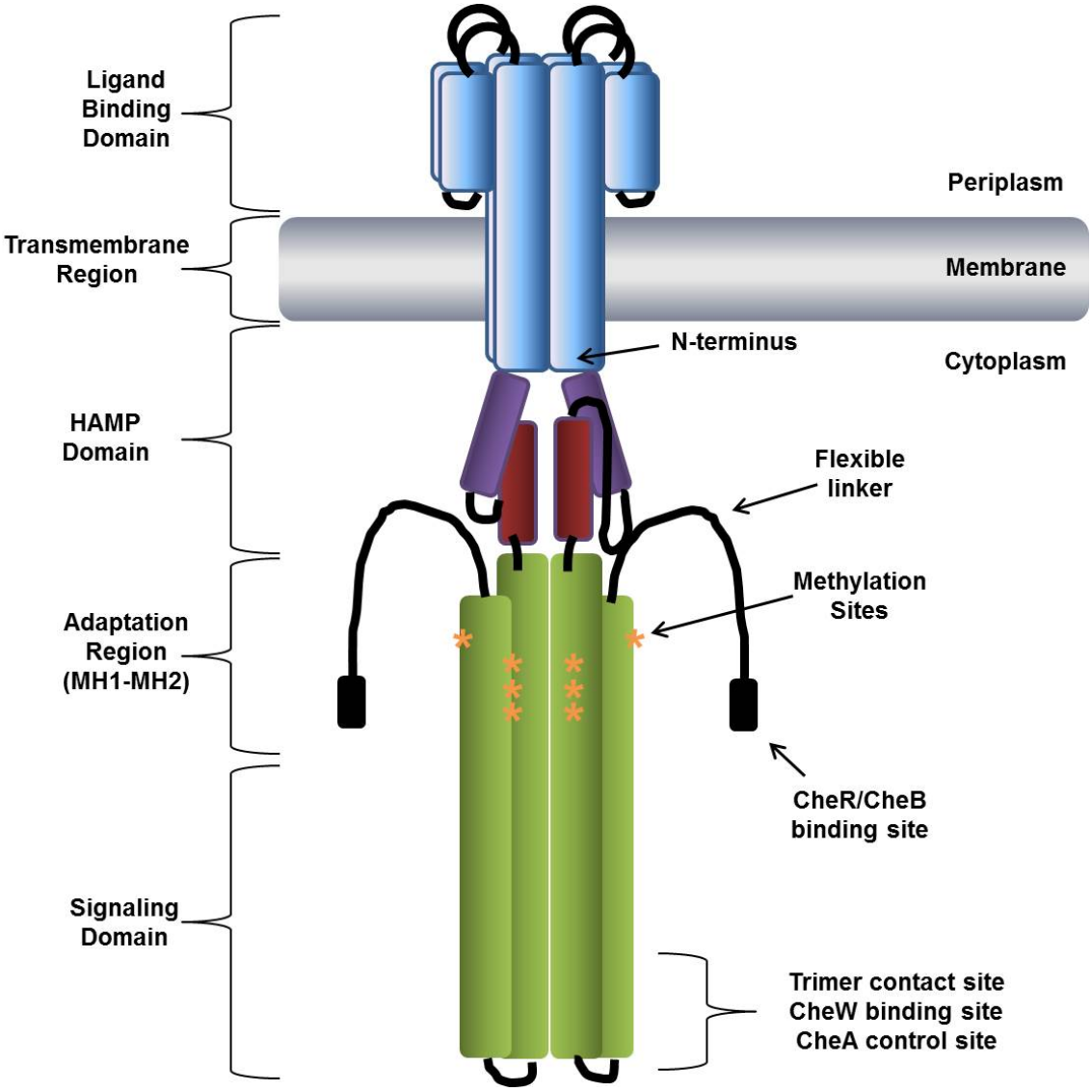

Figure 3. The functional domains of the chemoreceptor. The schematic illustration shows three-dimensional organization of the domains in relation to the receptor dimer in the cell membrane. Domains are distinct based on color and labeled in the center, and important features are labeled to the right.

transducing a signal across the cellular membrane. TM1 anchors the receptor in the membrane and stabilizes the homodimer. Bound ligand signals are transduced by TM2 across the membrane and into the cytoplasm. TM2 is directly linked to the receptor's cytoplasmic region by a Histidine kinase, Adenylate cyclase, Methyl-accepting chemotaxis proteins, Phosphatase (HAMP) domain.

The HAMP domain exists as a four helix bundle. Each of the dimeric subunits consists of parallel, alpha helical amphipathic sequences (AS1 and AS2). Each dimer is connected by a flexible linker of fourteen residues (*44-47*). The cytoplasmic domain, an extended four helix coiled coil, is adjacent to the HAMP domain and consists of the dimeric adaptation and signaling domains, located just downstream of HAMP.

Spatial chemical gradients and the changes in chemoeffector concentrations can be recorded through a sensory adaptation system governed by reversible covalent modifications. Four to six glutamyl residues in this adaptation region can be methylated by the chemoreceptor-specific CheR methyltransferase or demethylated by the CheB methylesterase. These adaptation enzymes continuously maintain the methylation record through both phosphorylation of CheB by CheA, and through conformational changes that alter the propensities for methylation or demethylation. In other words, when an attractant is bound, methylation propensity is high, while demethylation is low; the opposite is true for unbound kinase-active receptors (*48-50*). This allows the cell to maintain a memory of its surroundings, particularly in regard to the chemoeffector gradient in which it may find itself. This is very useful in dynamic environments such as the human gastrointestinal (GI) tract.

A two-component phosphorelay pathway governs receptor activity and ultimately flagellar rotation. Prior to ligand-binding at its periplasmic domain, a chemoreceptor exists in a kinase-activating state that initiates a phosphorelay to the flagellar motors. At the distal tip of the kinase control domain's four helix bundle, are bound the kinase CheA and the scaffolding protein CheW. These Che proteins are necessary for the receptors to cluster in their polar patches (*48, 49, 51*).

The CheA histidine kinase, when bound to a chemoreceptor, is activated several hundred fold in the absence of chemoeffector gradients (*52, 53*). CheA uses ATP to autophosphorylate at a highly conserved His48 residue (*54*). This phosphate group can then be transferred to the Asp57 residue of the CheY response regulator protein, allowing CheY-P to bind with high affinity to the flagellar basal body, specifically the FliM motor protein (*55-57*). Upon sufficient CheY-P binding, one or more flagella will rotate clockwise (CW), leading to the characteristic tumble of the cell (*58-61*). Another substrate for CheA-P is the methylesterase CheB. Upon phosphorylation CheB-P will set about removing methyl groups from specific glutamyl residues of the adaptation domain involved in sensory adaptation (*62*).

Stimulus input and signal transduction across the membrane

At the periplasmic domain of the chemoreceptor, the input stimulus is first recognized. Direct ligand-binding, as in the case of *L*-aspartate with Tar or *L*-serine with Tsr, occurs at one of two rotationally symmetric sites at the homodimer interface. Subsequently, the chemoreceptor displays negative half-of-the-sites cooperativity to an ex-

treme degree, preventing a second, identical ligand molecule from entering and binding at the second site (*63*). Along with adaptive methylation, this negative cooperativity aides the receptors in returning to their pre-ligand bound signaling state during chemotaxis.

Ligand binding induces a conformational change of the chemoreceptor to the effect of a 20-degree rotation along the helical axes of the subunits, breaking the rotational symmetry of the homodimer (*64*, *65*). This results in a slight downward displacement of helix 4, purportedly propagating the signal through TM2. This propagation through the transmembrane domain is not fully determined, but crosslinking studies with Tar suggest that attractant binding causes a piston-like, approximately 1.6 Ångstrom displacement of TM2 toward the HAMP domain, while methylation displaces it toward the periplasm in a return to the pre-ligand binding state (*66*-*68*).

Signal transduction passes through the transmembrane region and into the HAMP domain, where conformational changes link attractant binding at the periplasmic domain to kinase activity at the cytoplasmic domain. Here the evidence suggests that changes in stability of the four helix HAMP bundle are generated by helical sliding of TM2, which in turn modulates destabilization between AS2 of HAMP and the kinase-control region (*69*). Additional mutational and biochemical studies suggest that signal transduction is mediated through anti-symmetrical changes in helix-helix packing in the adaptation and cytoplasmic domains (*70, 71*). According to this predicted model, attractant binding information stabilizes the HAMP four helix bundle, thereby destabiliz-

ing the cytoplasmic domain and kinase control module, effectively turning off the kinase.

When an attractant binds at the periplasmic receptor domain, CheA autophosphorylation activity is inhibited, reducing the amount of CheY-P present in the cytoplasm, inducing counter-clockwise (CCW) flagellar rotation. The reduction of CheY-P is further enhanced through the activity of CheZ, a phosphatase that targets CheY-P, allowing the cell to quickly reduce its CheY-P levels in response to attractant binding. Bundles of CCW rotating flagella propel the cell in its characteristic run (*72*-*76*).

The receptors can be reset to a pre-stimulus state following attractant binding. This is achieved through methylation and demethylation of specific glutamyl residues that serve as substrates for the CheR (methyltransferase) and CheB (methylesterase) proteins that carry out adaptive methylation (*77*). These enzymes bind to the NWETF pentapeptide at the carboxyl terminus of the major chemoreceptors (Tsr and Tar). The glutamyl residues within the adaptation domain are reached due to a flexible coupling of the pentapeptide to the four helix bundle. The minor chemoreceptors (Trg and Tap) lack the pentapeptide at their carboxyl terminus, relying primarily on CheR and CheB enzymes bound to Tsr and Tar within the mixed receptor patch to undergo adaptive methylation (*77*). Adaptation enzymes interacting with one receptor can modify sites equivalent to those on approximately 6 neighboring dimers (*78*). The flexible tether of the receptor that binds CheR and CheB has been shown in molecular models to allow CheR to physically reach at least a few modification sites on eight of the neighboring receptors, indicating so-called assistance neighborhoods for adaptation response (*79*). Adaptive meth-

ylation serves to convey an environmental memory to the cells, allowing them to sense dynamic changes in their surroundings. This is achieved in part because the kinetic rates of the enzymes responsible for adaptation are slower than the time-scale of chemoeffector binding, allowing the cells to compare current ligand occupancy at the periplasmic binding sites with methylation of the glutamyl residues resulting from previous ligand binding (*39*, *80*). This serves as the basis for a chemotaxis response. A more complete view of the signaling cascade and adaptation is represented in Figure 4.

Quorum sensing and Autoinducer-2

Population density is a key factor in regulating various functions in bacteria, including control of pathogenesis and recruitment to and maintenance of biofilms (*81, 82*). Quorum sensing is the means by which bacteria can assess population density, and it relies on the recognition and determination of autoinducers (AIs). These compounds increase proportionally with population density, diffusing back into the cell upon reaching a certain concentration threshold, mediating the quorum sensing response. Some genes are induced by AIs, namely those that are involved in that specific AI's production, creating a positive feedback loop. Typically, the cell density must reach 10^8 cells per mL or higher in order to trigger AI effects on the population.

Quorum sensing through AIs also allows bacteria to communicate both in an intra- and interspecies manner. General autoinducer synthesis genes have been found in approximately half of the sequenced bacterial genomes (*81, 83*). While it was previously thought that intra-species communication and regulation were the most important

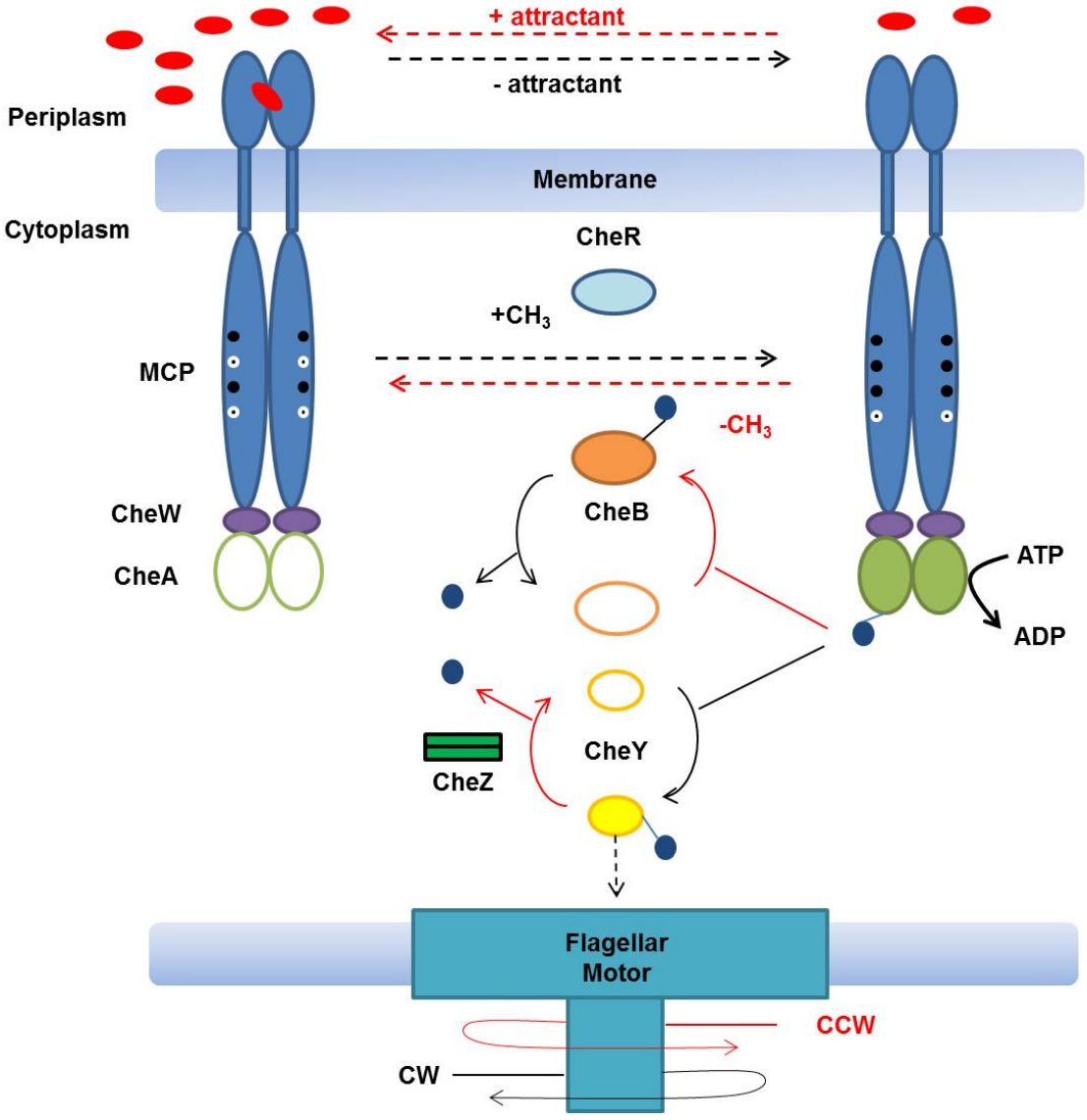

Figure 4. The chemoreceptor signaling cascade. Left receptor shows cascade effects following attractant ligand binding (red theme). CheA kinase is not phosphorylated, thus the phosphorelay of signal to the flagellar motor does not occur. Right receptor shows effects in the absence of attractant ligand (black theme). Inactive components are shown in white with color outline. Solid lines denote enzymatic reactions, while dashed lines denote binding interactions. Adaptation sites are shown as methylated (black circles) or unmethylated (white circles).

aspect of autoinducer production, as evidenced by the species specificity of particular AIs, newer studies have indicated cross talk between different species or genera of bacteria is equally important and can be achieved through the use of general AIs (*84*, *85*). Current knowledge indicates bacteria can integrate signals from their environments to determine if the AI being sensed comes from itself, from other microbes present, or from human stress hormones (*86*). This ability would be particularly useful in the human GI tract.

Species-specific autoinducers (AI-1s) in Gram-negative bacteria are acyl homoserine lactones and modified peptides in Gram-positive bacteria. A separate class of AI is more generally recognized across many Gram-negative and Gram-positive species. Autoinducer-2 is an example of a general AI, and is used in conjunction with species-specific AIs in certain bacteria. For example, the marine bacterium *Vibrio harveyi* requires the presence of both a specific AI-1 and AI-2 to fully induce bioluminescence (*87*). This bioluminescence study was the first in which AI-2 was identified.

Following its identification, AI-2 and its synthase enzyme LuxS have been found to be widely distributed in different bacteria across the kingdom Eubacteria (*83, 84, 88*). This discovery helped shape the prediction that AI-2 is used for interspecies communication. AI-2 is synthesized by LuxS, a homodimeric Fe^{2+} metalloenzyme involved in the activated methyl cycle of bacteria (*89-91*). In this cycle, *S*-adenosylmethionine (SAM) is converted back to homocysteine, through an *S*-adenosylhomocysteine (SAH) intermediate, although it can also be converted to 4,5-dihydroxy-2,3-pentanedione (DPD) from *S*-adenosylribosylhomocysteine (SRH) by LuxS cleavage (*84*, *92*, *93*). This DPD mole-

cule is highly unstable and quickly converted to a precursor for AI-2 (*93*). Both the activated methyl cycle and DPD cyclization pathway are shown in Figure 5. This DPD biosynthetic pathway in *Vibrio harveyi* has been shown to be identical for many bacteria, including *E. coli (92, 93)*.

Once the structure of AI-2 was determined through co-crystallization studies in *Vibrio harveyi*, it was determined that a borated DPD spontaneously cyclizes to form a furanosyl borate diester AI-2 compound, binding to its cognate receptor LuxP (*94*). A similar investigative approach was used in *Salmonella* to co-crystallize AI-2 with its cognate receptor, the Lsr (LuxS-regulated) binding protein, a product of the Lsr operon. The co-crystallization with its binding protein also revealed that *Salmonella* recognizes the chemically distinct, non-borated (2*R*,4*S*)-2-methyl-2,3,3,4-tetrahydroxytetrahydrofuran (*R*-THMF) form of AI-2 (*95*). Both the borated and non-borated forms exist in equilibrium with each other, though this can be influenced by the addition or removal of borate (*81, 94*).

The Lsr operon and its role in AI-2 uptake and chemotaxis

In *Salmonella enterica* serovar Typhimurium, AI-2 concentration is regulated by the seven Lsr operon gene products, including an ATP-binding cassette (ABC) transporter and AI-2 degradation proteins (*96*). In this system, AI-2 serves as a transcriptional activator, relieving LsrR repression of the *lsrACDBFGE* operon. This increases expression of the AI-2 transport apparatus: ABC transporter proteins LsrA, LsrC and LsrD, as well as the periplasmic binding protein LsrB. Peak extracellular AI-2 accumu-

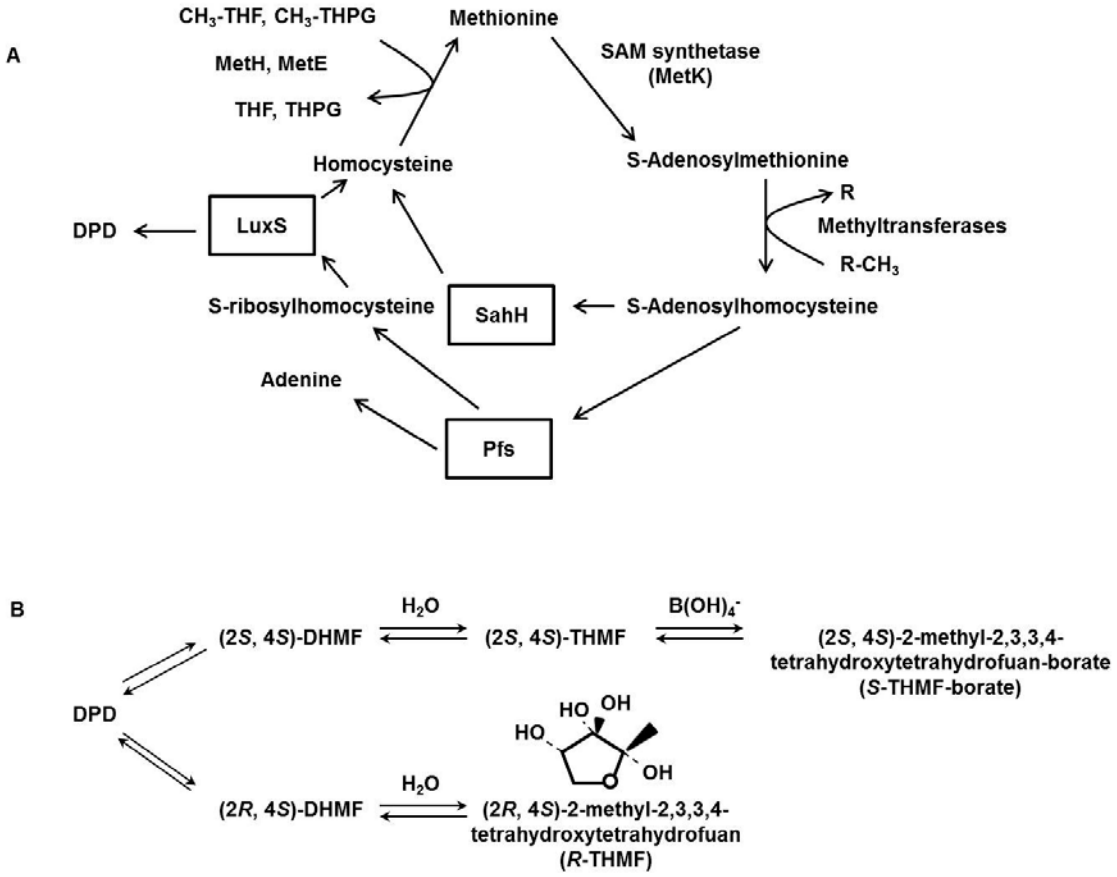

Figure 5. The synthesis pathways for DPD and AI-2. (a) The activated methyl cycle involves cleavage of *S*-ribosylhomocysteine (SRH) into homocysteine or dihydroxypentanedione (DPD), the precursor for AI-2. (b) DPD is highly unstable and spontaneously cyclizes in the presence of borate into borated and non-borated isomers that exist in equilibrium (*95*). Only the non-borated AI-2 (*R*-THMF) is sensed by *E. coli*.

lation occurs during mid to late exponential growth and declines rapidly at the onset of stationary phase as a result of its import through the transporter into the cytoplasm (*97*). The *lsrF*, *lsrG* and *lsrE* genes are required for processing and turnover of AI-2 once it reaches the cytoplasm (*96*). Two adjacent, but separately transcribed genes are *lsrR* and *lsrK*. The kinase product of *lsrK* phosphorylates internalized AI-2, and it is this AI-2-P that de-represses the LsrR repressor and activates transcription of the other *lsr* genes (Figure 6a) (*96*).

E. coli possesses a homologous *lsr* operon, the *b1513* operon (Figure 6b), encoding homologous genes and functions (*98*). Because of this homology, the *lsr* operon nomenclature will be used henceforth to describe *E. coli* genes and gene products pertaining to the *b1513* operon. The transport channel for AI-2 uptake is composed of LsrA, LsrC and LsrD and is located in the cytoplasmic membrane. Translated with a leader peptide, LsrB is exported to the periplasm via the Sec system. Here it is free to bind the extracellular AI-2 that remains in the periplasm following its export from the cell mostly via the TqsA protein (*99*). The remaining AI-2 molecules diffuse through outer membrane pores and accumulate externally, re-entering the periplasm via equilibration with the external environmental AI-2 when it reaches a concentration threshold.

Recent studies with AI-2 in *E. coli* revealed that only the *R*-THMF form is recognized as an attractant that stimulates chemotaxis, requiring both the Tsr chemoreceptor and the binding protein gene product of the Lsr operon, LsrB (*43, 100*). *E. coli* LsrB closely resembles *Salmonella* LsrB (Figure 7), to an 85% sequence identity (*101*). When LsrB is deleted chromosomally, *E.coli* does not respond to AI-2 in chemotaxis assays.

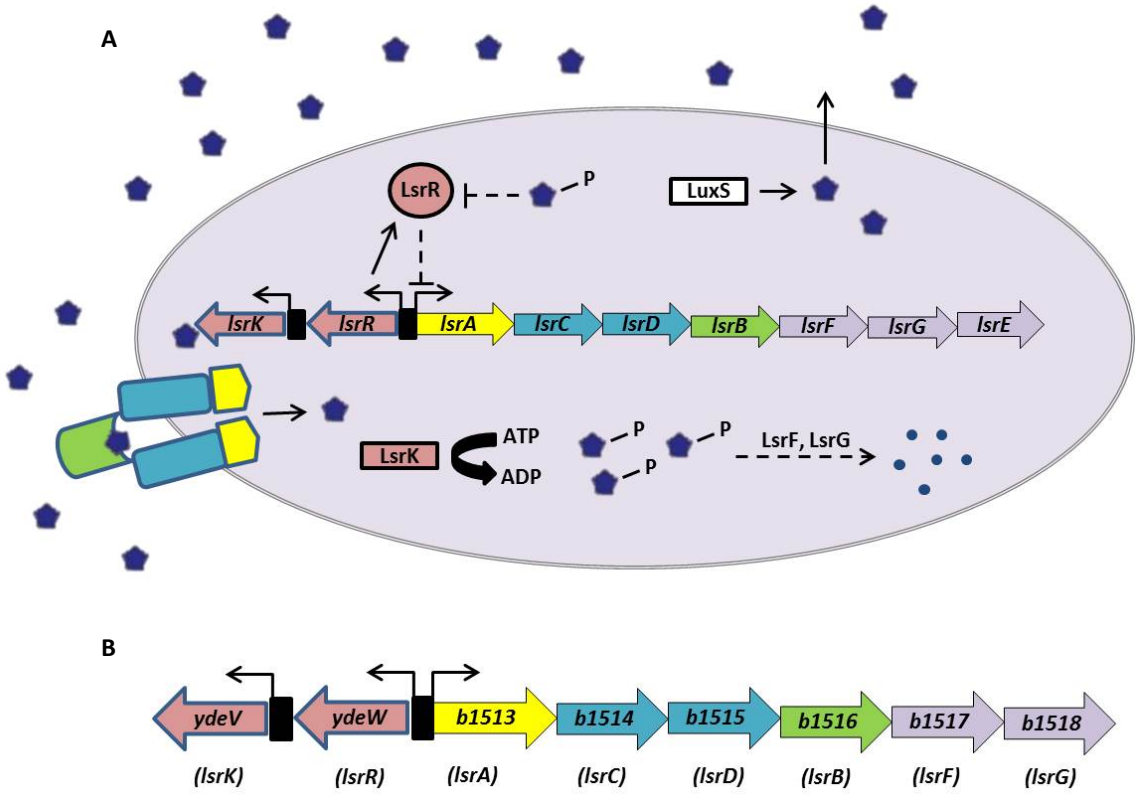

Figure 6. The *Salmonella lsr* operon and its homolog in *E. coli*. (a) The *lsr* locus in *Salmonella*. Transcription units are separated by black promoter boxes, and black arrows indicate direction of transcription for each unit. The small dark blue pentagons represent AI-2, which is made by LuxS and exported from the cell via the TqsA transporter (not shown). The Lsr ABC transporter reimports AI-2 into the cytoplasm, where it is phosphorylated by the LsrK kinase using ATP. Phosphorylated AI-2 relieves repression by LsrR, allowing expression of the *lsrACDBFGE* operon. LsrF and LsrG degrade AI-2-P. The function of LsrE is not clear, and it is absent in *E. coli*. (b) The *b1513* operon of *E. coli* is a homolog of the *Salmonella lsr* operon. The *E.* coli gene designations are given inside the arrows, and the *Salmonella* homologs are listed beneath each arrow. Figure adapted from Xavier and Bassler (*98*).

Figure 7. *Salmonella* LsrB crystal structure. The cartoon depicts the crystal structure of *Salmonella* LsrB in complex with the *R*-THMF isomer of AI-2. The amino and carboxyl terminals are labeled, as is the AI-2 ligand. The two subunits are asymmetrical, entering the closed conformation only when AI-2 is bound. *E. coli* LsrB is 85% identical to *Salmonella* LsrB, with only a few amino acid residue differences, and the AI-2 binding sites are identical. Only the *R*-THMF isomer of AI-2 binds in such a manner to elicit an attractant chemotaxis response in *E. coli*. Deletion of LsrB abolishes chemotaxis to AI-2 in *E* coli. PDB ID: 1TJY.

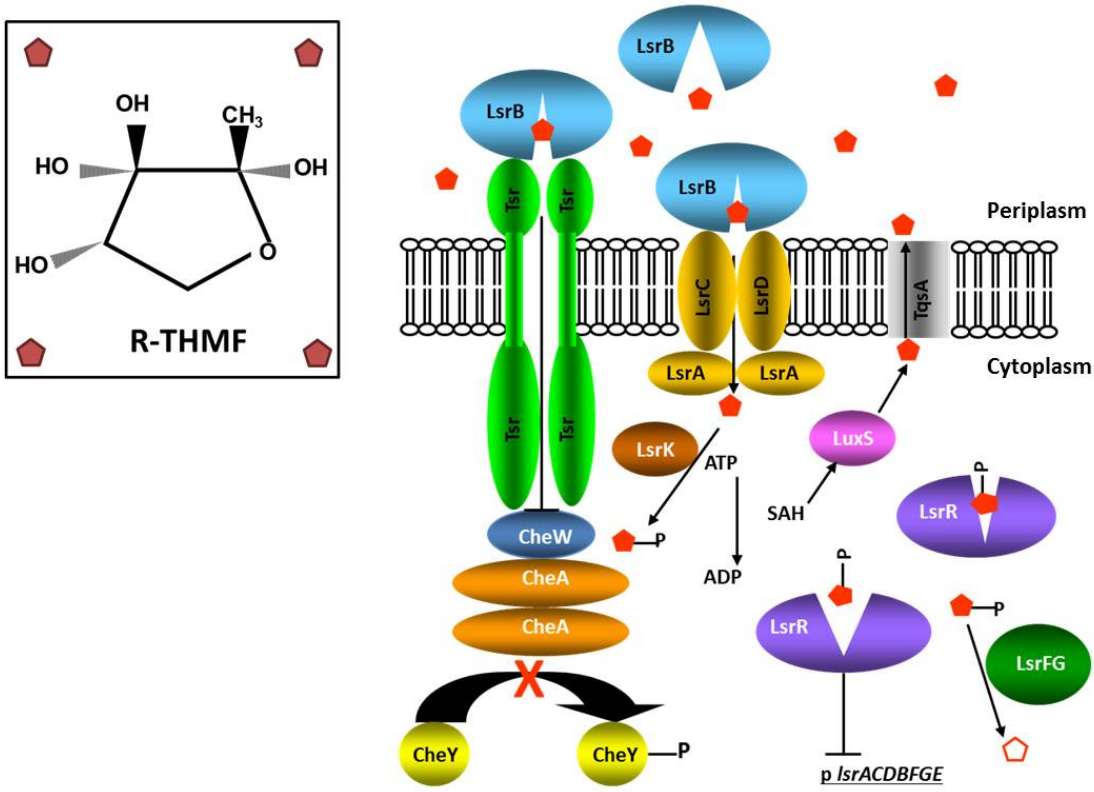

Figure 8. Proposed AI-2 chemotaxis pathway in *E. coli*. The *R*-THMF isomer of AI-2 is shown to the left (not to scale). The figure to the right shows the proposed pathway by which *E. coli* cells sense and respond to AI-2 (red pentagons) as a chemoattractant. The ABC transporter product of the *lsr* operon is shown in the cell membrane. AI-2-bound LsrB binds to the channel during AI-2 uptake as previously reported (*98*). Also present in the membrane is the Tsr chemoreceptor, complete with chemotaxis proteins for altering flagellar rotation. This model proposes that LsrB can interact with the Tsr receptor to elicit an attractant response, inhibiting phosphorylation along the phosphorelay pathway and causing a CCW rotation of the flagella to propel the cell in a run.

Conversely, deletion of the ABC transporter components of the *lsr* operon does not negatively affect AI-2 chemotaxis, suggesting that uptake of AI-2 to the cytoplasm is not necessary for chemotaxis to occur (*43*). Only deletion of Tsr was shown to abolish AI-2 chemotaxis (*43*). Thus, the study concluded that (i) both Tsr and LsrB were necessary for *E. coli* to perform chemotaxis to AI-2; and (ii) uptake into the cell is not required to elicit an attractant response. It was hypothesized, based on this information, that AI-2-bound LsrB in the periplasm likely interacts with the periplasmic domain of Tsr to produce a chemotactic signal (Figure 8).

Dissertation overview

Previous work in the field of chemotaxis had never identified a binding protein interaction with the Tsr chemoreceptor. Only recently has a binding protein interaction for Tsr been discovered, although the details surrounding this interaction remained unclear (*43*). The research undertaken and presented in this dissertation examines the interaction between Tsr and the AI-2-bound LsrB binding protein during AI-2 chemotaxis.

Chapter II describes my research in altering residues at the predicted interaction sites between Tsr and LsrB. The hypothesis was that individually altering select residues on both proteins would disrupt chemotaxis to AI-2 and give a better picture of the binding interaction and the critical residues involved in stabilizing the interaction to allow for signaling. The results suggest that the Lys-147 residue on the periplasmic shoulder regions of the Tsr homodimer are critical for AI-2 chemotaxis to occur. The results also suggest several residues in both the N-terminal and C-terminal domains of the LsrB monomer are important for this chemotaxis response, with Asp-59 in particular

showing a dominant negative phenotype for AI-2 chemotaxis when altered. All of the mutations generated were checked to make sure that that particular mutation did not prevent expression of the protein in an attempt to avoid false conclusions.

In Chapter III, my research attempted to correlate chemotaxis to AI-2 with various levels of LsrB expression. Plasmid-borne LsrB was induced with varying concentrations of IPTG to increase the amounts of the protein present in the cell during chemotaxis. It was determined that only about 23-25 copies of LsrB exists per cell under normal conditions, and that increasing the amount of LsrB present via induction drastically reduced chemotaxis to AI-2. Non-polar deletion mutants of the *lsr* operon were also used in attempt to determine how its components affect LsrB expression levels *in vivo*, and how these levels correspond to AI-2 chemotaxis.

Chapter IV describes my efforts in determining if (a) mutating residues crucial for the serine binding pocket also alter response to AI-2, and (b) if serine and AI-2 alter response to one another when the other is present at high concentrations. First, mutants for serine chemotaxis were exposed to a gradient of AI-2 and their response was determined. Results showed a lack of response to serine, but unimpaired response to AI-2. Additionally, mutations from Chapter II that reduced or abolished chemotaxis to AI-2 did not affect response to serine in those mutants. Second, exposing cells to high concentrations of one chemoeffector, then running chemotaxis assays to detect response to the other chemoeffector, gave an idea of the effect of the presence of one ligand on the other. Chapter V summarizes the experiments and discussion from my research and proposes future directions and experiments for this investigation.

CHAPTER II

EXAMINING THE TSR-LSRB BINDING INTERACTION THROUGH MUTATIONAL ANALYSIS

Introduction

Population density regulates many physiological activities and responses in bacteria, including formation of biofilms and expression of virulence factors. This regulation is accomplished through the use of quorum-sensing molecules that accumulate as population density increases. Autoinducer-2 (AI-2) is a general quorum-sensing molecule produced and secreted by numerous Gram-positive and Gram-negative bacteria. It is derived from the ribose moiety of *S*-adenosylhomocysteine following that molecule's conversion of that to *S*-ribosylhomocysteine and subsequent cleavage by the LuxS enzyme into 4,5-dihydroxy-2,3-pentanedione (DPD). The unstable, linear DPD molecule spontaneously cyclizes into either (2*S*,4*S*)-2-methyl-2,3,3,4-tetrayhydroxytetrahydrofuran borate (*S*-THMF borate) or (2*R*,4*S*)-2-methyl-2,3,3,4-tetrahydroxytetrahydrofuran (*R*-THMF).

S-THMF borate regulates bioluminescence and virulence in *Vibrio* species, including *Vibrio harveyi*. A periplasmic binding protein of *Vibrio*, LuxP, binds this borated form of AI-2 with high affinity (K_D of <1 μM) (*102, 103*). The *R*-THMF isomer of AI-2 is reported to bind to the LsrB periplasmic binding protein of *Salmonella*, *E. coli* and other enteric bacteria with an apparent K_D of 160 μM (*103*). This reported binding affinity for *R*-THMF AI-2 to LsrB is somewhat conjectural, due to the extreme instabil-

ity of AI-2 in solution, and the equilibrium between the two naturally occurring THMF isomers.

AI-2 is synthesized by LuxS and secreted into the periplasmic space, partly by the activity of TqsA efflux transport. Once in the periplasm, it can passively diffuse into the external environment to be sensed by neighboring cells. The ability of cells to take up AI-2 relies on the products of the *lsr* operon. The LsrB periplasmic binding protein binds AI-2 and interacts with an ABC transporter composed of a heterodimer of the two membrane-spanning LsrCD proteins and the cytoplasmic kinase LsrA.

The LsrK kinase phosphorylates the DPD intermediate of AI-2, creating phospho-DPD (DPD-P). This phosphorylated molecule binds the repressor of the *lsr* operon, LsrR, relieving repression and inducing transcription of *lsrACDBFG*. Two downstream gene products in this operon, LsrF and LsrG, degrade DPD-P, completing the regulatory cycle of AI-2 uptake and processing. This is an unconventional cycle, as AI-2 induces expression of factors needed both for its uptake and those required for its destruction.

Recently, it was shown that AI-2 is a potent chemoattractant for *E. coli* strain RP437, requiring the activity of both the LsrB periplasmic binding protein and the Tsr chemoreceptor (*43*). Import of AI-2 into the cytoplasm is not required for its being sensed as an attractant. A mutant lacking the ABC transporter protein LsrC was still able to perform normal chemotaxis to AI-2. Because of this finding, it was proposed that AI-2-bound LsrB interacts directly with the periplasmic domain of the Tsr chemoreceptor dimer. There is precedent for this type of interaction between binding protein and chemoreceptor, as evidenced with the *E. coli* aspartate receptor (Tar) and maltose bind-

ing protein (MBP) (*104, 105*). Periplasmic maltose must first bind to MBP, causing a conformational shift of MBP that can interact with Tar. Maltose-loaded MBP interacts with both subunits across the Tar dimer, involving certain residues on the surfaces of MBP and Tar (*104, 106*). This is also true of ribose and galactose binding proteins with Trg and DppA with Tap (*5,7,8,10*).

Based on the published Tar-MBP interaction, a computerized docking simulation was performed of the x-ray crystallographic structure of *Salmonella* LsrB, in its ligand-bound conformation (*95*), with the x-ray crystallographic structure of the ligand-free periplasmic domain of *E.coli* Tsr (*107*). In the Tar-MBP model, the ligand-free Tar was oriented to the most likely fit of MBP using SPOCK software (*108, 109*), then refined based on the experimental data.

Likewise, the Tsr-LsrB simulation was carried out using this software to obtain a testable model. Next, site-directed alanine scanning mutagenesis was used to probe the amino acid residues predicted to be at the sites of interaction between the two proteins. Tsr variants generated retained wild-type function for serine chemotaxis, and LsrB mutant proteins remained stable, and maybe functional for AI-2 uptake. The binding site for *R*-THMF was not affected by these residue changes.

The results reported here support the computer docking model for the LsrB-Tsr interaction and identify residues on both proteins that are critical for their interaction during binding and signaling, ostensibly without affecting the ability of LsrB to carry out its previously described AI-2 binding and transport functions.

Materials and methods

Bacterial strains, plasmids and media. Strain CV1, equivalent to strain RP437 (*110*), was used as the wild-type *E. coli* strain for chemotaxis. All relevant strains and plasmids are listed in Table 1. Plasmids pCA24N was used to express the wild-type and mutant Tsr and LsrB proteins at near-chromosomal levels. Additionally, plasmid pBAD18 was used to express *lsrB* from the arabinose-inducible pBAD promoter (*111*). Mutations were introduced into *tsr* and *lsrB* using the standard protocol for site-directed mutagenesis (Stratagene). Tryptone broth (TB; 10 g/L tryptone and 8 g/L NaCl) was used to culture cells at 30°C for all assays (*112*). Chemotaxis buffer (CB; 1X phosphate-buffered saline, 0.1 mM EDTA, 0.01 mM *L*-methionine and 10 mM *DL*-lactate) was used to wash cells and deliver attractants. AB medium contained 2 g/L casamino acids, 12.3 g/L magnesium sulfate heptahydrate, 17.5 g/L NaCl, 1 mM *L*-arginine, 1 % v/v glycerol and 10 mM potassium phosphate buffer, pH 7.0 (*113*). Chemically synthesized DPD (*114*) (17.57 mM) was purchased from the research group of Rita Ventura at the Insituto de Tecnologia Química e Biológica (ITQB-UNL) in Oeiras, Portugal. *L*-serine was purchased from Fisher Scientific (Fairlawn, NJ). *Vibrio harveyi* TL26 was a kind gift from Bonnie Bassler, Princeton University.

Measuring chemotaxis to attractants. Capillary assays, first developed by Adler *et al.* (*115*) were used to quantify the response to AI-2. Overnight cultures of cells expressing Tsr or LsrB mutant proteins from pCA24N were grown at 30°C in TB supplemented with streptomycin (50 μg/mL) and chloramphenicol (35 μg/mL). Cultures were back-diluted to a turbidity of ~0.050 at $O.D._{600}$ in 25 mL TB without antibiotic and then

Table 1. Bacterial strains and plasmids

Strain or plasmid	Genotype	Resistance[a]	Source
Escherichia coli			
CV1	Wild-type chemotaxis	Strep	(*110*)
CV5	CV1 Δ*tsr*	Strep	(*43*)[b]
AS2002	CV5 +pCA24N-*tsr*	Strep/Cm	This study[c]
CV1 (*ΔlsrB*)	Δ*lsrB*	Strep	This study[d]
AS2014	CV1 Δ*lsrB/luxS*	Strep	This study[e]
Vibrio harveyi			
TL26	Δ*luxN*/Δ*luxS*/Δ*cqsS*		(*116*)[f]
Plasmids			
pCP20	*oriR*^{ts} FLP recombinase	Amp	(*117*)[g]
pCA24N-*tsr*	pCA24N $_{PT5\text{-}lac}$::*tsr*	Cm	(*118*)
pCA24N-*lsrB*	pCA24N $_{PT5\text{-}lac}$::*lsrB*	Cm	(*118*)
pBAD-*lsrB*	pBAD $_{PBAD}$::*lsrB*	Amp	This study[h]

[a] Strep – streptomycin; Kan – kanamycin; Cm – chloramphenicol; Amp – ampicillin

[b] Contains Δ*tsr9101 (119)* introduced via phage transduction

[c] Constructed by transforming strain CV5 with pCA24N-*tsr*

[d] Constructed by removing Kan cassette (*120*) from MJ101(*43*)

[e] Constructed by removing the kanamycin resistance cassette from *lsrB* in MJ101 using FLP recombinase. This removal was selected for through lack of growth on Kan media and PCR was used to verify its removal. Phage transduction was then used to add the kanamycin resistance cassette to disrupt *luxS*. This was selected for through growth on Kan media and verified through PCR, then Kan cassette was removed using FLP recombinase.

[f] Disrupted for sensing AHLs and CAI-1. It senses only exogenously added AI-2.

[g] This plasmid was transformed into MJ101 and selected for through Amp-resistance. The recombinase recognizes flanking sites of the Kan-resistance cassette and removes it from the DNA. The plasmid is then cured by growth at 43°C, restricting its temperature sensitive origin of replication. The resulting strain is now both Kan- and Amp-sensitive.

[h] Constructed by cloning CV1 chromosomal *lsrB* into the pBAD18 vector.

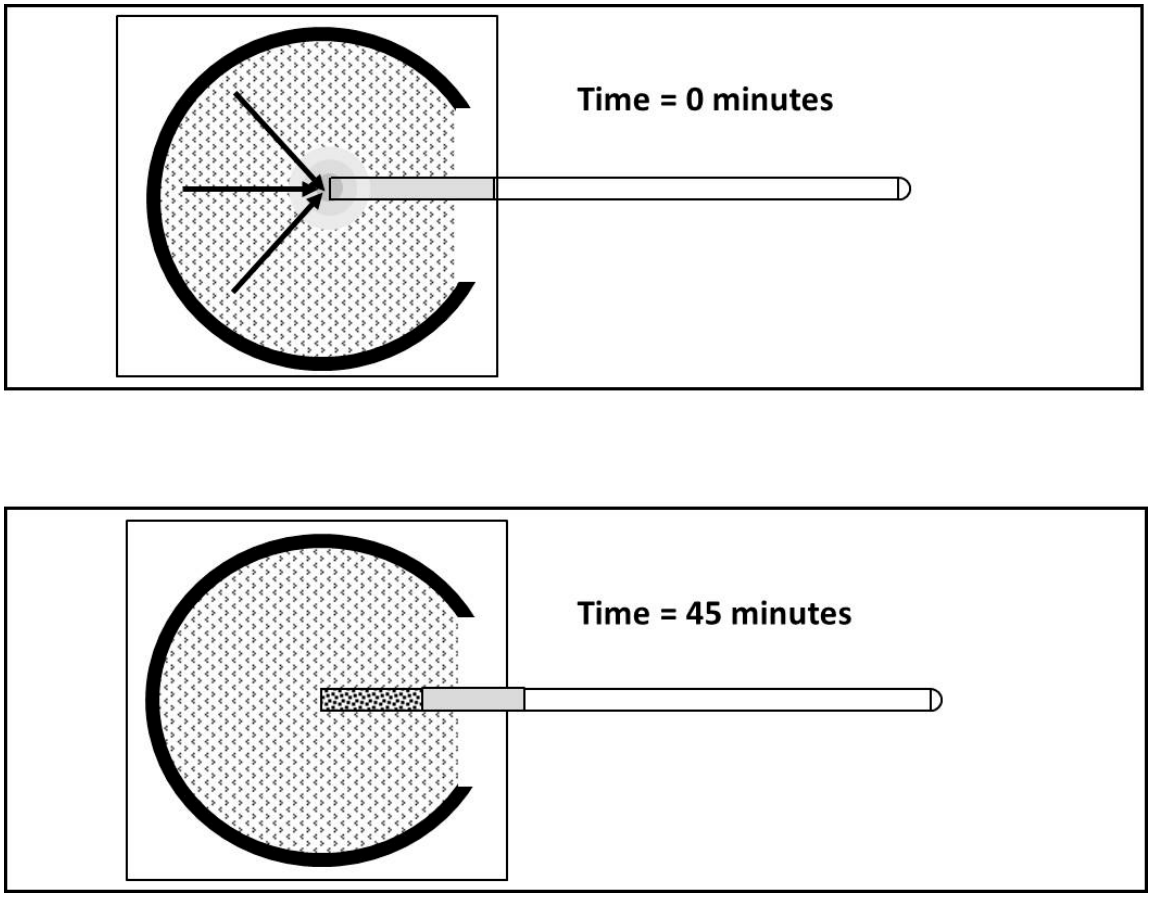

Figure 9. The capillary assay. Cell chamber ponds are created by placing a C-shaped plastic gasket onto a glass microscope slide, then adding a square, glass coverslip on top. Washed cells are loaded into the chamber to create the pond. 1 mm capillaries loaded with chemoeffector are inserted into the chamber pond and incubated for 45 minutes to allow diffusion and chemotaxis response. Capillaries are then removed and their contents expelled into dilution buffer for plating. Overnight incubation of plates allows for colonies to be counted and the number of cells accumulated inside the capillary can be calculated (*115*).

grown to mid-logarithmic phase at an $O.D._{600}$ = ~0.500. Expression of Tsr from AS2002 was induced with 100 µM IPTG (*121*) at $O.D._{600}$ = ~0.300 and allowed to continue growth to ~0.500. Expression of LsrB from AS2014 was not induced. Cells expressing plasmid pBAD-*lsrB* were prepared similar to cells expressing pCA24N-*lsrB* with the exception that expression of pBAD-*lsrB* was induced with 0.2% *L*-arabinose at the time of back dilution from overnight culture. Cell cultures of 5 mL were centrifuged at 600 x g for 10 minutes to separate the soft pellet from the growth media. The pellet was gently resuspended in an equal volume of CB and incubated for fifteen minutes of recovery time in a 30°C rotor set to low speed. The resuspended cells were used for the assay. Motility of the resuspended cells was confirmed through phase contrast microscopy.

Capillary assays used plastic gaskets sandwiched between a glass microscope slide and glass coverslip to create the pond chamber (Figure 9). About one sixth of the gasket was excised to provide an insertion point for both cells and capillaries into the chamber. A 1 microliter volume capillary was flame-sealed at one end and lowered into a solution containing the desired concentration of attractant to be tested. The CB-buffered attractant was pulled several millimeters into the capillary.

Capillaries contained either CB alone or CB supplemented with the different concentrations of *L*-serine or AI-2. The cells were inserted into the chamber ponds via gentle pipetting to avoid bubbles or flagellar shearing. Capillaries were then inserted through the opening of the chamber and cells were incubated at 30°C for 45 minutes. Diffusion of the chemoeffector from the open end of the capillary into the pond created a gradient that could be sensed by the cells (*115*). These cells migrated up the gradient

and into the capillary mouth if the attractant signal was strong enough. Once incubation finished, the capillaries were removed and their contents expelled into CB for dilution. Dilutions were plated on nutrient agar supplemented with appropriate antibiotic and allowed to grow at 37°C overnight. Colonies were counted and the number of cells that entered the capillaries was calculated. All data was normalized to CB background.

Computer generated docking model and residue selection. The MBP-Tar model (*122*) was used as a guide to generate a computerized docking model for LsrB-Tsr. SPOCK software (*108*) was used to align amino acid residues on the surface of AI-2-bound LsrB (*95*) (Protein Data Bank ID=1TJY) believed to be in contact with Tsr, based on the crystal structure for *E. coli* Tsr (*107*) (PDB ID=2D4U). Also taken into account were unpublished findings that replacements at particular residues in LsrB altered chemotaxis to AI-2. Care was taken to ensure these residues were oriented for close contact with Tsr. Molecular dynamics calculations were done by using AMBER (*123*) software to simulate docking, following the removal of all overlap between the Tsr and LsrB structures. A distance-dependent dielectric field, at an initial temperature of 300 Kelvin with a time step of 0.001 ps, was used to carry out all simulations, with the default force field suggested by the AMBER software.

Site-directed mutagenesis of tsr *and* lsrB. Point mutations were made in plasmid-borne *tsr* and *lsrB* genes using a site-directed PCR mutagenesis protocol closely following the protocol suggested by the Stratagene QuikChange™ II Site-Directed Mutagenesis Kit (Stratagene, La Jolla, CA). Amino acid residues in α-helix 3-4 (Gly144-Glu150) of the subunit 1 and 1' "shoulder" regions of the Tsr dimer were targeted and individual-

ly changed to alanine or other residues using primers designed according to well established principles for mutagenesis (*124*). Amino acid residues Leu56-Pro65 of β-strand 2, and Asp249-Glu256 of α-helix 8 of LsrB were targeted for individual replacement using the same guidelines. Primers were synthetic oligonucleotides (Integrated DNA Technologies™) containing the desired mutation, each complementary to opposite strands of the pCA24N-*tsr*, pCA24N-*lsrB* and pBAD-*lsrB* vectors. These primers were extended by the Pfu Ultra DNA polymerase during temperature cycling over multiple PCR cycles. Following PCR, the product is treated with the Dpn I endonuclease to eliminate methylated and hemi-methylated DNA (the parental template). Because the *tsr* and *lsrB* genes cloned into pCA24N and pBAD18 were derived from *E. coli*, this Dpn I digest selects for mutated synthesized DNA because plasmid DNA isolated from our *E. coli* strains is methylated. Mutated *tsr* and *lsrB* genes were then subjected to multiple rounds of PCR sequencing to confirm that only the desired point mutations were present. Plasmids containing desired mutant genes were then transformed into their competent cells (CV1 Δ*tsr* for *tsr* and CV1 Δ*lsrB* for *lsrB*) and frozen.

Creation of the ΔlsrB/ΔluxS *strain AS2014.* Strain MJ101 (*lsrB*ΩKan^r) was transformed with pCP20 (FLP recombinase/Cm^r) (*117*). Transformants were allowed to grow at plasmid's permissive temperature (30°C) to constitutively express FLP recombinase gene product. FLP recombinase removes the kanamycin cassette during growth phase of transformants to leave a clean, non-polar deletion of the targeted gene, a result confirmed by failure of the transformants to grow on kanamycin media (50 μg/mL) during replica plating. Transformants were then grown at restrictive temperature of pCP20

(43°C) to cure the cells of the plasmid. Plasmid curing was confirmed by replica plating cells onto media supplemented with chloramphenicol (35 μg/mL) and their subsequent failure to grow. The resulting strain MJ101was now Δ*lsrB* (no Kan cassette).

P1 phage transduction was performed to transduce the kanamycin cassette from a CV1 (*luxS*ΩKan^{r}) strain to the Δ*lsrB* strain. The transductants were grown on media supplemented with kanamycin (50 μg/mL). Isolated transductants were subjected to PCR with primers for the kanamycin cassette gene, the *lsrB* gene and the *luxS* gene. Following PCR the products were run on a 1% agarose gel supplemented with ethidium bromide, then viewed under ultraviolet light to confirm insertion of the kanamycin cassette and removal of the *luxS* gene. Removal of the kanamycin cassette disrupting *luxS* was done as explained above. Once these results were confirmed, strain AS2014 (Δ*lsrB*/Δ*luxS*) was made competent and ready for use.

Immunoblot analysis for LsrB expression. Overnight cultures of CV1 Δ*lsrB* containing pCA24N expressing LsrB protein were diluted into 500 mL TB and grown at 30°C with shaking to O.D.^{600} = 0.500. Cultures were centrifuged and the pellet was frozen at -80°C before resuspension in 25 mL lysis buffer (5 mM DTT, 50 mM Tris (pH 8.0), 300 mM NaCl, 1 mM PMSF). Resuspended pellets were then sonicated for 8 minutes (15 seconds ON / 45 seconds OFF, 37% amplitude). Centrifugation at ultra-high speed followed before the supernatant was collected in lysis buffer. This was then concentrated to 1 mL and quantified using the BCA assay. PAGE was performed on these whole cell protein preps (20 μL/well) in the presence of 10 μg DTT on 10 % Mini-PROTEAN TGX® Stain-Free™ Protein Gels (Bio-Rad). The separated proteins were

transferred onto a low-fluorescence PVDF membrane (Thermo-Fisher Scientific) at 100 volts for 1 hr using the Mini Trans-Blot® Electrophoretic Transfer Cell (Bio-Rad). The membrane was placed in blocking buffer (3% non-fat dry milk; 10 mM Tris pH 7.5, 100 mM NaCl, 0.1% Tween 20 (TBST)) and incubated with agitation for 1 hour at room temperature. It was then transferred into primary antibody solution (1:2500 Protein A purified anti-LsrB antibody in blocking buffer) and incubated with agitation for 1 hr at room temperature, followed by thorough washing in TBST (3x, 5 mins each). The membrane was then transferred into secondary antibody solution (1:25,000 anti-goat HRP (Sigma A5420) in blocking buffer) and incubated with agitation for 1 hr at room temperature, followed by thorough washing in TBST (3x, 5 mins each). The membrane was developed with Clarity™ ECL Blotting Substrate (Bio-rad) and imaged using the Chem-iDoc™ Touch Imaging System (Bio-Rad). ImageLab™ software (Bio-rad) was used for total protein normalization and estimation of relative LsrB levels.

AI-2 uptake assays with Vibrio harveyi. Overnight cultures of LsrB variants were diluted into 15 mL of TB at 30°C with shaking to $O.D._{600}$ = 0.500. Cultures were then distributed into separate tubes, AI-2 was added, and the samples were incubated at 30°C with shaking. Samples were collected every 30 min for a total of 10 hrs. Samples were centrifuged and the supernatants collected and frozen for use in the *Vibrio harveyi* TL26 bioluminescence assay. This reporter strain is disrupted for signaling pathways for acyl-homoserine lactones (AHLs) and the alpha-hydroxyketone (CAI-1), as well as for synthesis of AI-2 (Δ*luxS*); therefore, it responds only to exogenously added AI-2 and cannot produce AI-2 on its own. TL26 was diluted 1:5000 and 90 µL was added to each

reaction containing 10 μL of thawed samples. Bioluminescence was then measured every hour until the background began increasing. Fold induction in luminescence was measured as Relative Light Units (RLU) of sample / RLU of medium.

Confirmation of LsrB variant response from a separate vector. Because of the absence of tight control of the $P_{T5\text{-}lac}$ promoter in pCA24N, and a short C-termianl extension, key *lsrB* variants were constructed in an expression vector with tighter promoter control and no C-terminal extension. Site-directed mutagenesis was utilized as described previously to introduce point mutations D59A, V60A, T61A, D63A, R252A and E256A into pBAD-*lsrB*. These mutant proteins were then expressed through addition of 0.2% by volume *L*-arabinose to back diluted cultures growing at 30°C. Capillary assays were performed as described previously to measure chemotaxis to AI-2 gradients.

Results

Generation of the Tsr-LsrB docking model. Using the SPOCK and AMBER software programs, the best predicted interaction between the periplasmic domain of Tsr and the AI-2-bound LsrB binding protein was determined. This interaction and regions of interest are shown in Figure 10.

Mutagenesis of tsr. The effect of mutating individual residues from Gly144 to Glu150 to Ala in the "shoulder" regions of Tsr subunits 1 and 1' was tested. These amino acid residues and their relative positions are shown highlighted in red in Figure 11. The rest of the Tsr protein remains unchanged, including the published serine binding sites.

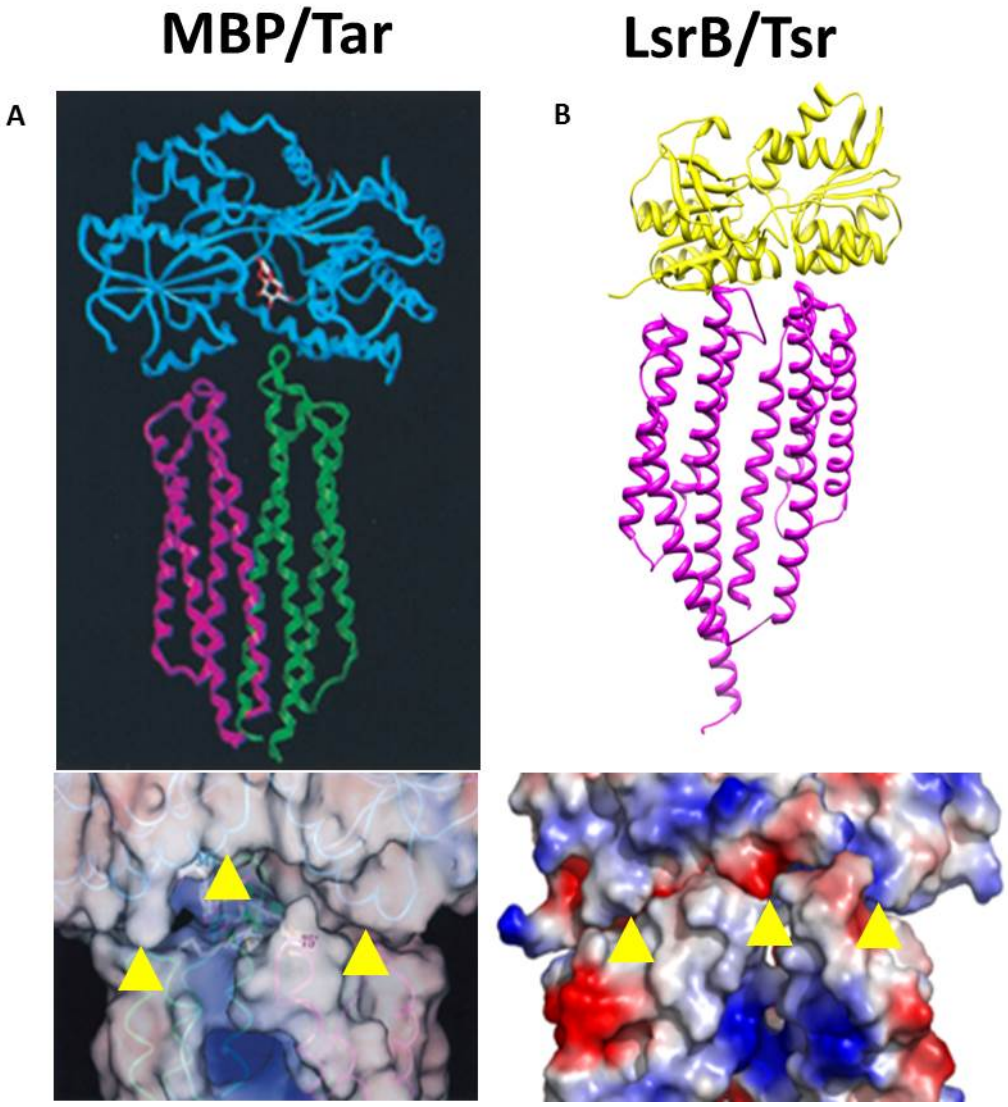

Figure 10. The Tsr-LsrB docking model. (a) The published docking model for the *E.coli* aspartate chemoreceptor (Tar) with ligand-bound maltose binding protein (MBP) (*122*). The upper image shows the likely conformation the proteins adopt during interaction. MBP is shown in blue, with maltose bound at its center. The periplasmic domain of Tar is colored by subunit. The lower image shows the "tightness" of the Tar-MBP interaction. Yellow arrows indicate critical binding sites. (b) The proposed docking model for Tsr-LsrB based on the SPOCK and AMBER software employed (unpublished). The upper image shows the likely interaction dynamics, while the lower image speculates on the strength of the binding. Yellow arrows indicate predicted critical residues that strengthen the binding.

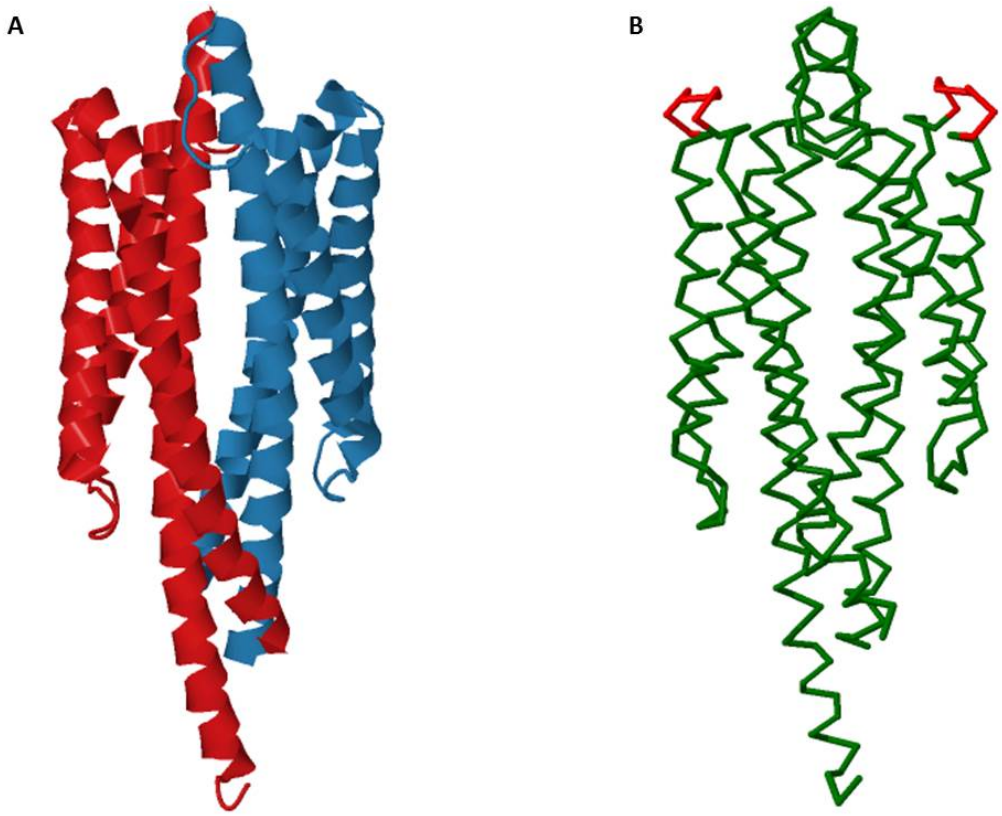

Figure 11. Tsr residues mutated based on docking model. (a) The cartoon structure of the dimerized Tsr periplasmic domain is shown. This model depicts the closed binding conformation of the receptor when serine is bound, and the monomeric subunits are defined by color. (b) The backbone structure taken from the image in (a) indicates amino acid residues predicted to be in closest contact with LsrB by highlighting them in red. This indicated portion extends from Gly144 to Glu150 of subunits 1 and 1'. Individual residues were subjected to site-directed mutagenesis to alanine or other amino acids. The serine binding pocket is unaffected by these mutations. Structures adapted from PDB ID: 2D4U (*107*).

Reviewing the components necessary for E. coli *cells to mediate AI-2 chemotaxis.* To quantify the AI-2 response and compare it to that of *L*-serine, capillary assays were performed (*115*). CV1 and CV4 (Δ*tar*) cells accumulated in capillaries containing either *L*-serine or AI-2. Cells that were Δ*tsr* (CV5) failed to accumulate in either capillaries containing *L*-serine or AI-2, confirming the original finding that the Tsr receptor is necessary to mediate AI-2 chemotaxis (Figure 12). Further confirmation of earlier findings that LsrB is required for AI-2 chemotaxis was supplied by the failure of MJ101 (*lsrB*ΩKan^r) cells to accumulate in capillaries containing AI-2, although they maintained a normal response to *L*-serine (Figure 13). Additionally, cells deleted for one of the membrane-bound transporter proteins (*lsrC*ΩKan^r) maintained the ability to respond to both *L*-serine and AI-2 (Figure 13).

The ability of tsr *variants to mediate chemotaxis to AI-2.* To quantify AI-2 response, and compare it to that of *L*-serine, capillary assays were again performed with the *tsr* variants generated from the docking model. The plasmid bearing wild-type *tsr* set the standard for comparison, while the CV5 (Δ*tsr*) strain served as the negative control. The point mutations were introduced into strain AS2002, and expression of the mutant proteins was induced with 100 μM IPTG. Four of the point mutants, G144A, G146A, I148A and N149A (position 145 is an Ala), showed little to no variation in AI-2 response, with dose response curves similar to that of the wild-type *tsr*. The E150A point mutant was noticeably impaired for response to AI-2, though not to a significant degree. The K147A point mutant showed little to no accumulation in the capillary in the presence of AI-2 (Figure 14). The response to 10 mM serine was not inhibited with any of

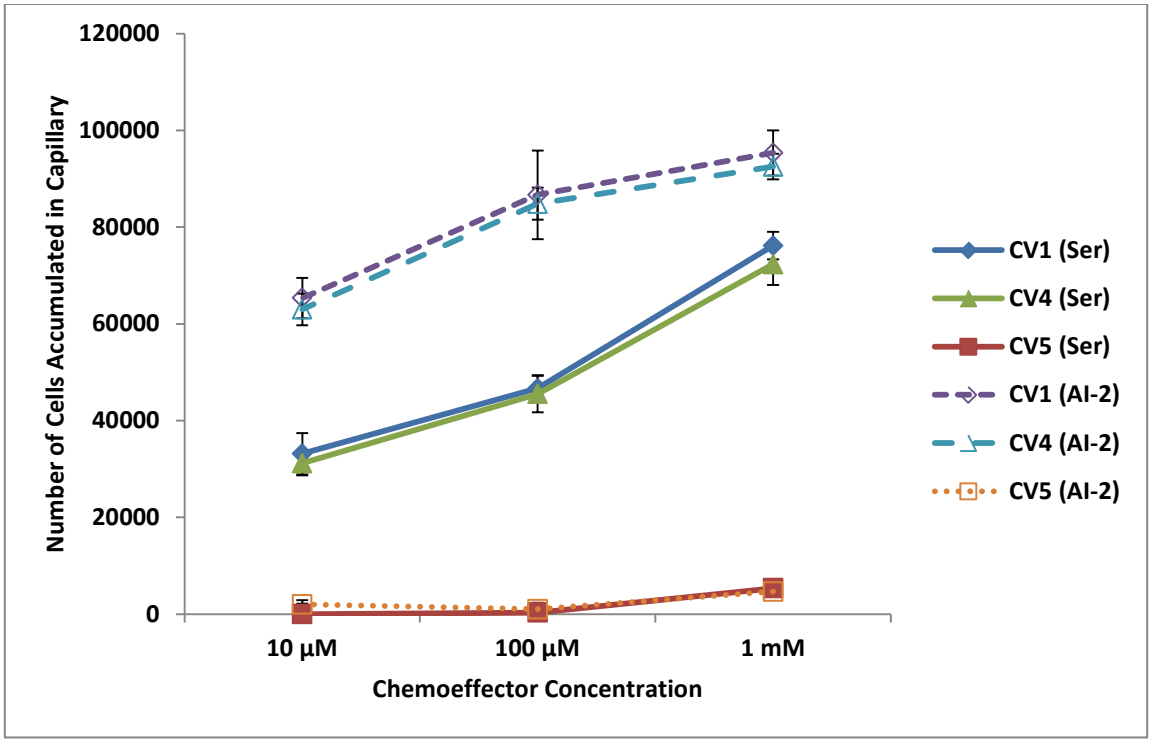

Figure 12. Response of WT and variant cells to chemoattractant. Shown are the normalized values (buffer-only controls subtracted) of CV1 (WT), CV4 (Δ*tar*) and CV5 (Δ*tsr*) cells responding to capillaries containing either *L*-serine or AI-2. Incubation of cells occurred for 45 minutes at 30°C. Trials were performed in triplicate with three biological replicates each. Cells deleted for the Tsr chemoreceptor failed to respond significantly to either attractant. Cells deleted for the Tar chemoreceptor responded to gradients of AI-2 at near wild-type levels.

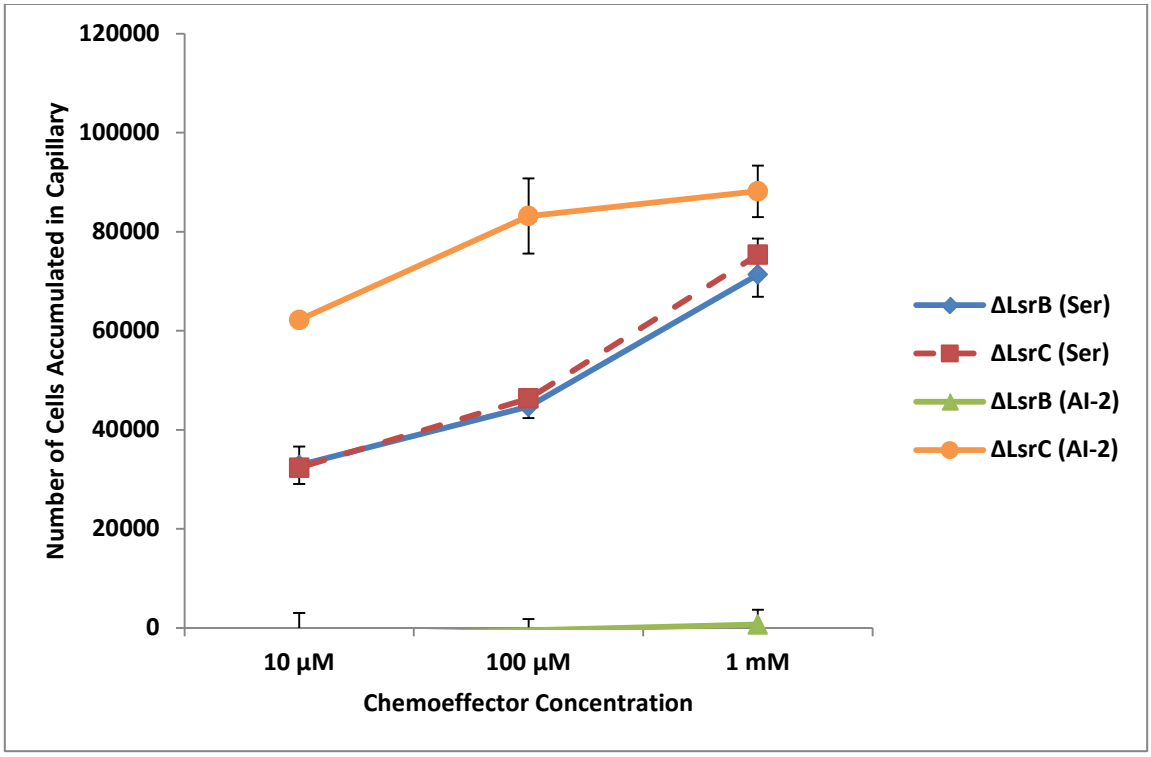

Figure 13. Response to chemoeffector by *lsr* operon variants. Shown are normalized values of Δ*lsrB* (*lsrB*ΩKan^r) and Δ*lsrC* (*lsrC*ΩKan^r) cells responding to either *L*-serine or AI-2. Cells were incubated at 30°C for 45 minutes. Trials were performed in triplicate for three biological replicates. Cells lacking the AI-2 binding protein LsrB were unable to respond to a gradient of AI-2. Cells lacking one of the AI-2 transport channel proteins LsrC were able to respond normally to gradients of AI-2.

the mutant proteins except for a 10% decrease with E150A (Figure 15). Glu-150 is the residue closest to the serine-binding site.

The amino acid residues Lys147 and Glu150 were selected for charge reversal point mutation to further investigate their importance. The Ile148 residue was also selected as a control since its dose response curve showed near wild-type level response in the alanine scanning mutant testing. K147E, I148E and E150K were introduced separately into AS2002 and tested in the capillary assay for response to *L*-serine and AI-2. The K147E variant showed a complete lack of response to AI-2. The I148E variant responded with a near wild-type response curve, whereas the E150K variant gave a slightly weaker response than its E150A counterpart – lower than the wild-type response but not significantly (Figure 16). Again, serine response was not affected by these mutations.

The ability of lsrB *variants in the N-terminal region (β-strand-2) to mediate chemotaxis to AI-2*. Capillaries assays were used to measure the chemotactic ability of *lsrB* variants to AI-2. The docking model was again consulted to determine which amino acid residues in the N-terminal region of LsrB should be subjected to alanine-scanning mutagenesis. The plasmid bearing wild-type LsrB was used as the standard for comparison for AI-2 chemotaxis. MJ101 (*lsrB*ΩKan^r) was the negative control for chemotactic response to AI-2, showing no response in the assay. Several alanine-scanning variants in β-strand-2 showed little to no difference in dose response to AI-2 from the capillary assay. These included L56A, G57A, V58A, Y62A, G64A and P65A. The most severe dose response alteration was exhibited by the D59A variant, with elim-

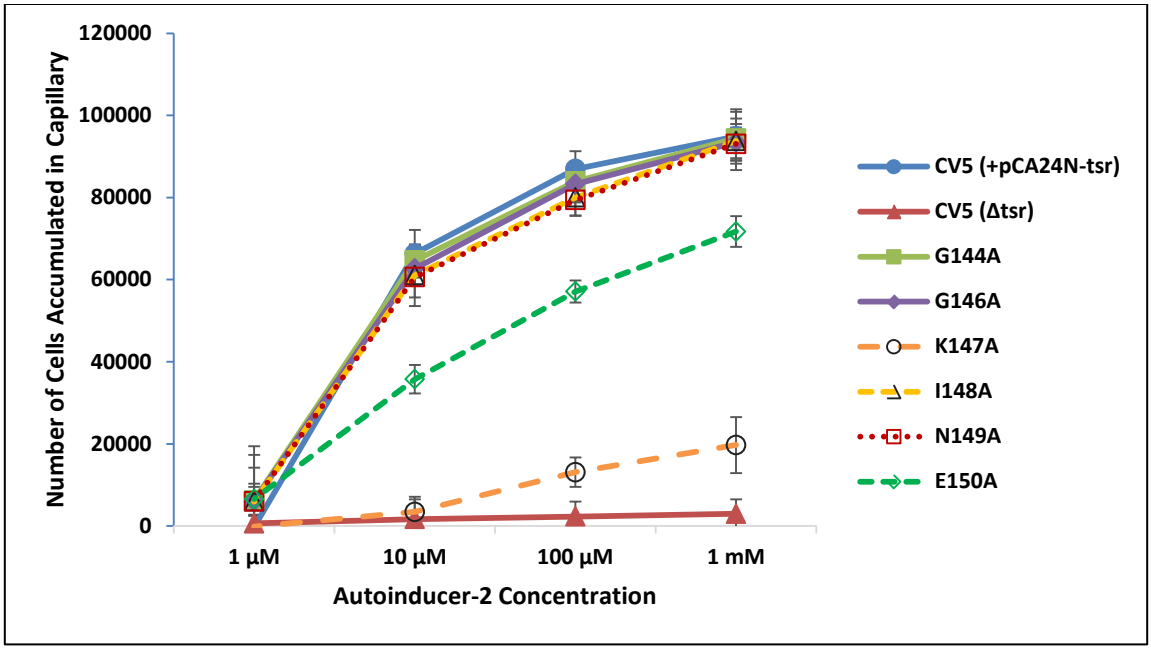

Figure 14. Tsr alanine-scanning mutant response to AI-2. Background accumulations in buffer-only capillaries were between 7,000 and 15,000. Shown are the normalized values (buffer-only controls subtracted) of CV5+pCA24N-*tsr* (AS2002), CV5 (Δ*tsr*) and AS2002 *tsr* point mutant cells responding to capillaries containing AI-2. Capillary assays were performed over a 45 minute incubation at 30°C in a slide warming chamber. Trials were performed in triplicate for three biological replicates. Tsr variants were expressed from pCA24N with 100 µM IPTG induction. The K147A variant accumulated only slightly more than the negative control. Also reduced for AI-2 chemotaxis was the E150A Tsr variant. All other point mutants responded at near wild-type levels.

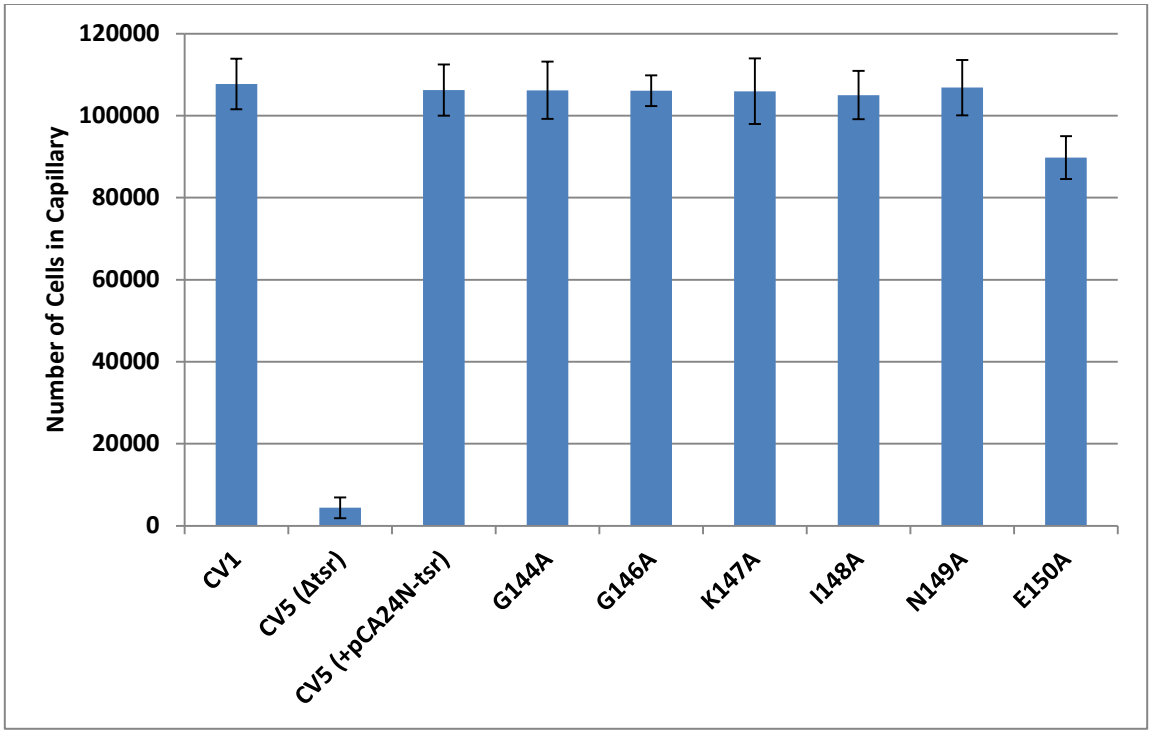

Figure 15. Tsr alanine-scanning mutant response to 10 mM *L*-serine. Background accumulations in buffer-only capillaries were between 7,000 and 15,000. Assays were carried out in triplicate for three biological replicates. Cells were incubated for 45 minutes at 30°C. Variants were induced at 100 μM IPTG from plasmid pCA24N. Capillary assays were performed over a 45 minute incubation period at 30°C.

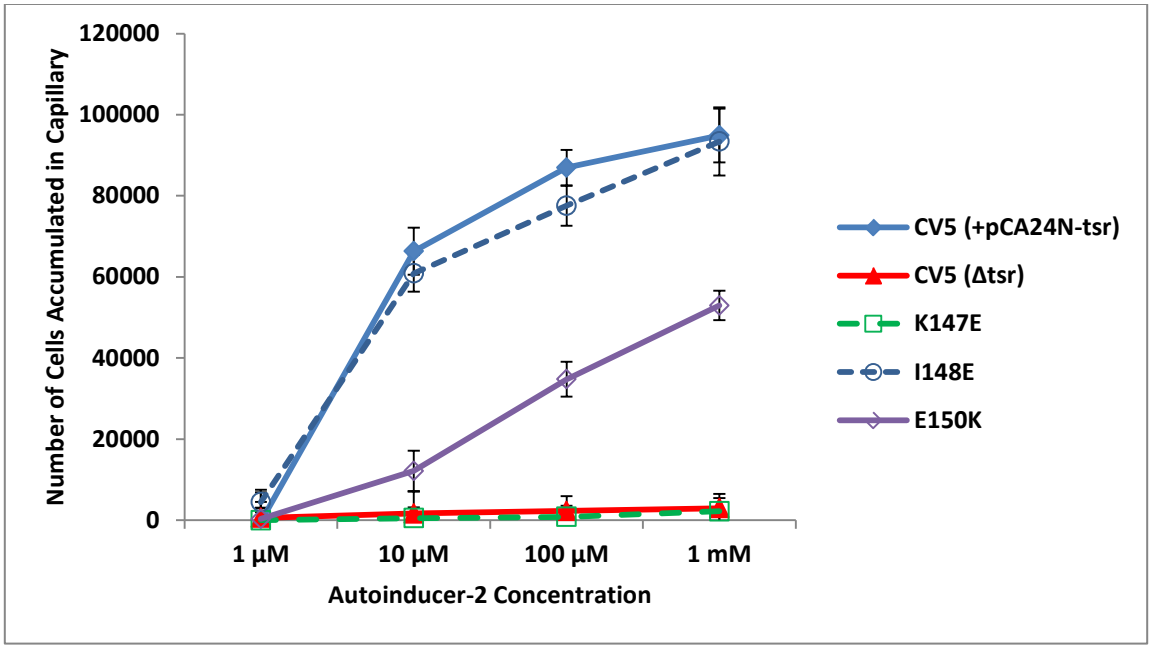

Figure 16. Tsr charge reversal mutant response to AI-2. Background accumulations in buffer-only capillaries were between 7,000 and 15,000. Charge reversals of three selected residues were carried out and variants were induced from plasmid pCA24N with 100 µM IPTG. K147E loses any ability to mediate AI-2 chemotaxis. E150K response to AI-2 is relatively unchanged from E150A. Capillary assays were performed over a 45 minute incubation period at 30°C. Trials were carried out in triplicate for three biological replicates.

ination of the dose response to varying degrees in the V60A, T61A and D63A variants (Figure 17).

The ability of lsrB *variants in the C-terminal region (α-helix-8) to mediate chemotaxis to AI-2*. Amino acids in α-helix-8 of the LsrB C-terminus were subjected to alanine-scanning mutagenesis based on the docking model. These variant responses were again compared to the chemotactic response of wild-type LsrB expressed from plasmid pCA24N, and negative control MJ101. Based on the results of these capillary assays, only the N249A mutant retained a wild-type dose response curve. The R252A and E256A variants showed significantly altered response compared to wild-type, and the R252A/E256A double mutant failed to respond (Figure 18). Charge reversal mutations were then introduced at these positions both singly and in a tandem. Both the R252E and E256R variants showed a severe alteration in the AI-2 response compared to wild-type, with the double mutant (R252E/E256R) losing all ability to respond to AI-2 in the capillary assay (Figure 19).

Ability of LsrB variants to transport AI-2 in uptake assay. Each of the LsrB variants was tested for its ability to participate in AI-2 uptake using the *Vibrio harveyi* TL26 bioluminescence assay. All variants in β-strand-2 showed a decrease in bioluminescence similar to wild-type LsrB between the 3 to 4 hour time points (Figure 20). AI-2 uptake was not hindered in the D59A, V60A, T61A or D63A AI-2 chemotaxis mutants. Likewise, variants in α-helix-8 were not hindered in their ability to transport AI-2 relative to wild-type (Figure 21). Only double mutants T61A/D63A and R252A/E256A showed

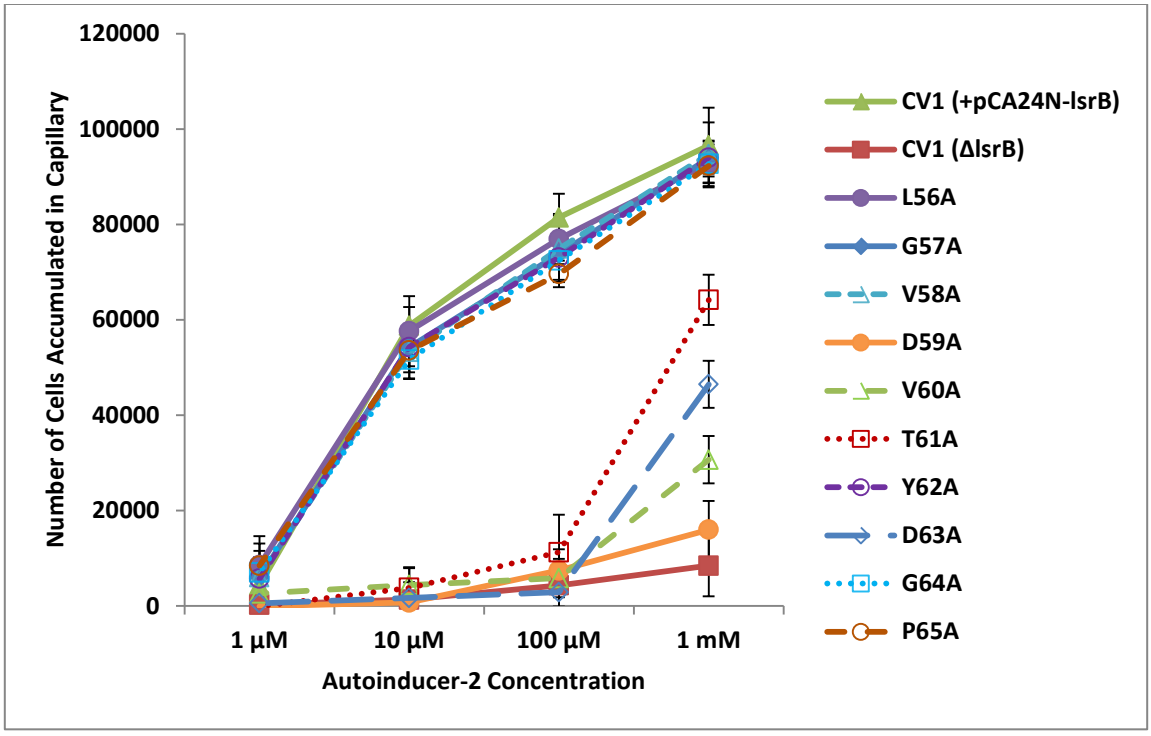

Figure 17. LsrB β-strand 2 variant response to AI-2. Background accumulations in buffer-only capillaries were between 7,000 and 15,000. Most variants retain a wild-type dose response curve. Variants D59A, V60A, T61A and D63A, all show a drastically different dose response to a range of AI-2. The D59A variant loses nearly all of its ability to respond to AI-2 via chemotaxis. No induction was necessary as uninduced plasmid-born LsrB levels were similar to those of chromosomally produced LsrB. Capillary assays were performed over a 45 minute incubation period at 30°C. Trials were carried out in triplicate with three biological replicates.

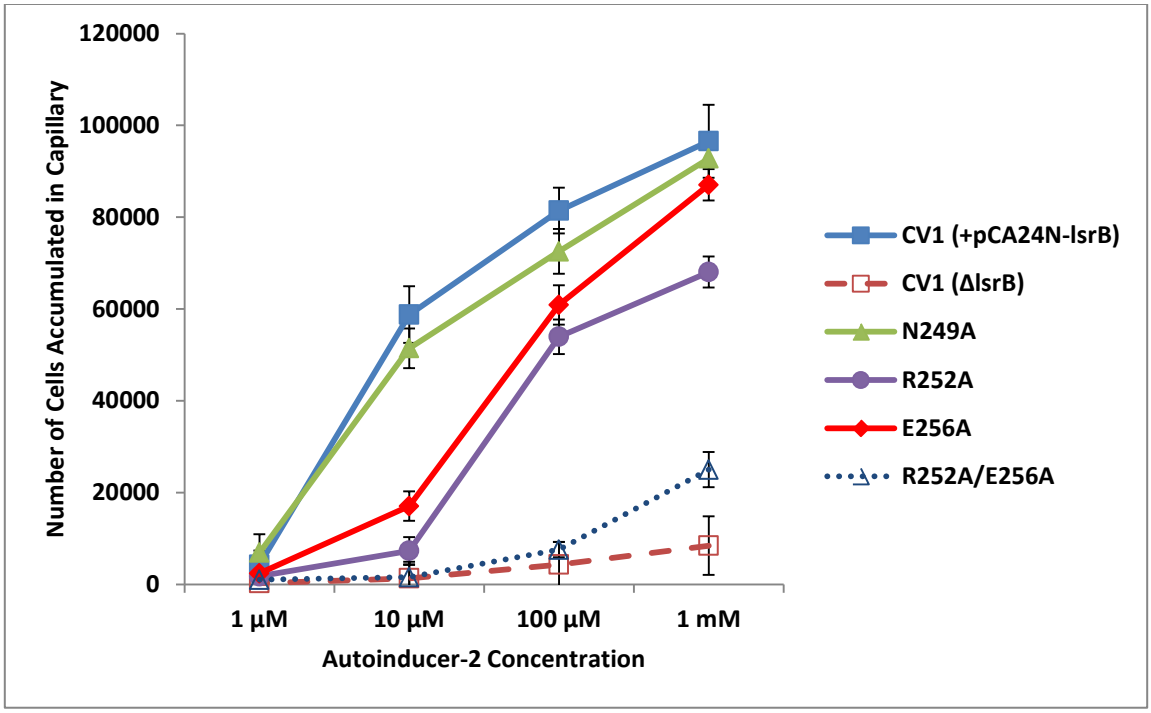

Figure 18. LsrB α-helix 8 variant response to AI-2. Background accumulations in buffer-only capillaries were between 7,000 and 15,000. Most variants retain a wild-type dose response curve. Notable variants include R252A, E256A and the R252A/E256A double mutant, all of which show a lowered dose response to a range of AI-2. No induction was necessary as uninduced plasmid-born LsrB levels were similar to those of chromosomally produced LsrB. Capillary assays were performed over a 45 minute incubation period at 30°C. Trials were carried out in triplicate with three biological replicates.

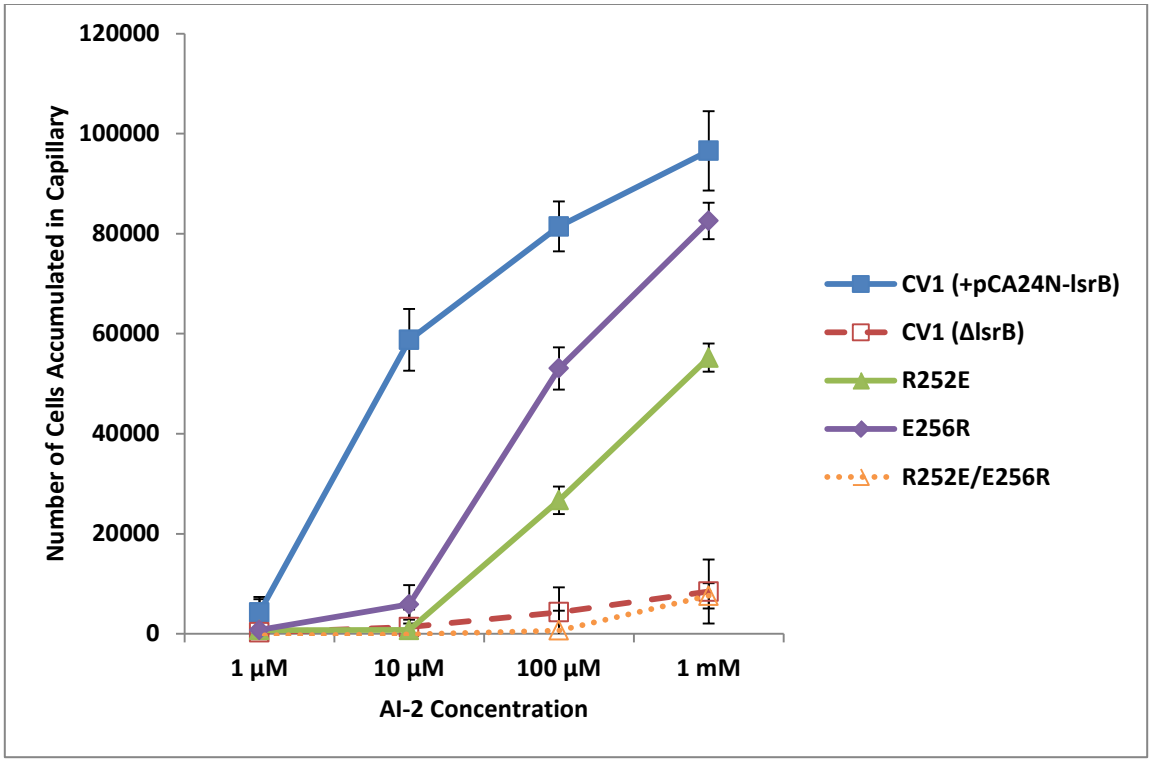

Figure 19. LsrB α-helix 8 charge reversal variant response to AI-2. Shown are the selected point mutants that were subjected to charge reversal. No induction from pCA24N was necessary since LsrB levels were similar to chromosomal levels. Background accumulations ranged between 7,000 to 10,000 cells in buffer only. Cells were incubated at 30°C for 45 minutes. Trials were carried out in triplicate for three biological replicates. Charge reversal at R252 and E256 severely reduced AI-2 chemotaxis at higher concentrations and eliminated it at lower. A charge reversal double mutant completely lost ability to mediate AI-2 chemotaxis.

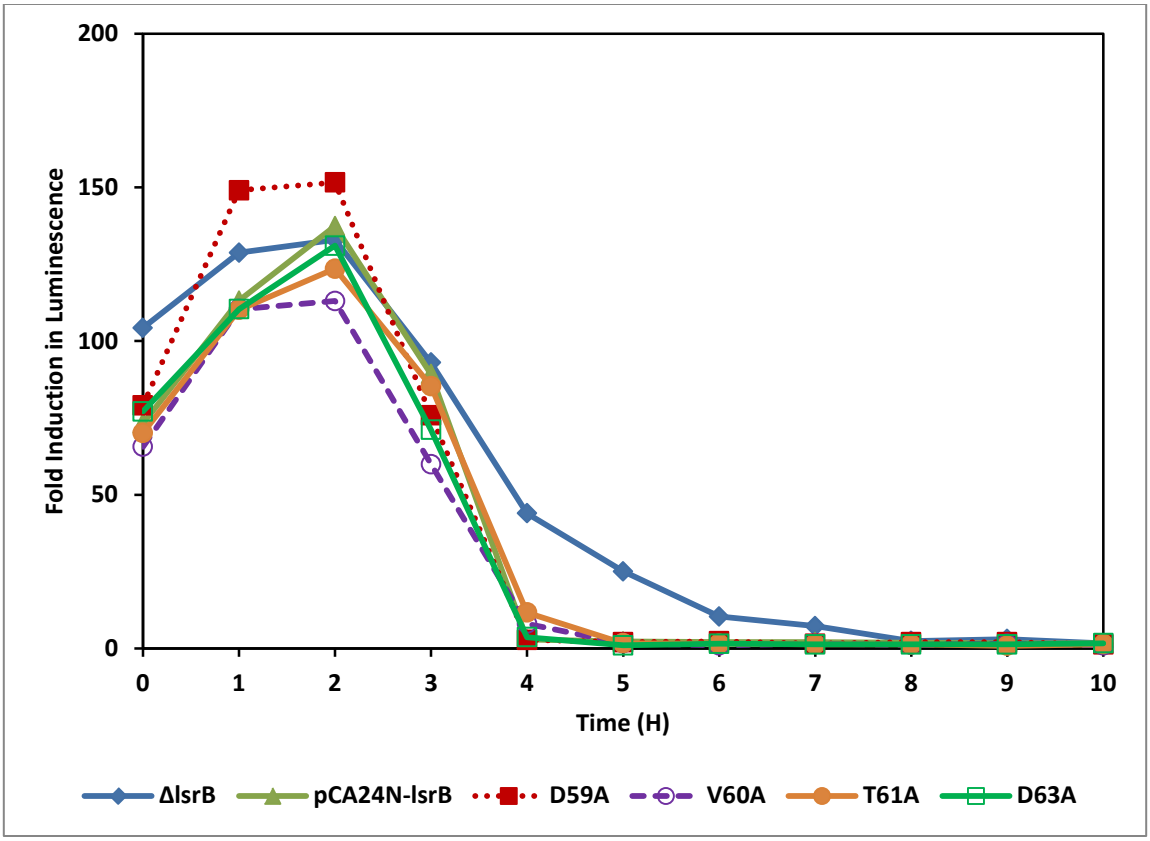

Figure 20. Ability of LsrB β-strand 2 variants to uptake AI-2. Shown is the fold induction in luminescence in *Vibrio harveyi* TL26 following addition of *E. coli* supernatant from various growth time points. Bioluminescence is measured in relative light units (RLU) and is defined as RLU of the sample / RLU of the culture medium. All LsrB β-strand 2 point mutants show the same reduction in luminescence profile as that observed with wild-type (~2 to 4 hours). As a negative control, the *ΔlsrB* mutant continued to induce bioluminescence out to nearly 8 hours.

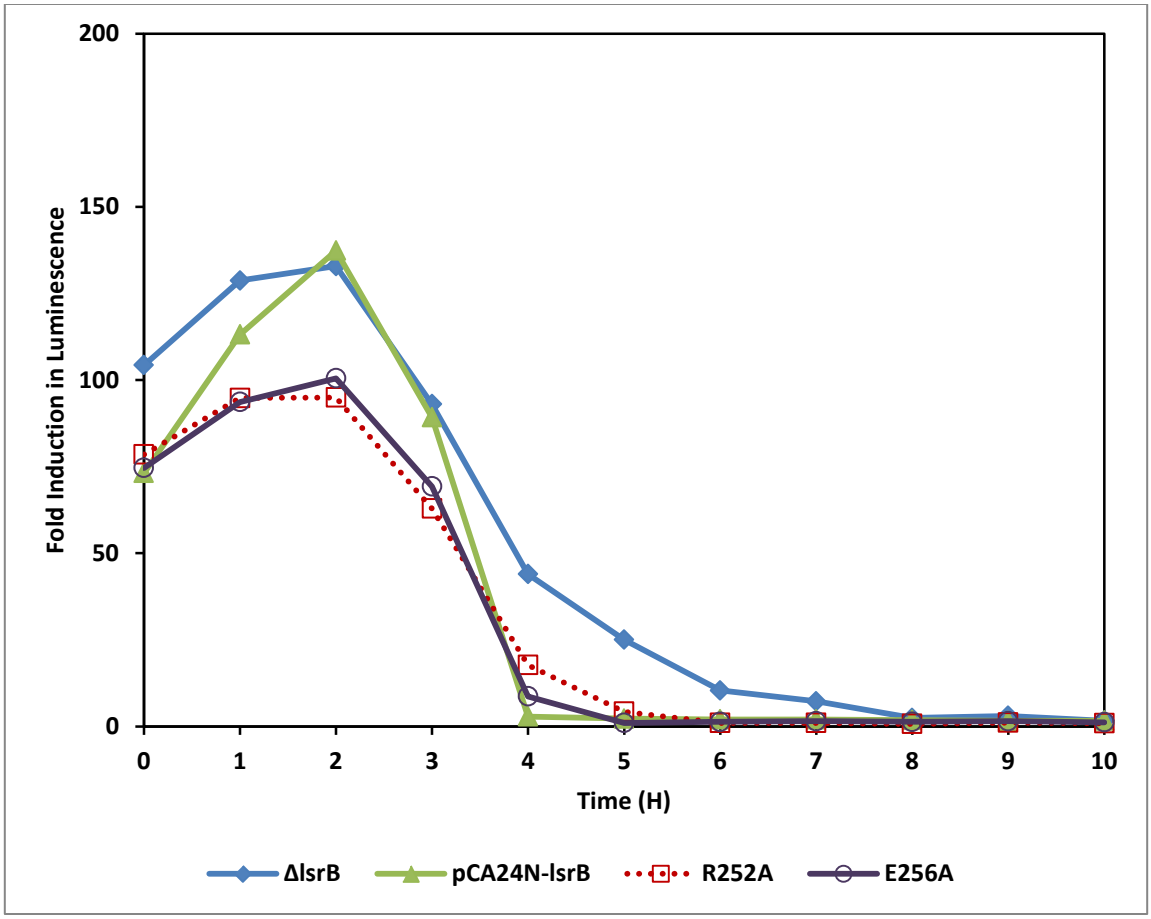

Figure 21. Ability of LsrB α-helix 8 variants to uptake AI-2. Shown is the fold induction in luminescence in *Vibrio harveyi* TL26 following addition of *E. coli* supernatant from various growth time points. Bioluminescence is measured in relative light units (RLU) and is defined as RLU of the sample / RLU of the culture medium. All LsrB α-helix 8 point mutants show the same reduction in luminescence profile as that observed with wild-type (~2 to 4 hours). As a negative control, the Δ*lsrB* mutant continued to induce bioluminescence out to nearly 8 hours.

any difference in uptake, with a delay of approximately one hour, though uptake still occurred (Figure 22).

Ability of key lsrB *variants to respond to only exogenously sensed AI-2.* To ensure mutant response was to AI-2 sensed from the outside environment, plasmids carrying key *lsrB* variants were transformed into cells deleted for the *luxS* gene. LuxS is involved in the production of AI-2 from *S*-adenosylhomocysteine, and deleting it removes the cell's capability of producing any endogenous AI-2. This serves the purpose of confirming that certain LsrB variants are not simply being overwhelmed by endogenously produced AI-2 within the cytoplasm and being sequestered away to give the negative chemotaxis result. In a Δ*luxS* background, D59A, T61A, D63A and R252A showed no AI-2 chemotaxis improvement in the capillary assay when compared to strains carrying intact *luxS*. Additionally, wild-type cells deleted for *luxS* were still able to mediate chemotaxis to AI-2 (Figure 23).

Complementation of lsrB *variants in a wild-type background.* In an attempt to determine if any of the LsrB variants deficient for AI-2 chemotaxis could be complemented by the presence of wild-type protein, I transformed these variants into wild-type CV1 cells and tested their ability to respond to AI-2 in the capillary assay. Protein levels of chromosomally-encoded and plasmid-encoded wild-type LsrB were already found to be nearly identical, so induction with IPTG was not necessary. Interestingly, the dose response of the LsrB mutant D59A was not restored to wild-type level when the wild-type LsrB protein was present (Figure 24). The V60A variant dose response became similar to wild-type, while the dose responses of the other variants tested fell somewhere

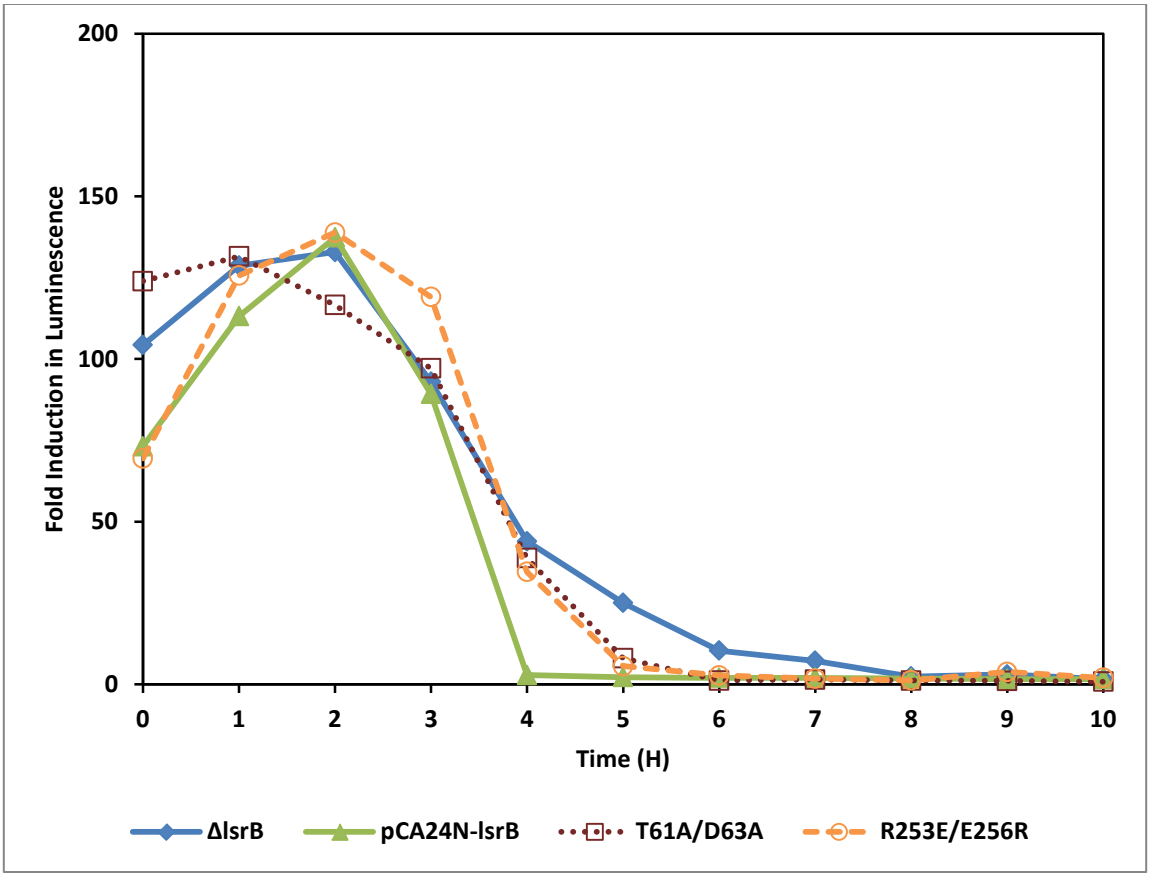

Figure 22. Ability of *E.coli* cells carrying an LsrB double mutant to uptake AI-2. Shown is the fold induction in luminescence in *Vibrio harveyi* TL26 following addition of *E. coli* supernatant from various growth time points. Bioluminescence is measured in relative light units (RLU) and is defined as RLU of the sample / RLU of the culture medium. Both the T61/D63A and R252A/E256A double mutant show a delay in quenching of bioluminescence in *V. harveyi* of approximately one hour relative to wild-type.

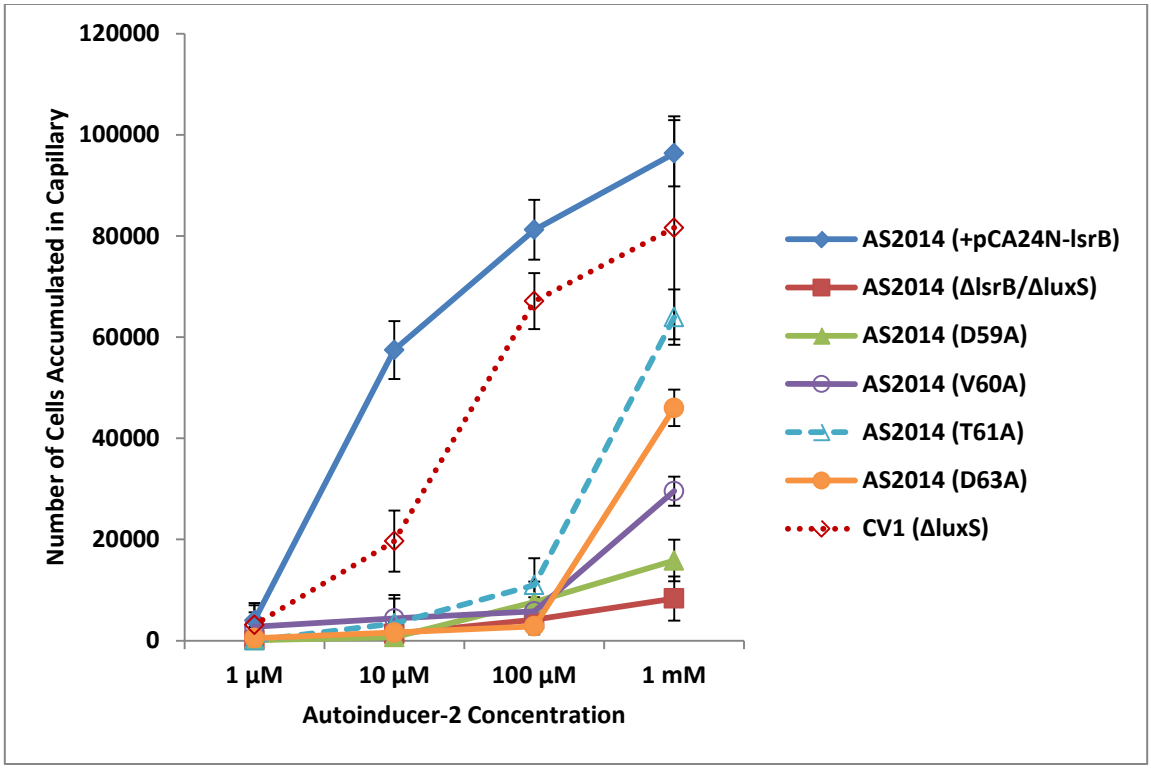

Figure 23. AI-2 chemotaxis by LsrB variants in a Δ*luxS* background. Key LsrB variants were expressed without induction from plasmid pCA24N in cells carrying a chromosomal deletion for the *luxS* gene (strain AS2014). Capillary assays were performed at 30°C for 45 minutes. Each trial represents three biological replicates carried out in triplicate.

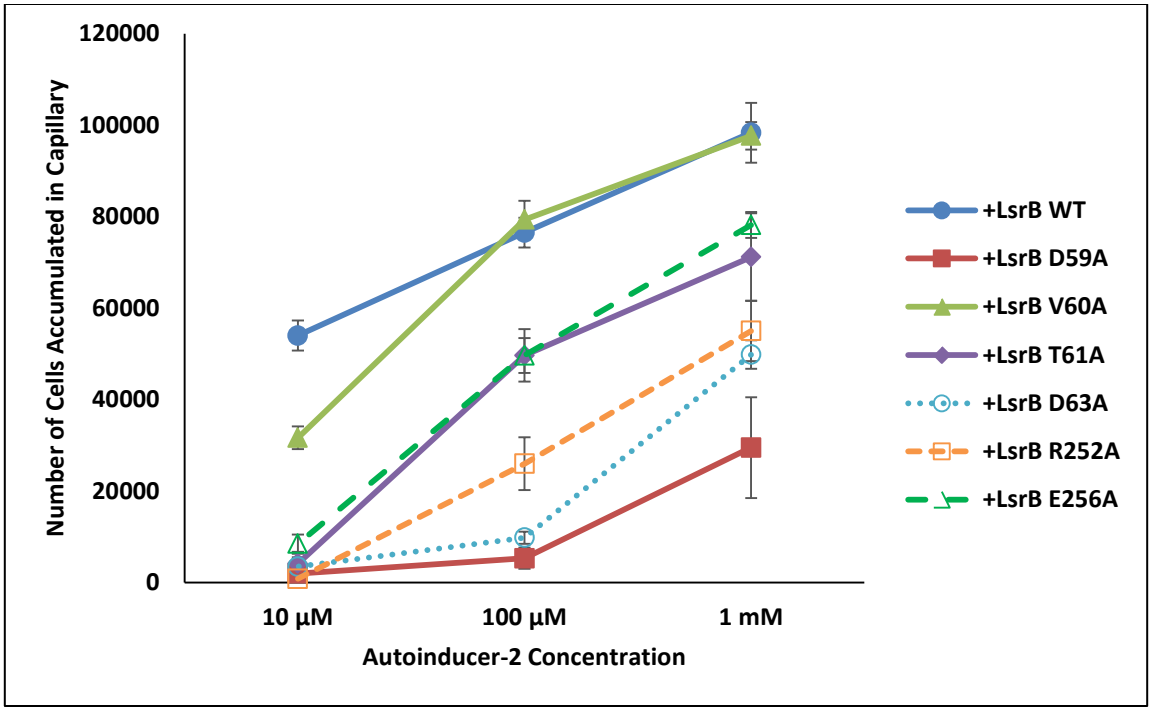

Figure 24. AI-2 chemotaxis by LsrB variants in a CV1 background. Key LsrB variants were expressed without induction from plasmid pCA24N in cells carrying a chromosomal wild-type copy of LsrB. Response to AI-2 gradients was rescued to some degree for most variants, with V60A being rescued to nearly wild-type levels. Capillary assays were performed at 30°C for 45 minutes. Each trial represents three biological replicates carried out in triplicate.

in between. These results suggest the D59A mutant may exhibit a dominant-negative phenotype, a condition not unlike that described in previous studies with MBP and Tar (*122*).

Ability of pBAD-LsrB variants to mediate response to AI-2 gradients. LsrB variants expressed under control of the P_{BAD} promoter were exposed to serine and AI-2 gradients in the capillary assay. The accumulation of *lsrB* variant cells above background levels was within 97% of the response measured for those same over-expressed mutants carrying the C-terminal extension in pCA24N-*lsrB* (Figure 25). There was no significant variation in AI-2 response in the presence or absence of the C-terminal extension.

Discussion

The docking of ligand-bound maltose binding protein (MBP) to Tar has been investigated extensively (*105, 122, 125-127*). The resulting docking model has provided an excellent point of reference for our own proposed docking model of LsrB with Tsr. Because of the large degree of sequence and structural similarity between Tsr and Tar, orienting a binding protein for potential interaction with Tsr can be patterned somewhat after the MBP-Tar model. Using this published model a proposed docking model for the interaction of ligand-bound LsrB and the periplasmic domain of Tsr was generated (Figure 10). Residues of interest were highlighted for genetic analysis. Figure 26 illustrates the location of the amino acid residues of interest in both the N-terminal and C-terminal regions of the ligand-bound conformation of LsrB. Figure 11 indicates residues of particular interest in the shoulder regions of the Tsr homodimer.

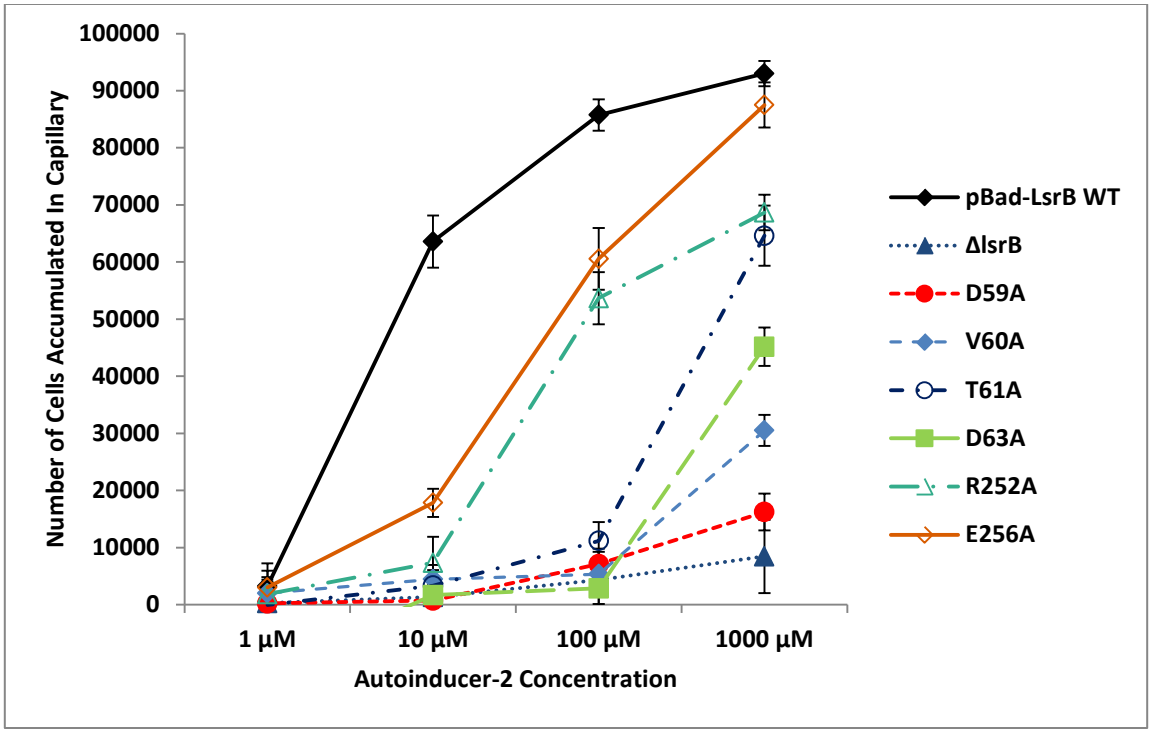

Figure 25. Response to AI-2 by pBAD-*lsrB* variants. Key LsrB variants were cloned into pBAD. Mutants were induced with 0.2% arabinose for full induction. Each key alanine substitution showed the same chemotaxis to AI-2 as it did when expressed from pCA24N. Capillary assays were performed at 30°C for 45 minutes. Each trial represents three biological replicates carried out in triplicate.

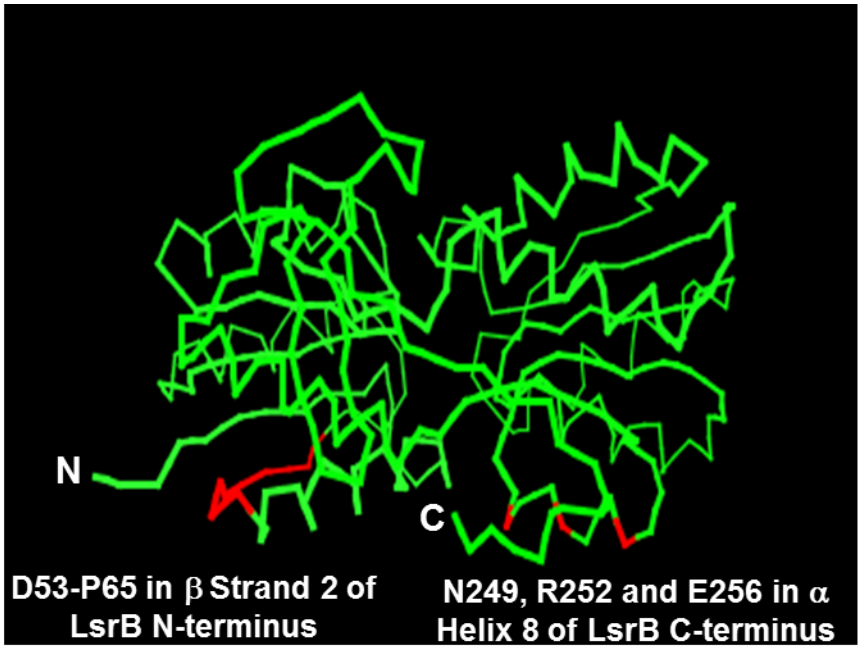

Figure 26. Structure of *E. coli* LsrB with residues of interest. This structure of the LsrB binding protein is adapted from the published LsrB of *Salmonella typhimurium* (*95*). The β-strand 2 residues D53-P65 are highlighted in red in the N-terminus, while residues N249, R252 and E256 of α-helix 8 are highlighted in red in the C-terminus of the protein. Each of these residues was chosen due to its proximity and likelihood of binding calculated from the generated Tsr-LsrB docking model.

Alanine scanning mutagenesis of both proteins revealed particular amino acid residues that are critical for AI-2 chemotaxis to occur. In Tsr the positively charged lysine at position 147 and negatively charged glutamate at position 150 must be present for *E. coli* cells to perform chemotaxis to AI-2. Mutating these residues to alanine greatly depresses chemotaxis to AI-2, but has little effect on response to serine, leading us to conclude these alterations likely do not change the overall structure or function of the Tsr protein, only its ability to interact with LsrB and signal. The fact that these are charged residues led us to surmise that electrostatic forces were likely at work during the interaction with LsrB. I tested this theory by introducing charge reversals at these positions. The result was a complete elimination of AI-2 response in cells carrying the K147E mutation, and a further attenuation of response in cells with the E150K mutation. Reversing the charge at 147 likely resulted in electrostatic repulsion between the two proteins, causing the failure of the cells to respond to AI-2. Because Tsr is a homodi- mer, lysine-147 is present in both shoulder regions and likely serves as an anchoring point for the interaction with LsrB during chemotaxis.

In LsrB the critical amino acids identified during the alanine-scanning mutagenesis were a mix of charged and non-polar residues. Asp-59, Val-60, Thr-61, Asp-63, Arg-252 and Glu-256 each seem to play a role in supporting chemotaxis to AI-2. Changing each of these to Ala negatively affected AI-2 response to some degree, with D59A showing the greatest deficiency. The T61/D63 and R252A/E256 double mutants were removed from consideration due to the delay they showed in transporting AI-2 into the cell. This delay compared to wild-type is a likely indicator that these proteins either

couldn't bind AI-2 well, or couldn't interact with the LsrACD transport channel to import AI-2. Based on the location of the negatively charged aspartate residues (D59 and D63) in β-strand 2, they are likely candidates to electrostatically interact with the positively charged Lys-147 of Tsr on one homodimer shoulder. In α-helix 8 is where the negatively charged Glu-256 possibly interacts with the other Lys-147 of the opposite shoulder in Tsr. Due to their proximity, mutating the Val-60 and Thr-61 residues in β-strand 2 of LsrB may affect the positioning of the Asp-59 and/or Asp-63 residues needed for interaction with Tsr. Perhaps the alteration of these LsrB residues disrupts the tight interaction with Tsr, resulting in an inability to propagate a signal through transmembrane helix-2 of the chemoreceptor. Additionally, the positively charged Arg-256 in α-helix 8 may stabilize the LsrB-Tsr docking by interacting with the aforementioned Glu-150 of Tsr. These results lend credibility to our proposed docking model and elucidate the nature of the protein-protein interaction taking place during chemotaxis to AI-2.

Of obvious note is the wide range of expression levels detected in the LsrB mutants expressed from pCA24N (data not shown). While these results are curious, they likely do not affect AI-2 chemotaxis. The fact that each of the LsrB mutants mentioned here maintains its ability to import AI-2 into the cell, according to the *Vibrio harveyi* bioluminescence assay, indicates the reduction in AI-2 chemotaxis is not simply the result of altering the export and subsequent periplasmic concentration of LsrB with the C-terminal extension. In other words, they perform their native function at wild-type levels, thus the mutations affect only chemotaxis. This is further supported by the fact that

LsrB variants expressed from the pBAD plasmid respond to AI-2 at identical levels of those from the pCA24N plasmid.

While the protein expression levels are curious, it is certainly possible that AI-2 chemotaxis is not directly correlated to LsrB expression in *E. coli*. Further investigation into this issue will be discussed in Chapter V. Overall, it appears that docking of LsrB to Tsr and signaling during AI-2 chemotaxis relies primarily on tight interaction with the N-terminal domain, specifically β-strand 2 of LsrB. The C-terminal domain, specifically α-helix 8, likely serves to further stabilize the interaction and facilitate signaling.

Furthermore, the ability of the cells to produce their own AI-2 through the activity of LuxS doesn't appear to affect their response to extracellular AI-2. Key LsrB mutants expressed in a LuxS deletion strain showed no variation in AI-2 response compared to strains with intact LuxS. Production of AI-2 in the cytoplasm and its subsequent export apparently does not inhibit those cells from recognizing and responding to environmental AI-2. This may be due to the fact that by the time cells are producing enough AI-2 themselves, the chemotaxis response to environmental AI-2 has already occurred.

Lastly, when attempts to complement mutant LsrB proteins with copies of wild-type LsrB were made, the D59A and D63A variants failed to complement. The reason for this is unclear, though perhaps they represent dominant negative phenotypes, where the mutant proteins are able to dock with Tsr but are unable to elicit signal propagation through the chemoreceptor. If this is true, the interaction is still tight enough to block wild-type LsrB from complementing the mutation. The investigation of these mutants will be further discussed in Chapter V.

CHAPTER III

CORRELATING LSRB EXPRESSION LEVELS WITH AI-2 CHEMOTAXIS

Introduction

The expression of the periplasmic LsrB protein is regulated within the *lsr* operon of *E. coli*. When population density is low, and a quorum sensing threshold of AI-2 is not achieved in the environment, the *lsr* operon is repressed by the LsrR protein. Following sufficient addition of AI-2 to the local environment, this LsrR repression is relieved by interaction with phosphorylated AI-2 (AI-2-P). Thus, the operon produces LsrB, which in turn binds periplasmic AI-2 and transports it into the cytoplasm via the LsrACD transporter, resulting in the presence of more AI-2-P to relieve repression of the operon. It is not until the last components of the operon (LsrFG) are made in sufficient quantities that AI-2-P is deconstructed and recycled, returning the operon to a repressed state (in concert with waning levels of environmental AI-2 presumably).

As I have shown in the previous chapter, wild-type levels of chromosomal LsrB are sufficient to elicit a chemotaxis response to the *R*-THMF form of AI-2 in *E. coli* (Figure 12). I wanted to determine (a) how much LsrB was produced in cells at various growth phases and its correlation to AI-2 chemotaxis, and (b) what affect stepwise induction of LsrB expression from a plasmid had on the ability of the cells to perform chemotaxis to AI-2. For the first question, cells were grown to increasing optical densities before protein levels and chemotaxis response were measured. Log phase growth in *E. coli* is considered to begin when cells reach an $O.D._{600}$ just below 0.3; it progresses to

mid-logarithmic growth near 0.5; and enters late logarithmic growth between 0.7 and 0.9. During early log growth, cells would likely produce little AI-2, as the components of the *lsr* operon are not being highly expressed. During mid-logarithmic growth, cells would begin expressing more of the LsrB binding proteins in order to transport AI-2 into the cells, leading to more expression of the *lsr* operon. Once they reach later log growth, cells should have high amounts of AI-2 present.

In the second scenario, an induction series was performed on plasmid-borne LsrB and response to AI-2 was measured in the capillary assay. I found that increasing LsrB within the cells correlated negatively with AI-2 chemotaxis, though there was little effect on serine chemotaxis, and optimal response to AI-2 as a chemoattractant occurred during mid-log phase growth.

Furthermore, I hypothesized that LsrB expression would change when different components of the *lsr* operon were independently deleted. For instance, I expected more LsrB to be present when LsrR, the operon repressor, was deleted. Conversely, I surmised that deleting components of the ABC transporter LsrACD or the AI-2 degradation pathway LsrFG would have little to no effect on expression of LsrB. I also tested the effect of deleting LuxS and TqsA on LsrB expression. Likewise, I investigated whether deletions of these different genes affected chemotaxis to AI-2, and if these effects could be correlated to LsrB expression in these mutants. Lastly, I tested effect on AI-2 chemotaxis in cells at various growth phases when the *luxS* gene was deleted. Deletion of the LuxS enzyme ensures the cells are not producing endogenous AI-2, allowing us to ex-

amine whether accumulation of endogenous AI-2 at earlier and later phases of growth influenced response to exogenous AI-2 added to the medium.

I found there were few variations in LsrB expression in the individual deletion mutants. I also found there was little to no difference in the AI-2 dose response curves of the individual deletion mutants, whether the component deleted was involved in synthesis of AI-2, export of AI-2, or even import of AI-2. Additionally, I saw a decrease in AI-2 response at later growth phases compared to mid-log phase growth, and observed strains carrying the *luxS* deletion varied little in chemotaxis response from their counterparts able to produce their own AI-2. Overall, expression of LsrB did not seem to correlate to AI-2 chemotaxis.

Materials and methods

Bacterial strains, plasmids and media. Wild-type strain CV1 was used for the growth phase tests. Deletion mutant strains were derived from CV1 using phage transduction to disrupt target genes with a kanamycin resistance cassette before its removal as previously described (*43*). Cassette was then removed by transforming cells with the pCP20 plasmid encoding an FLP recombinase (*117*). The pCP20 plasmid was removed through a temperature-sensitive growth restriction and PCR was used to verify a clean gene deletion with removal of the kanamycin resistance cassette. Table 2 lists the target genes deleted for use in this study. IPTG-inducible plasmid pCA24N was employed to produce stepwise increases in LsrB expression in strain MJ101. All strains were grown in tryptone broth media (10 g/L tryptone; 8 g/L NaCl) supplemented with antibiotic

where appropriate. IPTG was added to inducible strains when optical density reached 0.300 at wavelength 600 nm.

Measuring chemotaxis to AI-2 and serine at different growth phases. Strain CV1 was grown overnight in TB supplemented with streptomycin (50 µg/mL), then back-diluted into four separate flasks to a turbidity of approximately 0.05 at $O.D._{600}$ in 25 mL tryptone broth without antibiotic. Cells were then grown at 30°C with shaking to $O.D^{600}$ = 0.3, 0.5, 0.7 and 0.9 respectively. All densities were either concentrated or diluted to $O.D_{600}$ = 0.5 with chemotaxis buffer for uniform density upon addition to the cell reservoirs. Motility was confirmed through microscopy. Capillary assays (*115*) were used to quantify response to AI-2 and *L*-serine at the four different growth phases. Centrifugation at 600 *x g* for 10 minutes separated the cell pellet from the growth media. After removal of the supernatant, cells were gently resuspended in an equal volume of chemotaxis buffer and given fifteen minutes of recovery time in a 30°C rotor. Motility was again confirmed through microscopy before use in the capillary assay. Cells were exposed to gradients of 1 mM, 100 µM, 10 µM and 1 µM AI-2 in chemotaxis buffer.

Measuring chemotaxis to attractants in the deletion strains. Capillary assays (*115*) were chosen to quantify the chemotaxis responses to AI-2. Overnight cultures of cells deleted for various AI-2 pathway genes were grown at 30°C in TB supplemented with streptomycin (50 µg/mL). Cultures were back-diluted to a turbidity of ~0.05 at $O.D._{600}$ in 25 mL TB without antibiotic and grown to mid-logarithmic phase at an $O.D._{600}$ = ~0.5. Cells were then centrifuged at 600 *x g* for 10 minutes to separate the soft pellet from the growth media. The supernatant was removed and the pellet then gently

Table 2. Bacterial strains and target genes for deletion studies

Strain	Target Gene	Function
Escherichia coli		
CV1[a]	*lsrA*	Kinase for LsrACD transporter
	lsrB	Periplasmic binding protein for AI-2
	lsrC	ABC transporter membrane channel protein
	lsrD	ABC transporter membrane channel protein
	lsrF	AI-2 degradation
	lsrG	AI-2 degradation
	lsrK	Kinase for phosphorylating AI-2
	lsrR	*lsr* operon repressor
	luxS	Synthesis of AI-2 precursor DPD
	tqsA	Export of AI-2 from the cell

[a]Kanamycin resistance cassettes were transduced to disrupt individual genes and then removed by FLP recombinase via temperature sensitive plasmid pCP20 (*117*). Deletion of the gene of interest and removal of the kanamycin cassette were confirmed through PCR.

resuspended in chemotaxis buffer as described previously. The cells were given fifteen minutes of recovery time in a 30°C rotor set to low speed before use. Motility of washed cells was confirmed through phase contrast microscopy before their addition to the cell reservoirs for exposure to attractant-laden capillaries.

Immunoblots for LsrB expression. Whole cell protein preps were performed. Overnight cultures were diluted into 500 mL TB and grown at 30°C with shaking to $O.D._{600}$ = 0.5. Cultures were centrifuged and the pellet was frozen at -80°C before being resuspended in 25 mL lysis buffer (5 mM DTT, 50 mM Tris (pH 8.0), 300 mM NaCl, 1 mM PMSF). Resuspended pellets were then sonicated for 8 minutes (15 seconds ON / 45 seconds OFF, 37% amplitude). Centrifugation at ultra-high speed followed before the supernatant was collected in lysis buffer. This was then concentrated to 1 mL and quantified using the BCA assay. Polyacrylamide gel electrophoresis was used with purified LsrB antibody to compare LsrB levels of growth phase variants and mutants to wild-type LsrB expressed from either the chromosome or the pCA24N plasmid.

IPTG induction series. Strain CV1 with the *lsrB* deletion, carrying the pCA24N-*lsrB* plasmid, was grown overnight in TB supplemented with chloramphenicol (35 μg/mL) to select for the plasmid. The overnight was back-diluted into 25 mL of TB and grown at 30°C with shaking (250 rpm) to $O.D._{600}$ = 0.3. At this point, varying concentrations of IPTG (purchased from Fisher Scientific) were added to the culture to induce *lsrB* expression. Concentrations of IPTG used in the series included 0 μM, 1 μM, 10 μM, 100 μM and 1000 μM. Cells were then returned to growth at 30°C until reaching an

$O.D._{600}$ of 0.5. The cultures were then prepared for use in the capillary assay as described previously, and capillary assays were performed to measure chemotaxis ability to AI-2. Western blots were carried out as previously described to measure LsrB expression with regard to increasing concentrations of IPTG.

Results

Growth phase effects on AI-2 chemotaxis in wild-type cells. Growth of CV1 cells to varying phases showed obvious effects on AI-2 chemotaxis. All growth phases ($O.D._{600}$ = 0.3, 0.5, 0.7 and 0.9) were tested at an $O.D._{600}$ = 0.5 for uniform testing in the capillary assay. Because there is some evidence that *E.coli* cells begin to accumulate endogenously produced AI-2 in early log-phase growth (Sneha Jani, unpublished), I tested from this point to late log phase growth. At $O.D._{600}$ = 0.3 the dose response never saw an accumulation of more than 21,000 colony-forming units (CFUs) at any of the tested concentrations of AI-2. This represented only 22% the response of cells at that same concentration during mid log phase growth, with the accumulation even lower at other points along the dose response curve. Background accumulation of CFUs was also nearly 3 times lower at this growth phase compared to mid log, despite the densities being identical at the time of the assay. At $O.D._{600}$ = 0.7, peak accumulation reached 33,000 CFUs (1 mM AI-2), approximately 35% of the response at the same concentration in mid log phase. At $O.D._{600}$ = 0.9 the maximum response was observed at 1 mM AI-2 and numbered 17,500 CFUs. This was calculated to be 18% of the CFUs accumulated at mid log phase (Figure 27).

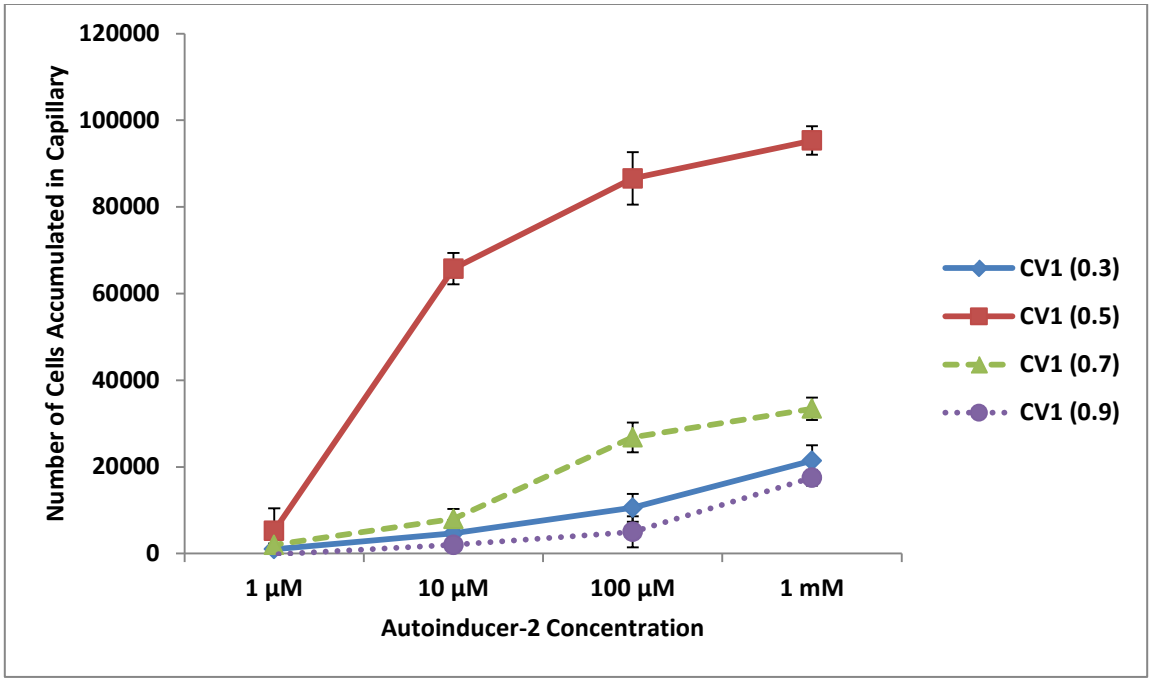

Figure 27. Response of log phase growth variants to AI-2 gradients. Cells were grown to appropriate optical density, washed, and then resuspended in chemotaxis buffer to a final $O.D._{600}$ = 0.500. Capillary assays were incubated at 30°C for 45 minutes, and data points represent three biological replicates with each concentration done in triplicate.

Growth phase effects on L-*serine chemotaxis in wild-type cells.* Effects on chemotaxis to *L*-serine across the various growth phases tested were less extreme. However, at $O.D._{600}$ = 0.3 the serine dose response curve was noticeably depressed compared to mid log phase (Figure 28). Peak accumulation to serine at mid log phase occurred at 1 mM (97,000 CFUs), but showed just 71,000 CFUs in cells grown to $O.D._{600}$ = 0.3, 73% of the accumulation at 0.5. The dose response curves for the remaining densities (0.7 and 0.9) were nearly identical to the mid log phase dose response curve (Figure 28).

Growth phase effects on AI-2 chemotaxis in ΔluxS *cells.* When exposed to exogenous AI-2 in a Δ*luxS* background, early log phase cells ($O.D._{600}$ = 0.3) and late log phase cells ($O.D._{600}$ = 0.7 and 0.9) all showed peak accumulation at 1 mM, though none garnered much more than 30,000 CFUs, approximately one-third the response by mid log phase cells at the same concentration (Figure 29). Response by these same growth phase variants to *L*-serine (Figure 30) generated a dose response curve nearly identical to that previously shown for wild-type cells.

*IPTG induction of pCA24N-*lsrB *and its effect on LsrB expression and AI-2 chemotaxis*. CV1 (Δ*lsrB*) was transformed with pCA24N-*lsrB* and induced with varying concentrations of IPTG. Western blots indicated that the amount of LsrB produced varied with increasing concentration of IPTG added during early log phase cell growth (Figure 31). At 1 and 10 μM IPTG induction, the amount of LsrB was actually less than uninduced. The increases in LsrB levels were significant at 100 μM IPTG, producing nearly 3 times that of uninduced. At 1 mM IPTG, LsrB expression was approximately 6 times that of un-induced wild-type.

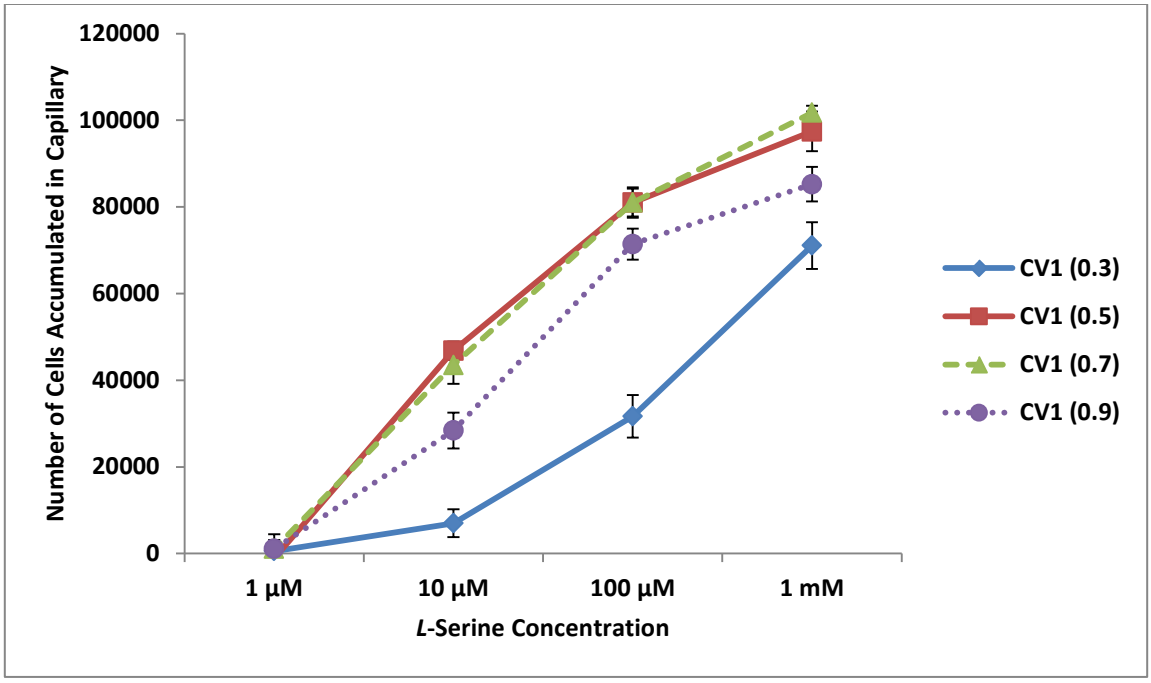

Figure 28. Response of log phase growth variants to serine gradients. Cells were grown to appropriate optical density, washed, then resuspended in chemotaxis buffer to a final $O.D._{600}$ = 0.500. Peak accumulation occurred at 1 mM serine concentration. At an earlier stage of growth, *E.coli* CV1 cells responded at 73 % of the response at the same serine concentration along the dose response curve at mid log phase (0.500). Later log stages of growth were at or near mid log phase dose response. Capillary assays were incubated at 30°C for 45 minutes, and data points represent three biological replicates with each concentration done in triplicate.

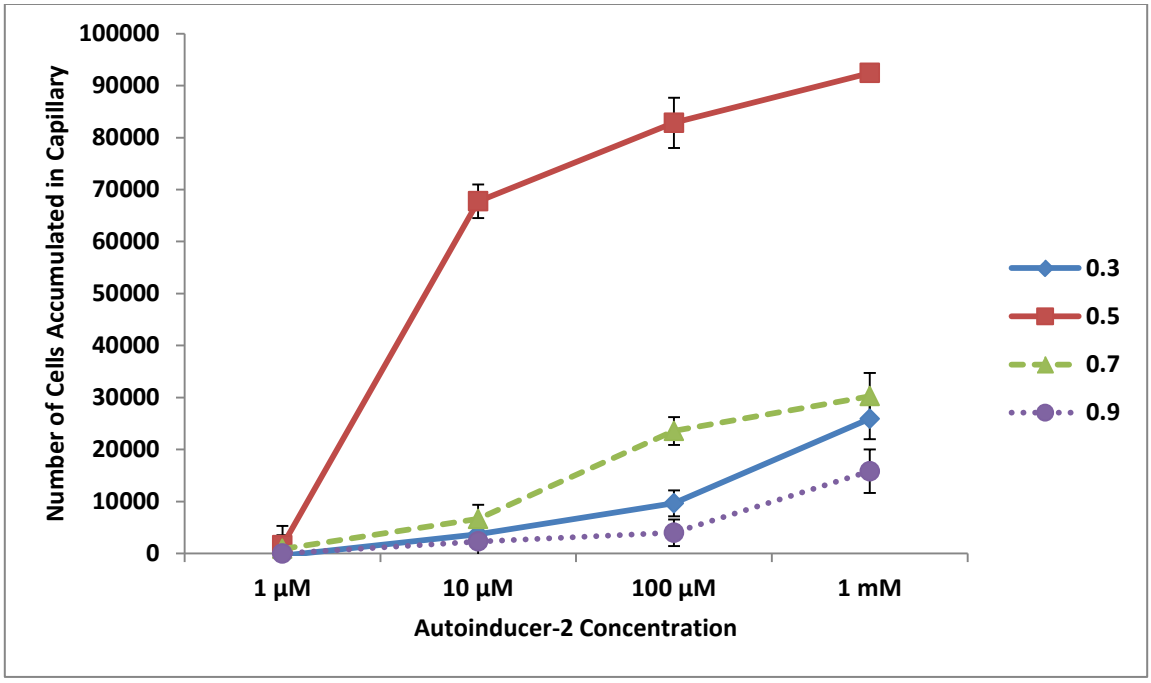

Figure 29. Response of Δ*luxS* log phase growth variants to AI-2 gradients. Cells were grown to appropriate optical density, washed, then resuspended in chemotaxis buffer to a final $O.D._{600}$ = 0.500. Peak accumulation occurred at 1 mM AI-2 concentration. Capillary assays were incubated at 30°C for 45 minutes, and data points represent three biological replicates with each concentration done in triplicate.

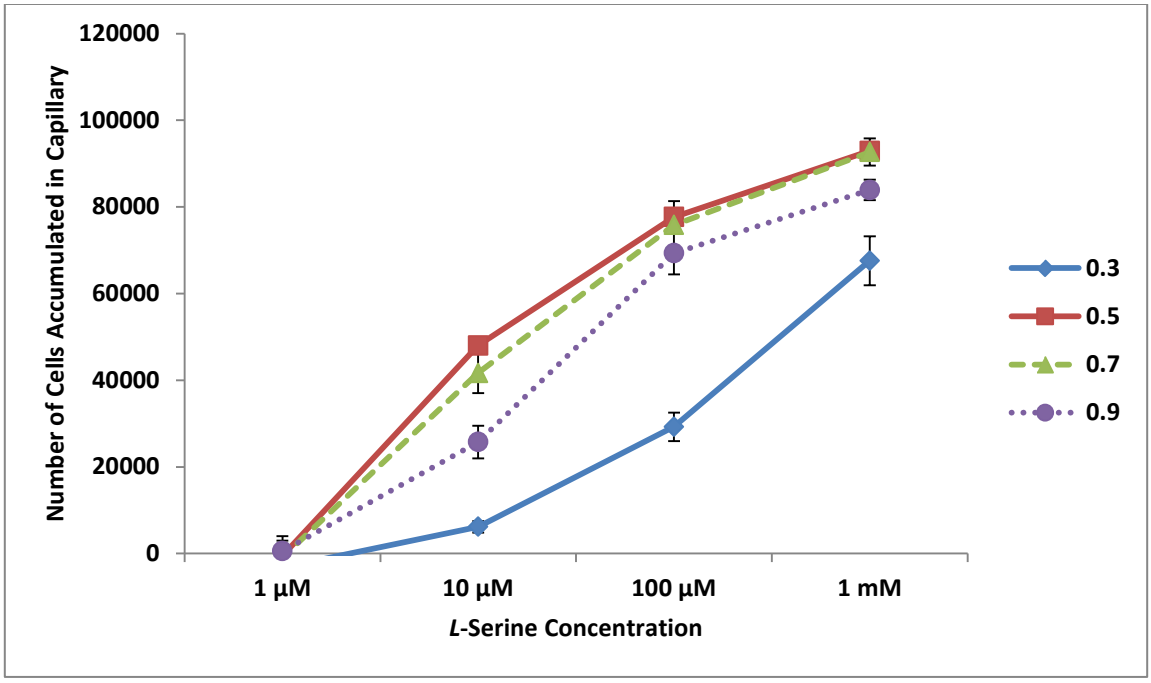

Figure 30. Response of Δ*luxS* log phase growth variants to serine gradients. Cells were grown to appropriate optical density, washed, then resuspended in chemotaxis buffer to a final $O.D._{600}$ = 0.500. Peak accumulation occurred at 1 mM serine concentration. At an earlier stage of growth, cells responded at 73 % of the response at the same serine concentration along the dose response curve at mid log phase (0.500). Later log stages of growth were at or near mid log phase dose response. Capillary assays were incubated at 30°C for 45 minutes, and data points represent three biological replicates with each concentration done in triplicate.

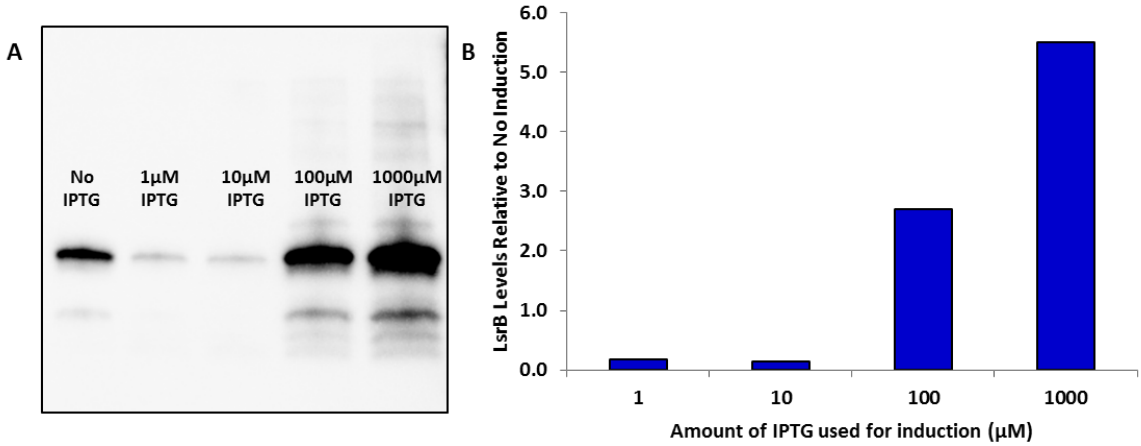

Figure 31. Western blots for IPTG induction of LsrB expression. Plasmid pCA24N was used to express LsrB with varying amounts of IPTG induction during growth. Induction ranged from 0 µM to 1000 µM IPTG, and whole cell extracts were prepared. Samples were detected with anti-LsrB antibody and LsrB levels were calculated based on chemiluminescence intensity. (a) Western blot image shows little LsrB production at 1 and 10 µM IPTG induction, while bands are significantly darker for 100 and 1000 µM IPTG induction compared to uninduced samples from the same plasmid. (b) LsrB levels relative to undinduced samples were estimated. At 1 and 10 µM IPTG induction, LsrB levels are less than 50 % of uninduced amount. At 100 µM IPTG induction, there is approximately 3 time as much LsrB produced compared to uninduced. At 1000 µM IPTG induction, there is approximately 6 times as much LsrB produced compared to uninduced sample.

The chemotaxis assays for these inductions exhibited a negative correlation between amount of LsrB induced and ability of the cells to respond to AI-2 (Figure 32). The dose response curves were similar between the un-induced and 1 μM induction strains, though they shifted significantly beyond 1 μM induction. Without induction, cells carrying plasmid-borne LsrB accumulated approximately 96,000 colony-forming units (CFUs) compared to approximately 95,000 CFUs of the 1μM induction strain at 1 mM AI-2. They decreased similarly along the same dose response curve with decreasing AI-2 concentration. The difference in dose response at 10 μM IPTG was significantly lower, with no single accumulation garnering more than 78% of the un-induced value. The results were even more drastic at 100 μM and 1 mM IPTG induction, with no single response point for either garnering more than 33% and 4%, respectively, of un-induced response. As a control, 100 mM *L*-serine was used in the capillary assay as well. All of the induction strains accumulated CFUs of a similar number as the un-induced strain.

Effect of single gene knockouts on LsrB expression. The LsrB gene product is the fourth gene in the *lsr* operon to be transcribed during expression, preceded by the components of the ABC transporter – LsrACD. The expression of LsrB in the absence of both upstream and downstream flanking genes in the *lsr* operon was investigated. Figure 33 shows the relative LsrB protein levels in the various deletion mutant backgrounds. The amount of LsrB produced was noticeably higher than wild-type in the Δ*lsrR* knockout and slightly lower in the Δ*lsrK* and Δ*luxS* knockouts.

Effect of single gene knockouts on AI-2 chemotaxis. In addition to investigating

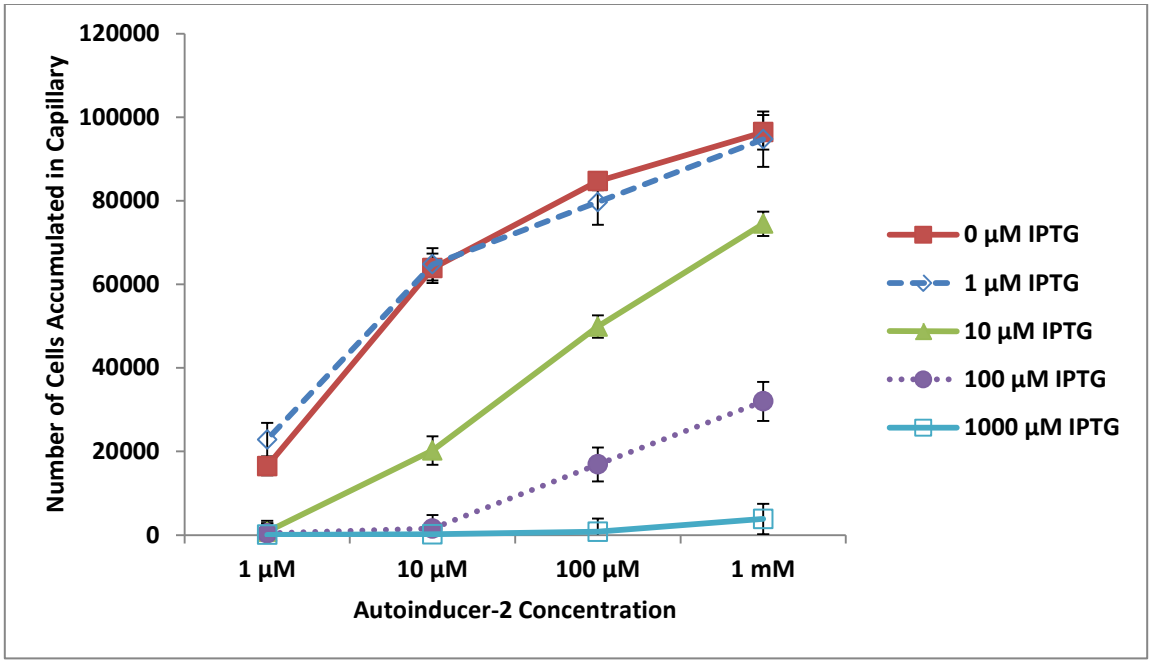

Figure 32. IPTG induction series response to AI-2. LsrB was expressed from pCA24N using various amounts of IPTG (0 to 1000 µM) during early log phase growth, then exposed to AI-2 gradients after growth to mid log phase. Serine response was not altered to any significant degree by overexpression of LsrB in this manner.

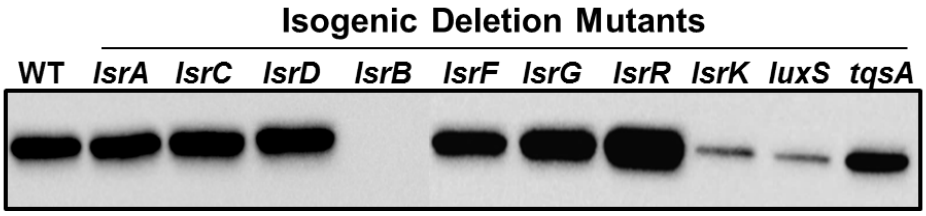

Figure 33. Expression of LsrB in select deletion mutants. Strain CV1 was deleted for each of the components of the *lsr* operon, as well as genes involving AI-2 synthesis (*luxS*) and export (*tqsA*). Western blots were performed on whole cell extracts of deletion mutants using anti-LsrB antibody. Most knockouts showed wild-type levels of LsrB. Knockouts for *lsrK* and *luxS* showed reduced expression of LsrB relative to wild-type. Knockouts for *lsrG* and *lsrR* showed increased expression. Deleting the repressor LsrR boosted LsrB expression the most of any of the deletion mutants.

how the LsrB levels within the cell are affected when flanking *lsr* operon genes are deleted, I also tested the ability of these knockout mutants to perform AI-2 chemotaxis in the capillary assay. The wild-type strain produced its maximum response at 1 mM AI-2, with 95,000 CFUs, then decreased to 86,000 CFUs at 100 μM, 66,000 CFUs at 10 μM and 6,000 at 1 μM. Most of the deletion mutants in the primary transcription unit of the *lsr* operon (*lsrACDBFG*) produced similar dose response curves to AI-2 compared to wild-type *E.coli* (Figures 34 and 35). Only the Δ*lsrD* strain showed a higher response at each point along the dose response curve compared to wild-type, yet even that increase was minimal at no more than 10%. The other *lsr operon* transcription unit knockouts, consisting of Δ*lsrR* and Δ*lsrK*, along with both Δ*luxS* and Δ*tqsA* were observed for AI-2 chemotaxis. Only the Δ*lsrK* mutant deviated from wild-type along the dose response curve (Figure 35). Though similar to wild-type with 92,000 CFUs at 1 mM AI-2, it dropped to approximately 84% of wild-type at 100 μM AI-2 and only 71% at 10 μM AI-2 before bottoming out at 1 μM AI-2. The Δ*lsrR* mutant actually showed slightly higher dose response than wild-type, though not significant at any point along the curve.

Discussion

The expression of LsrB is regulated by the *lsr* operon and the presence of AI-2. When present at sufficient concentration in the periplasm, AI-2 is bound to LsrB which aids in importing AI-2 into the cytoplasm via the membrane transporter comprised of LsrA, LsrC and LsrD. Once internalized, AI-2 is phosphorylated by the kinase LsrK. It then binds to the *lsr* operon repressor LsrR, relieving repression of *lsrACDBFG*. LsrF

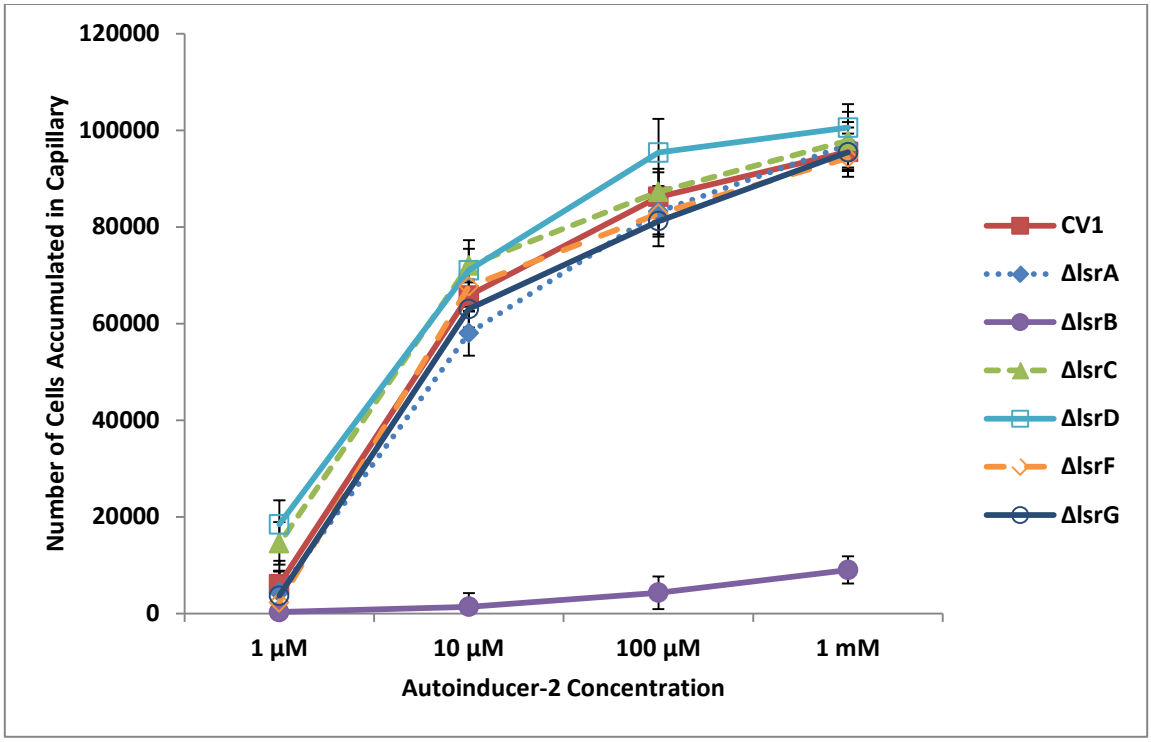

Figure 34. Response to AI-2 by *lsr* operon knockouts. Components of the *lsrACDBFG* operon were deleted individually in CV1, then tested for ability to respond to AI-2 gradients. All knockouts were able to perform chemotaxis at wild-type levels to AI-2, the exception being the *lsrB* deletion. Capillary assays were performed at 30°C for 45 minutes. Each trial represents three biological replicates carried out in triplicate.

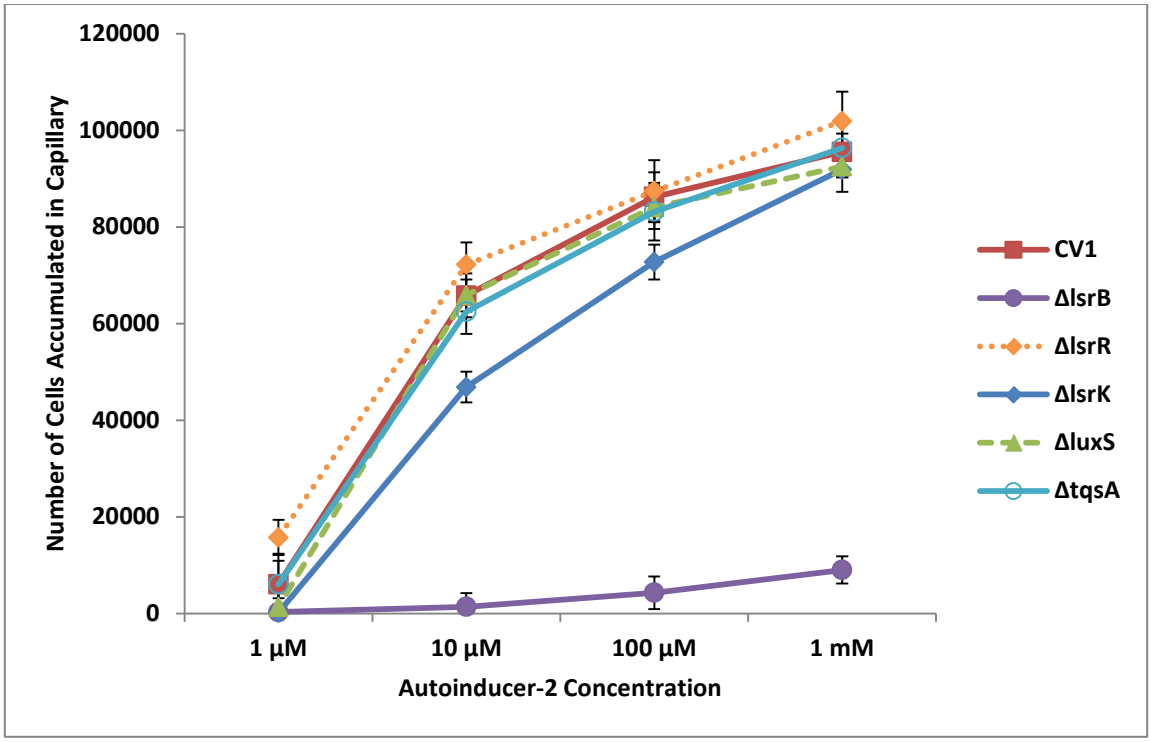

Figure 35. Response to AI-2 by *lsr*-associated knockouts. Regulatory genes *lsrK* and *lsrR*, as well as AI-2 synthesis protein LuxS and AI-2 exporter TqsA were deleted individually in CV1, then tested for ability to respond to AI-2 gradients. Capillary assays were performed at 30°C for 45 minutes. Each trial represents three biological replicates carried out in triplicate.

and LsrG are involved in breaking down phosphorylated AI-2 so it doesn't accumulate to high levels in the cytoplasm. Because of the feedback loop created by the presence of AI-2, altering any one of these components should have an effect on the levels of LsrB in the cell, and likewise the ability of the cells to respond to AI-2 gradients via chemotaxis.

Our approach to investigate the correlation between abundance of LsrB and chemotaxis response was three-fold. First, I checked to see if cells naturally produce more LsrB by growing them to later log phase. Our western blots for protein levels confirmed expression of LsrB increases with growth phase, with approximately 300 copies per cell present during mid logarithmic growth (S. Jani and M. Manson, unpublished), so I checked the chemotaxis ability of these growth variants in the capillary assay. By growing wild-type cells to different densities and introducing them in the chemotaxis assays at a uniform density, I restricted the variables to growth phase rather than growth phase and density combined. Contrary to our hypothesis, allowing more LsrB production had a negative effect on chemotaxis to AI-2. Optimal AI-2 response occurred at mid log phase and decreased significantly with later phases of growth. I considered this may be due to the accumulation of endogenous AI-2 in the periplasm, so I repeated the assays with cells unable to produce their own AI-2 (Δ*luxS*). These cells would be exposed only to exogenous AI-2. The fact that these *luxS* mutants responded to the same degree as wild-type cells at each growth phase leads us to believe endogenous AI-2 does not contribute to the reduced chemotaxis response. This lack of robust response could also be due to the fact that cells are less motile and less chemotactic during late log to

stationary phase as compared to mid log phase (*128, 129*). Quantitative studies have also shown that flagellar synthesis and mean run speed peak during mid log phase then decrease significantly as cells progress to late log and stationary phase (*130*). In our particular strain (CV1) it has been observed that a roughly inverse relationship exists between run speed and tumble frequency during later stages of growth, and that it is more difficult to achieve full adaptation of a ligand-bound chemoreceptor during this timeframe (*131*). Indeed, I found that response to *L*-serine was reduced as growth phase progressed. A combination of these factors, in addition to various other global changes that occur as growth progresses, may make it difficult to accurately characterize chemotaxis at later stages of growth.

The second approach involved deleting components of the uptake and regulation pathway, including components of the transporter *lsrACD* and the kinase and repressor *lsrK* and *lsrR*, respectively. This series also included *luxS* and *TqsA*, a membrane protein involved in export of newly synthesized AI-2 from the periplasm. When protein levels of LsrB were measured through western blotting, the amount of LsrB in the Δ*lsrR* knockout was nearly six times the amount of expression as wild-type. This did not dramatically increase the chemotaxis response to AI-2 in Δ*lsrR*, however, as its dose response was nearly identical to wild-type. On the other end of the expression spectrum, LsrB was expressed at only 20% of wild-type levels in Δ*lsrK* and only 10% of wild-type in Δ*luxS*. Neither of these deficiencies appeared to affect AI-2 chemotaxis, however, as the dose response to AI-2 in these deletion mutants remained virtually identical to wild-type, suggesting relatively few LsrB proteins can mediate a strong response to AI-2.

A third approach involved inducing LsrB from a plasmid promoter. Under P_{TAC} control LsrB was overexpressed to a large degree, yet this had a negative impact on AI-2 chemotaxis as measured in the capillary assay. Western blots showed increasing levels of LsrB with increasing induction (with the exception of 1 and 10 μM IPTG induction), but with those increases came less chemotaxis to AI-2. This was puzzling since the limiting step of AI-2 chemotaxis seemed to be the amount of available LsrB to bind AI-2 and interact with Tsr. These results implied a negative correlation between amount of periplasmic LsrB and chemotaxis to AI-2. It remains unclear why expression of LsrB actually decreased at lower levels of IPTG induction (1 and 10 μM) from the plasmid.

These results further solidify our hypothesis that optimal AI-2 chemotaxis occurs when LsrB copy level is at our just below 300 molecules per cell at mid log phase, and that the binding between Tsr and LsrB must be very tight to elicit such a strong response despite so few molecules present. Further studies are required to fully understand the correlation between LsrB expression levels and chemotaxis to AI-2. These ideas will be discussed in Chapter V.

CHAPTER IV

DETERMINING THE EFFECT ON CHEMOTAXIS WHEN SERINE AND AI-2 ARE PRESENT SIMULTANEOUSLY

Introduction

A mechanism for simultaneous sensing of two chemoeffectors by the same chemoreceptor has been described previously. The Tar receptor can mediate chemotaxis to two independently binding ligands: *L*-aspartate and substrate-loaded maltose binding protein (MBP) (*126*). Saturating concentrations of one ligand can and do affect response to the opposite ligand. A more detailed analysis revealed that when forced to signal through the same Tar subunit, aspartate and maltose competed for signaling.

Serine is a known, potent attractant for *E.coli* during chemotaxis. Its receptor is one of the more abundant receptors present in the polar chemoreceptor signaling patches of *E. coli* cells (*34*). The serine chemoreceptor (Tsr) binds *L*-serine directly at a known binding site consisting of a pocket formed by an arginine 69 residue on one Tsr monomer and a threonine 156 on the other (*107, 132, 133*). Sensing of AI-2 should not involve these binding pockets and does not occur through direct ligand-binding. Based on the docking model generated for the proposed interaction between ligand-bound LsrB and Tsr, AI-2 is sensed indirectly by Tsr through LsrB docking at its periplasmic shoulder regions.

To ensure sensing of AI-2 does not in some way involve intact serine binding sites, I used the known binding site mutants to test the cells' ability to respond to extra-

cellular AI-2. If the cells respond similar to wild-type, I surmise signaling for AI-2 neither involves direct sensing at the binding pockets, nor requires intact binding pockets comprised of Arg-69 and Thr-156 to transduce a response to AI-2.

Using the Tar-MBP model as a starting point, I hypothesized that high concentrations of one ligand could possibly affect the ability of the cells to respond to the other ligand in the capillary assay. The serine chemoreceptor is one of the more abundant MCPs in *E.coli* cells, with Tar numbering nearly 15,000 at mid-log growth (*34, 134*), but those cells contain only about 300 copies of LsrB (S. Jani and M. Manson, unpublished) at mid-log phase growth. Thus, I believed that high concentrations of AI-2 would have little effect on the ability of cells to respond to serine. Conversely, I hypothesized that high concentrations of serine would render the cells blind to AI-2 gradients. In other words, I looked for a shift near half maximal effective concentration (EC_{50}) of response when the second ligand was present.

Materials and methods

Bacterial strains, plasmids and media. Strain CV1 was used as our wild-type strain. Strain CV5 (Δ*Tsr*) and CV1 (Δ*lsrB*) were derived from CV1 as previously described. Plasmid pPA114, a relative of pKG116 (*18, 135*) carrying serine binding site mutations in *tsr* under sodium salicylate control, was used to express Tsr variants (*136*). The pPA114 plasmid was induced with 0.6 μM sodium salicylate. All strains were grown in tryptone broth media (10 g/L tryptone; 8 g/L NaCl) supplemented with antibiotic where appropriate.

Measuring chemotaxis to attractants by mutants for serine chemotaxis. Capillary assays (*114*) were employed to quantify the ability of mutants for serine chemotaxis to respond to varying concentrations of AI-2. Overnight cultures were grown at 30°C in TB supplemented with streptomycin (50 μg/mL) and chloramphenicol (30 μg/mL) for selection of the pPA114 plasmid. Back dilutions were made to a turbidity of ~0.05 at $O.D._{600}$ in 25 mL TB without antibiotic. Cells were grown to mid-logarithmic phase ($O.D._{600}$ = ~0.5) and centrifuged at 600 *x g* for 10 minutes to isolate them from the growth media. Once the supernatant was removed, an equal volume of chemotaxis buffer was used to resuspend the cells. They were given 15 minutes incubation at 30°C in a low speed test tube roller for recovery. Motility was confirmed through direct observation with phase contrast microscopy.

Measuring chemotaxis to attractants in the presence of second ligand. Capillary assays (*115*) were chosen to quantify the response to the chosen chemoattractant. Overnight cultures of cells were grown at 30°C in TB supplemented with streptomycin (50 μg/mL). Cultures were back-diluted to a turbidity of ~0.05 at $O.D._{600}$ in 25 mL TB. A 100 μM concentration of the second ligand was also added to the growth media at this time. When testing the response to AI-2 in the capillary assay, 100 μM *L*-serine was added; when testing for response to serine, 100 μM AI-2 was added. Cells were then grown to mid-logarithmic phase at an $O.D._{600}$ = ~0.5. Cells were then centrifuged at 600 *x g* for 10 minutes to separate the cells from the media. The supernatant was removed and the pellet gently resuspended in chemotaxis buffer containing 100 μM of the second ligand as described above. The cells were given fifteen minutes of recovery time in a

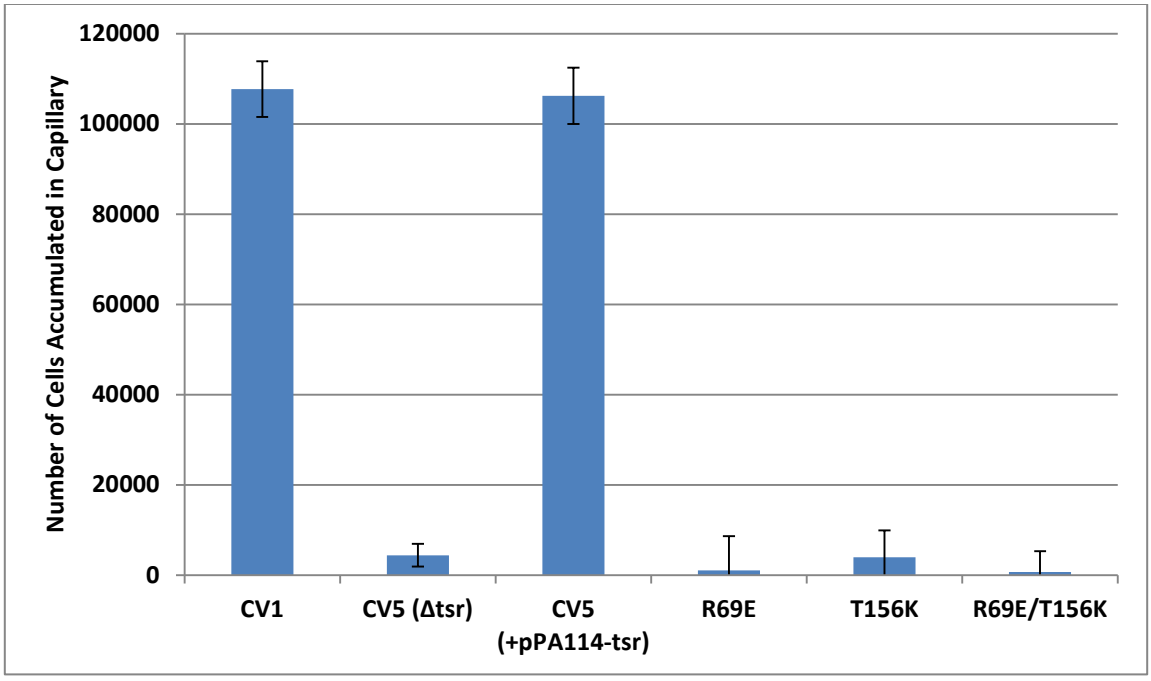

Figure 36. Response to *L*-serine by Tsr binding site knockout mutants. Cells carrying substitutions at the major and minor serine binding sites of the Tsr receptor were exposed to 10 mM *L*-serine and their response was measured in the capillary assay. Mutant Tsr proteins were expressed from sodium salicylate-inducible plasmid pPA114 (*136*). Capillary assays were performed at 30°C for 45 minutes. Each trial represents three biological replicates carried out in triplicate.

30°C rotor at low speed. Motility of cells was then confirmed through phase contrast microscopy. Second ligand was also added to dilutions of target ligand to ensure constant exposure during the capillary assay.

Results

Ability of cells mutated for serine binding site to respond to AI-2. Previous genetic studies have shown that mutations of the residues forming the serine-binding pocket between the Tsr subunits of its periplasmic domain negatively affect chemotaxis to *L*-serine (*137-139*). I confirmed this *L*-serine chemotaxis deficiency in the capillary assay. Cells carrying the R69E mutation (minor binding site) accumulated at less than 1% of the response by wild-type CV1 cells; cells carrying the T156K mutation (major binding site) showed only 3.5% wild-type response; binding pocket double mutants (R69E/T156K) accumulated to only 0.6% wild-type levels (Figure 36). These binding pocket mutants, however, were not affected for chemotaxis to AI-2 (Figure 37). Each of the mutants tested accumulated to within 97% or better of the wild-type dose response curve for AI-2 in the capillary assay. Cells lacking either Tsr or LsrB failed to accumulate significantly to an AI-2 gradient.

Effects of second ligand on response to target ligand. When cells exposed to saturating concentrations of AI-2 during growth were exposed to *L*-serine in the capillary assay, the dose response to serine (normalized to background control) was 105,000 cells at 1 mM (92% serine only); 72,000 cells at 100 µM (85% serine only); 31,000 cells at 10 µM (62% serine only); and 1,500 cells at 1 µM (35% serine only) (Figure 38). The

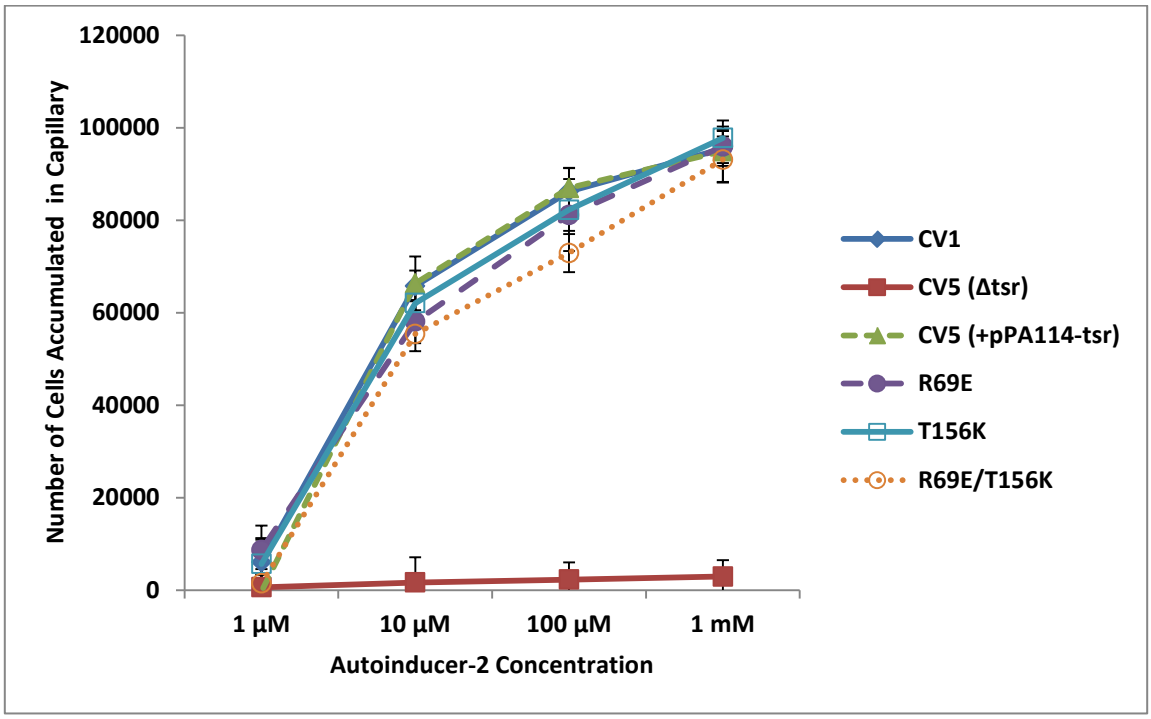

Figure 37. Response to AI-2 by serine binding site mutants. Mutations were selected based on previous findings of their affecting chemotaxis to serine. Mutant Tsr proteins were expressed from sodium salicylate-inducible plasmid pPA114 (*136*). Capillary assays were performed at 30°C for 45 minutes. Each trial represents three biological replicates carried out in triplicate.

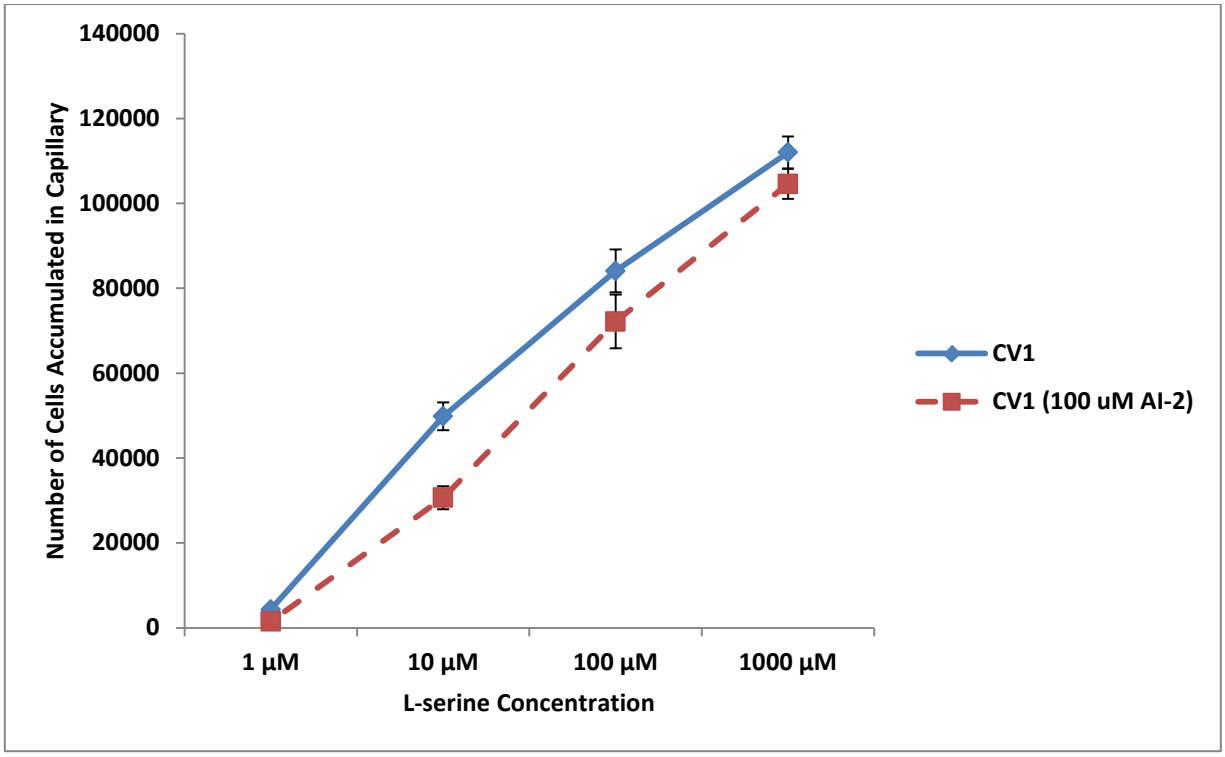

Figure 38. Response to serine by cells grown with AI-2. Wild-type CV1 cells were grown in the presence of 100 µM AI-2, then continuously exposed to this concentration of AI-2 during the capillary assay. AI-2 was also present in the capillaries containing the *L*-serine concentrations for dose response. Capillary assays were performed at 30°C for 45 minutes. Each trial represents three biological replicates carried out in triplicate.

background only control (saturating AI-2 present) averaged 9,500 cells accumulated, an amount similar to chemotaxis buffer lacking saturating ligand. Response to AI-2 in the presence of saturating serine concentration (100 μM), again normalized to background, was quite different. At 1 mM AI-2 exposure 43,000 cells accumulated (44% AI-2 only); at 100 μM exposure 7,000 cells accumulated (8% AI-2 only); at 10 μM exposure 1,500 cells accumulated (2% AI-2 only); and at 1 μM exposure 800 cells accumulated (14% AI-2 only) (Figure 39). Controls of background only (saturating *L*-serine present) averaged 60,000 cells accumulated, whereas the background only response when no saturating chemoattractant was present averaged only 12,000 cells.

Discussion

Each of the methyl accepting chemotaxis proteins (MCPs) of *E. coli* interact with a cognate binding protein carrying a particular ligand. Some also sense ligands through direct binding interactions. These interactions take place at the periplasmic region of the MCPs and the signal is transduced across the membrane to the distal tip of the chemoreceptor. In cases where multiple ligands are recognized by a single chemoreceptor, as in the case with both aspartate and maltose in Tar, independent binding sites exist for the different ligands and have been genetically analyzed (*41*, *125*).

Our recent work showed that AI-2 is sensed through *E. coli* Tsr with the aid of the AI-2 binding protein LsrB (Chapter II, Figures 8 and 13). I surmised that the known ligands of Tsr utilize distinct binding sites of the receptor's periplasmic domain. I reasoned, simply, that if distinct sites existed for serine and AI-2 binding, a disruption in the

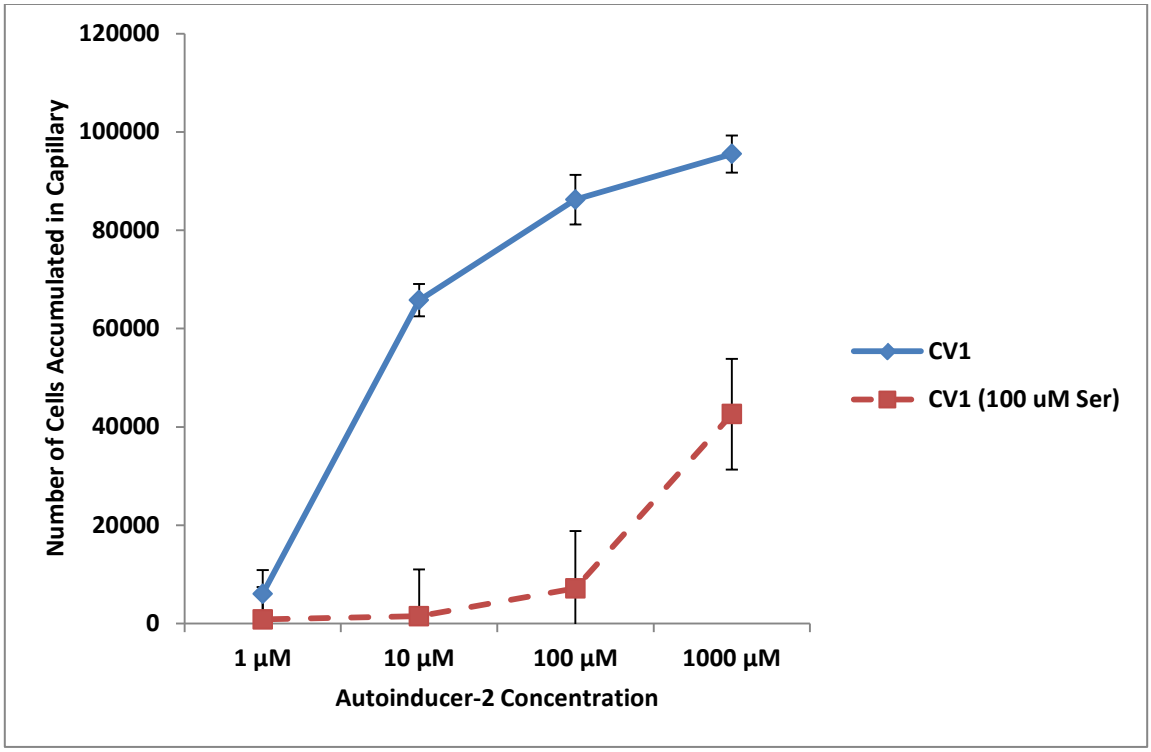

Figure 39. Response to AI-2 by cells grown with serine. Wild-type CV1 cells were grown in the presence of 100 µM *L*-serine, then continuously exposed to this concentration of serine during the capillary assay. Serine was also present in the capillaries containing the AI-2 concentrations for dose response tests. Capillary assays were performed at 30°C for 45 minutes. Each trial represents three biological replicates carried out in triplicate.

ability of the cells to respond to serine should not affect chemotaxis toward AI-2, or vice versa. To elucidate this I tested for AI-2 chemotaxis in Tsr receptors that are unable to bind and respond to serine. I already knew *E. coli* carrying Tsr mutations making them deficient for AI-2 chemotaxis were still able to respond to serine (Figure 15). Quantifying response to AI-2 in serine chemotaxis negative cells would allow us to quickly confirm this hypothesis.

Our results here support this hypothesis. Mutations in the serine binding pockets of the Tsr homodimer, Arg-69 and Thr-156, did not affect response to varying concentrations of AI-2, as these mutants responded to this ligand just as well as wild-type. This was not a surprise, however, as our docking model suggested AI-2 cannot directly bind to Tsr, and the binding protein LsrB interacts with Tsr at its periplasmic shoulder regions.

A second approach involved exposing Tsr to hyper-physiological concentrations of one ligand prior to introducing the other. Much as in the case of Tar with aspartate and maltose binding protein, I believed exposure to and binding of one ligand might preclude binding and or response to the other. Therefore, cells were grown in the presence of a high concentration of serine before use in chemotaxis assays, and serine was even added to the chemotaxis buffer solution to ensure constant exposure over the course of the assays. The same was done using AI-2 as the second ligand. Due to the abundance of Tsr in mid-logarithmic growth phase cells, and the relatively paltry amount of LsrB in comparison (roughly 300 molecules per cell) at this same growth phase, I hypothesized

response to serine would not be affected by the presence of AI-2, but that response to AI-2 gradients would be nearly impossible.

The results gathered here seem to support this specific hypothesis, though testing various background concentrations of the second ligand is necessary to make broader conclusions. Response to serine was largely unaffected by the presence of exogenous AI-2, likely because at mid log phase cells produce an abundance of Tsr chemoreceptor in comparison to AI-2 binding proteins. With so many receptors for serine and so few LsrB proteins present to bind the added AI-2, cells have little problem recognizing serine gradients and responding accordingly. On the other hand, when serine is present at high concentrations it renders the *E. coli* cells blind to gradients of AI-2. Even if all of the approximately 300 molecules of LsrB were loaded with AI-2, they would be unable to occupy all of the available Tsr receptors.

With so little LsrB present in wild-type cells, the window for response to AI-2 appears to be very particular. Perhaps overexpression of LsrB to levels closer to those of Tsr would allow for a level playing field in terms of opportunity for binding, although this does not align with our observations from Chapter III, where increasing levels of LsrB leads to decreased chemotaxis response to AI-2. Further experiments along this line of thinking shall be discussed in Chapter V.

CHAPTER V

SUMMARY AND DISCUSSION

Summary

Until recently, a periplasmic binding protein had not been identified for the Tsr chemoreceptor in *E. coli*. The other MCPs (Tar, Tap, Trg) and the interactions with their cognate binding proteins have been studied extensively. When the identification of a periplasmic binding protein for Tsr was proposed, a genetic analysis of the proposed interaction, and a correlation between protein expression and chemotaxis became the goal of this thesis work. In this dissertation I address the accuracy of the proposed docking model for the interaction between *E.coli* Tsr and AI-2-bound LsrB through site-directed mutagenesis, and I attempt to correlate chemotaxis to AI-2 with expression of LsrB and interference by the presence of a potential competing ligand.

The results from Chapter II suggest that the shoulder regions of the Tsr homodimer, and residues in β-strand 2 and α-helix 8 of LsrB are critical for the interaction of Tsr and substrate-bound LsrB during AI-2 chemotaxis in *E. coli*. The findings in Chapter II support the proposed docking model developed and discussed in that chapter. Results from Chapter III indicate that LsrB is present in low copy number (~300 molecules per cell) at mid log phase compared to the high-abundance chemoreceptors Tsr and Tar (~15,000 molecules per cell), and that overexpression of LsrB does not directly correlate to AI-2 chemotaxis. Results here also showed that deleting various components of the *lsr* operon and production pathways, while slightly altering the expression levels of

LsrB, had little effect on AI-2 chemotaxis. Only when the periplasmic binding protein for AI-2 (LsrB) was deleted was chemotaxis negatively affected. Results from Chapter IV indicate that the presence of high concentrations of *L*-serine in the environment virtually blind the cells to the presence of AI-2, though the opposite is not true. A high concentration of AI-2 does little to reduce chemotaxis to serine in mid-log phase cells. Here, it was also confirmed that the serine binding pockets of Tsr are not necessary for dose response to AI-2. In this chapter, I discuss the likely mechanism of interaction between Tsr and LsrB, and explore the possible relationship between cellular levels of AI-2, LsrB and chemotaxis. I also suggest potential experiments to elucidate this relationship, including biochemical studies involving investigation of binding affinity between Tsr and LsrB.

Discussion

A docking model for the Tsr-LsrB interaction. A docking model for the interaction between AI-2 bound LsrB and the Tar chemoreceptor was proposed and tested in Chapter II. This model was based on the published model generated from studies of the Tar chemoreceptor and maltose binding protein (MBP), and an established experimental approach was available (*105*). Single amino acid residues were shown to be vital for maltose chemotaxis to occur. Mutation of these residues negatively affected response to maltose, presumably by disrupting the Tar-MBP interaction.

The results in this chapter support our proposed docking model and identify key residues in both proteins that must be present for AI-2 chemotaxis to take place. Alanine

substitutions in Tsr at Lys-147 and Glu-150 reduced AI-2 chemotaxis response in the capillary assay. The Lys-147-Ala mutant lost nearly all ability to respond to AI-2 gradients. The Glu-150-Ala mutant was significantly reduced for AI-2 chemotaxis, though it was nowhere near as depressed as the Lys-147-Ala mutant. In LsrB alanine substitutions at Asp-59, Val-60, Thr-61, Asp-63, Arg-252 and Glu-256 reduced AI-2 chemotaxis to varying degrees. I will discuss the likely role of each of these residues in the Tsr-LsrB interaction.

Cells expressing the Tsr variant Lys-147-Ala failed to mediate more than 20% of the wild-type AI-2 chemotaxis response. Lysine is a positively charged residue capable of forming a salt bridge with residues of the opposite charge in close proximity. The docking model intimates a very tight coupling between Tsr and LsrB, conditions conducive for electrostatic interactions to predominate. Seeing as how the most critical residues in LsrB for AI-2 chemotaxis appear to be Asp-59 and Asp-63, positively charged amino acids, a salt bridge between Lys-147 in Tsr and Asp-59 or Asp-63 in LsrB is possibly a stabilizing force for this docking, and furthermore may be crucial for eliciting a signal after binding. Because the Lys-147 is present in the other half of the Tsr homodimer, this positive charge may also attract the Glu-256 of the LsrB C-terminal domain to form a second salt bridge, further stabilizing the interaction.

The Glu-150 of Tsr potentially forms a salt bridge with the Arg-252 of the LsrB C-terminal domain, adding additional support to the interaction. Taken together with the other likely salt bridges formed, the predominant stabilization forces behind the docking of Tsr to LsrB seem to be electrostatic. When these forces are unperturbed, the two pro-

teins could come together tightly enough to elicit a strong chemotaxis response despite a large disparity between the number of Tsr and LsrB molecules present in each cell. Such a tight interaction suggests a low dissociation constant and high affinity between Tsr and LsrB, much higher than the binding affinity of Tar for MBP. Further biochemical studies are necessary to make firm conclusions in this area.

The remaining residues of interest likely contribute to the overall stability of the binding. The LsrB Thr-61, a polar residue, likely forms a supporting hydrogen bond with a residue in Tsr or a water molecule. Water molecules have been shown to play roles in ligand-protein interaction. Why the hydrophobic Val-60 in LsrB's N-terminal domain is critical remains uncertain. Substituting alanine for valine is simply swapping two hydrophobic amino acids, though valine is typically buried to a greater degree, and changing it to alanine possibly disrupts the conformation of LsrB enough to prohibit the Asp-59 to Lys-147 salt bridge from forming without affecting the affinity of LsrB for the LsrACD transport channel during AI-2 uptake.

None of these critical single amino acid mutations affect the ability of LsrB to bind AI-2 in the periplasm and transport it back into the cell via the LsrACD transport apparatus. Bioluminescent assays measuring AI-2 uptake in *Vibrio harveyi* show each of the point mutants perform AI-2 uptake along the same time frame as wild-type LsrB cells. Therefore, I conclude these residues are critical for the Tsr-LsrB interaction, and play seemingly no role in normal *lsr* operon function. These findings ensure the negative effects on response to AI-2 result from disrupting chemotaxis rather than protein expression.

Additional mutations outside the proposed areas of interaction in LsrB and Tsr, and their effects on AI-2 chemotaxis, are needed as controls to support our docking model. If mutations in areas of the proteins away from the interaction sites do not alter AI-2 chemotaxis, it would lend support to the nature of our proposed docking interaction.

The failure of wild-type LsrB to rescue the negative phenotype for AI-2 chemotaxis resulting from the Asp-59-Ala and Asp-63-Ala point mutations remains an interesting result. This finding of a potential dominant-negative phenotype requires further consideration. It may result from a stronger binding of this mutant LsrB with Tsr, precluding binding of wild-type LsrB to the chemoreceptor. If this is the case, notably it does not seem to inhibit response to serine. This scenario suggests the Asp-59 and Asp-63 mutants are AI-2 signaling mutants rather than binding mutants. A separate scenario for this effect may be dimerization of mutant and wild-type LsrB proteins, though AI-2 uptake remained consistent with wild-type monomeric LsrB in the bioluminescence assay. Complementation studies in which residues in Tsr are mutated, beginning with Lys-147, could reverse this dominant negative phenotype to some degree. Exchanging charges between Tsr and LsrB (Lys-147-Glu and Asp-59/63-Arg, respectively) could potentially counteract the disruption of salt bridge formation.

A second possibility is that the LsrB protein could be locked into a closed conformation resulting from this point mutation. While it is unlikely a surface mutation would have this effect, dominant negative phenotypes have been observed for maltose chemotaxis in *E. coli* and were the result of crosslinking event that locked MBP into its

substrate-free/closed conformation (*140*). Perhaps introducing inter-domain cysteine-cysteine crosslinks into wild-type LsrB could be used to test this. If the dominant negative phenotype is the result of a closed conformation mutation, the dose response curve for this crosslinking mutant could look similar to the D59A or D63A mutants.

The amount of LsrB present does not correlate directly with chemotaxis to AI-2. As mentioned in Chapter I, the expression of LsrB from the *lsrACDBFG* operon is regulated by the presence of phosphorylated AI-2 (AI-2-P). When a threshold of environmental AI-2 is reached and it accumulates within the periplasm, it is imported into the cell via an ABC transporter. Some amount of LsrB is present to bind the AI-2 and interact with the LsrACD transport channel. Once imported, AI-2 is phosphorylated by the kinase LsrK, at which point it can bind to LsrR and relieve repression of the *lsr* operon. When this occurs, more transport channel proteins are expressed (LsrACD) and more LsrB is produced, allowing more AI-2 to be taken into the cell. Growing cells to later log phase allows up to six times as much LsrB to be present compared to the approximately 300 molecules per cell during mid logarithmic growth.

Our initial hypothesis was that cells might respond to increasingly higher levels of AI-2 if more LsrB was available for binding and interacting with Tsr. Not only was this assumption incorrect, the response actually decreased with increasing LsrB levels at later phase growth. This result was confirmed with overexpression from an LsrB-bearing plasmid. To us, this suggests an optimal window for response to AI-2, namely at mid log phase cell growth and roughly 300 copies of LsrB per cell. This suggests a scenario where *E. coli* cells growing and dividing in the gastrointestinal tract receive

quorum sensing information via AI-2 concentration and respond quickly, taking them to areas of higher cell density where nutrients may be more readily available, such as a pyre's patch. Once in these areas, the increasing levels of LsrB allow for import and degradation of AI-2 by the *lsrFG* gene products whose expression is also induced as repression is relieved, thus returning the *lsr* operon to its pre AI-2 threshold state.

Due to the numerous global changes occurring during later phase growth (*128, 130*), it is difficult to make direct correlations between protein levels and chemotaxis response. As cells move into later stages of the growth curve, swim speed and motility decrease in general, and frequency of tumbling increases. Perhaps even the changing profile of the high abundance chemoreceptors Tsr and Tar at later log growth (*141*) makes chemotaxis to attractants, AI-2 among them, difficult to measure.

Chemotaxis to AI-2 is reduced in the presence of serine. Studies involving simultaneous exposure to gradients of *L*-aspartate and maltose for the *E. coli* Tar chemoreceptor have suggested a preference by cells for one attractant over another. Under conditions where the ligands were forced to bind and signal through the same Tar subunit, saturating concentrations of maltose only moderately inhibited aspartate chemotaxis, while the opposite showed a more drastic effect. When saturating aspartate was present at the time the cells were exposed to maltose gradients, the response to maltose was virtually eliminated (*126*). The ligands were characterized as competing and aspartate was the winner. This competition did not occur when ligands were forced into signaling through opposite subunits of Tar.

My studies with background concentrations of serine and AI-2 have suggested these two ligands can signal through the same subunit as well. Disrupting the binding pocket for serine at either Arg-69 or Thr-156 did not interfere with AI-2 chemotaxis. Likewise, mutants deficient in AI-2 chemotaxis still responded at wild-type levels to serine gradients. When both attractants were present at the same time, however, the cells were unable to mount a dose response to AI-2. When saturating levels of serine remained constant throughout the exposure to AI-2, cells failed to perform any significant response to the latter in the capillary assay. On the other hand, when AI-2 was the saturating ligand at constant exposure, it did not reduce the chemotaxis response to serine relative to wild-type.

It is already apparent that LsrB is present at lower copy number per cell during mid logarithmic growth compared to Tsr, and this may be the central reason for the lack of response to AI-2 when serine is present. If the cells have more opportunity to interact with serine due to the abundance of Tsr, they may become blind to AI-2 gradients at higher serine concentrations. My results lean toward this conclusion. With saturating AI-2 present, at 1 mM serine the response was within 93% of wild-type in the absence of competing ligand; at 100 μM serine the response fell to 85% of no competitor; and at 10 μM serine it dropped to 63% of wild-type without AI-2 present (Figure 38). This suggests that only when levels of serine are low enough will cells begin to recognize the presence of AI-2 in the environment.

In the gastrointestinal tract of humans, *E.coli* does well to respond to serine as a priority to AI-2 since serine is a nutrient source for the cells. Autoinducer-2 serves as a

signaling molecule, not a nutrient source; therefore, in this case it is in the cells' best interest to respond to a nutrient source over a non-nutrient source, especially considering that stable biofilms are not likely to appear in the dynamic gut. Perhaps this is why so few copies of LsrB are present in the cells at a given time relative to Tsr or Tar. When it serves the best interest of the cells to migrate away from low nutrient areas toward higher population densities – a potential indicator of plentiful nutrients –AI-2-laden LsrB has little competition for binding to Tsr and eliciting a chemotactic response. Perhaps the grand balance of a healthy microbiome within the human gut is partially achieved through regulated response to nutrient sources and signaling molecules.

Future Studies

My work here has provided a docking model for the interaction of AI-2-bound LsrB with Tsr during AI-2 chemotaxis in *E. coli*. It has also shown there is no direct correlation between increasing levels of LsrB and chemotaxis to AI-2. Furthermore, it has indicated that the presence of a high concentration of *L*-serine can reduce the ability of the cells to perform chemotaxis to AI-2. However, there are certain aspects of AI-2 chemotaxis that remain unanswered.

First, it can be determined whether serine and AI-2 compete to signal through the same subunit of Tsr. Tsr can exist as a heterodimer of wild-type and mutant proteins when point mutants and wild-type versions of Tsr are expressed from compatible plasmids within the same cell. These heterodimers will allow serine to bind in only one conformation, causing it to signal through a particular subunit. If mutant LsrB proteins can

be forced to interact with Tsr and signal through that same subunit, it might be determined if serine and AI-2 signals compete for signaling. This same scenario was studied with aspartate and MBP in Tar, and it was determined that when forced to signal through the same subunit of Tar, competition did occur (*122*).

Second, we can elucidate the effects of the presence of secondary attractants on response to either serine or AI-2. Varied background concentrations of either serine or AI-2 would give a better picture of the amount of secondary ligand necessary to inhibit response to the first. Up to this point, only 100 µM of either serine or AI-2 was used as background, but testing higher and lower concentrations would give us a better idea of the EC_{50} for each. Furthermore on this point, expressing LsrB to levels higher than the 300 copies produced by the chromosome at mid-log phase would clarify the ability of serine at 100 µM to reduce AI-2 chemotaxis. By expressing extra LsrB from an inducible plasmid, perhaps AI-2 chemotaxis would not be affected by the presence of serine. Even more useful would be the use of tethered cell assays or microfluidic assays that test the response of cells to multiple ligands in real time. The capillary assay gives only a measure of the end result of exposure to chemoeffectors.

Next, what roles do the aspartates in LsrB at positions 59 and 63 play during chemotaxis? My results suggest both are critical to the ability of cells to respond to gradients of AI-2. It is unclear if they help stabilize the Tsr-LsrB interaction, or if they allow for signaling through Tsr to occur post-binding. It would be useful to see the chemotaxis response of a D59A/D63A double mutant to determine if the charge or the position is the important aspect.

Additionally, determining the binding affinity of LsrB for Tsr is important. Due to its unstable nature, AI-2 has been an issue here. According to our hypothesis, it must be present and bound to LsrB to get a closed conformation of LsrB that can interact with Tsr. This is a problem for most biochemical assays that can help determine binding affinity. It is also a problem for obtaining a co-crystal structure of LsrB-Tsr. If we could obtain either a stable form of AI-2, or a closed conformation of LsrB that interacts with Tsr, it would make it possible to carry out the necessary biochemical assays for determining binding affinity and the nature of the interaction. Assays such as isothermal titration calorimetry, or equilibrium gradient ultracentrifugation could be employed.

REFERENCES

1. Berg, H. C., and Anderson, R. A. (1973) Bacteria swim by rotating their flagellar filaments, *Nature 245*, 380-382.

2. Berg, H. C., and Turner, L. (1995) Cells of *Escherichia coli* swim either end forward, *Proceedings of the National Academy of Sciences of the United States of America 92*, 477-479.

3. Berg, H. C., and Brown, D. A. (1972) Chemotaxis in *Escherichia coli* analysed by three-dimensional tracking, *Nature 239*, 500-504.

4. Silverman, M., and Simon, M. (1977) Chemotaxis in *Escherichia coli*: methylation of che gene products, *Proceedings of the National Academy of Sciences of the United States of America 74*, 3317-3321.

5. Kondoh, H., Ball, C. B., and Adler, J. (1979) Identification of a methyl-accepting chemotaxis protein for the ribose and galactose chemoreceptors of *Escherichia coli*, *Proceedings of the National Academy of Sciences of the United States of America 76*, 260-264.

6. Hazelbauer, G. L., and Engstrom, P. (1980) Parallel pathways for transduction of chemotactic signals in *Escherichia coli*, *Nature 283*, 98-100.

7. Hazelbauer, G. L., Engstrom, P., and Harayama, S. (1981) Methyl-accepting chemotaxis protein III and transducer gene *trg*, *Journal of Bacteriology 145*, 43-49.

8. Manson, M. D., Blank, V., Brade, G., and Higgins, C. F. (1986) Peptide chemotaxis in *E. coli* involves the Tap signal transducer and the dipeptide permease, *Nature 321*, 253-256.

9. Springer, M. S., Goy, M. F., and Adler, J. (1977) Sensory transduction in *Escherichia coli*: two complementary pathways of information processing that involve methylated proteins, *Proceedings of the National Academy of Sciences of the United States of America 74*, 3312-3316.

10. Hazelbauer, G. L. (1988) The bacterial chemosensory system, *Canadian Journal of Microbiology 34*, 466-474.

11. Bibikov, S. I., Biran, R., Rudd, K. E., and Parkinson, J. S. (1997) A signal transducer for aerotaxis in *Escherichia coli*, *Journal of Bacteriology 179*, 4075-4079.

12. Bibikov, S. I., Miller, A. C., Gosink, K. K., and Parkinson, J. S. (2004) Methylation-independent aerotaxis mediated by the *Escherichia coli* Aer protein, *Journal of Bacteriology 186*, 3730-3737.

13. Rebbapragada, A., Johnson, M. S., Harding, G. P., Zuccarelli, A. J., Fletcher, H. M., Zhulin, I. B., and Taylor, B. L. (1997) The Aer protein and the serine chemoreceptor Tsr independently sense intracellular energy levels and transduce oxygen, redox, and energy signals for *Escherichia coli* behavior, *Proceedings of the National Academy of Sciences of the United States of America 94*, 10541-10546.

14. Krikos, A., Conley, M. P., Boyd, A., Berg, H. C., and Simon, M. I. (1985) Chimeric chemosensory transducers of *Escherichia coli*, *Proceedings of the National Academy of Sciences of the United States of America 82*, 1326-1330.

15. Mowbray, S. L., and Koshland, D. E., Jr. (1990) Mutations in the aspartate receptor of *Escherichia coli* which affect aspartate binding, *The Journal of Biological Chemistry 265*, 15638-15643.

16. Reader, R. W., Tso, W. W., Springer, M. S., Goy, M. F., and Adler, J. (1979) Pleiotropic aspartate taxis and serine taxis mutants of *Escherichia coli*, *Journal of General Microbiology 111*, 363-374.

17. Englert, D. L., Adase, C. A., Jayaraman, A., and Manson, M. D. (2010) Repellent taxis in response to nickel ion requires neither Ni2+ transport nor the periplasmic NikA binding protein, *Journal of Bacteriology 192*, 2633-2637.

18. Ames, P., Studdert, C. A., Reiser, R. H., and Parkinson, J. S. (2002) Collaborative signaling by mixed chemoreceptor teams in *Escherichia coli*, *Proceedings of the National Academy of Sciences of the United States of America 99*, 7060-7065.

19. Kim, K. K., Yokota, H., and Kim, S. H. (1999) Four-helical-bundle structure of the cytoplasmic domain of a serine chemotaxis receptor, *Nature 400*, 787-792.

20. McAndrew, R. S., Ellis, A. E., Lai, R. Z., Manson, M. D., and Holzenburg, A. (2005) Identification of Tsr and Tar chemoreceptor arrays in *E. coli* inner membranes, *Microscopy Microanalysis 11*, 1190-1191.

21. Studdert, C. A., and Parkinson, J. S. (2005) Insights into the organization and dynamics of bacterial chemoreceptor clusters through in vivo crosslinking studies, *Proceedings of the National Academy of Sciences of the United States of America 102*, 15623-15628.

22. Maddock, J. R., and Shapiro, L. (1993) Polar location of the chemoreceptor complex in the *Escherichia coli* cell, *Science 259*, 1717-1723.

23. Liu, J., Hu, B., Morado, D. R., Jani, S., Manson, M. D., and Margolin, W. (2012) Molecular architecture of chemoreceptor arrays revealed by cryoelectron tomography of *Escherichia coli* minicells, *Proceedings of the National Academy of Sciences of the United States of America 109*, E1481-1488.

24. Briegel, A., Beeby, M., Thanbichler, M., and Jensen, G. J. (2011) Activated chemoreceptor arrays remain intact and hexagonally packed, *Molecular Microbiology 82*, 748-757.

25. Briegel, A., Ladinsky, M. S., Oikonomou, C., Jones, C. W., Harris, M. J., Fowler, D. J., Chang, Y. W., Thompson, L. K., Armitage, J. P., and Jensen, G. J. (2014) Structure of bacterial cytoplasmic chemoreceptor arrays and implications for chemotactic signaling, *eLife 3*, e02151.

26. Briegel, A., Li, X., Bilwes, A. M., Hughes, K. T., Jensen, G. J., and Crane, B. R. (2012) Bacterial chemoreceptor arrays are hexagonally packed trimers of receptor dimers networked by rings of kinase and coupling proteins, *Proceedings of the National Academy of Sciences of the United States of America 109*, 3766-3771.

27. Lybarger, S. R., and Maddock, J. R. (2000) Differences in the polar clustering of the high- and low-abundance chemoreceptors of *Escherichia coli*, *Proceedings of the National Academy of Sciences of the United States of America 97*, 8057-8062.

28. Albert, R., Chiu, Y. W., and Othmer, H. G. (2004) Dynamic receptor team formation can explain the high signal transduction gain in *Escherichia coli*, *Biophysical Journal 86*, 2650-2659.

29. Bray, D., Levin, M. D., and Morton-Firth, C. J. (1998) Receptor clustering as a cellular mechanism to control sensitivity, *Nature 393*, 85-88.

30. Shimizu, T. S., Aksenov, S. V., and Bray, D. (2003) A spatially extended stochastic model of the bacterial chemotaxis signalling pathway, *Journal of Molecular Biology 329*, 291-309.

31. Sourjik, V., and Berg, H. C. (2002) Receptor sensitivity in bacterial chemotaxis, *Proceedings of the National Academy of Sciences of the United States of America 99*, 123-127.

32. Mesibov, R., Ordal, G. W., and Adler, J. (1973) The range of attractant concentrations for bacterial chemotaxis and the threshold and size of response over this range. Weber law and related phenomena, *The Journal of General Physiology 62*, 203-223.

33. Segall, J. E., Block, S. M., and Berg, H. C. (1986) Temporal comparisons in bacterial chemotaxis, *Proceedings of the National Academy of Sciences of the United States of America 83*, 8987-8991.

34. Li, M., and Hazelbauer, G. L. (2004) Cellular stoichiometry of the components of the chemotaxis signaling complex, *Journal of Bacteriology 186*, 3687-3694.

35. Feng, X., Baumgartner, J. W., and Hazelbauer, G. L. (1997) High- and low-abundance chemoreceptors in *Escherichia coli*: differential activities associated with closely related cytoplasmic domains, *Journal of Bacteriology 179*, 6714-6720.

36. Weerasuriya, S., Schneider, B. M., and Manson, M. D. (1998) Chimeric chemoreceptors in *Escherichia coli*: signaling properties of Tar-Tap and Tap-Tar hybrids, *Journal of Bacteriology 180*, 914-920.

37. Lai, R. Z., Manson, J. M., Bormans, A. F., Draheim, R. R., Nguyen, N. T., and Manson, M. D. (2005) Cooperative signaling among bacterial chemoreceptors, *Biochemistry 44*, 14298-14307.

38. Milligan, D. L., and Koshland, D. E., Jr. (1988) Site-directed cross-linking. Establishing the dimeric structure of the aspartate receptor of bacterial chemotaxis, *The Journal of Biological Chemistry 263*, 6268-6275.

39. Hazelbauer, G. L., Falke, J. J., and Parkinson, J. S. (2008) Bacterial chemoreceptors: high-performance signaling in networked arrays, *Trends in Biochemical Sciences 33*, 9-19.

40. Bowie, J. U., Pakula, A. A., and Simon, M. I. (1995) The three-dimensional structure of the aspartate receptor from *Escherichia coli*, *Acta Crystallographica. Section D, Biological Crystallography 51*, 145-154.

41. Milburn, M. V., Prive, G. G., Milligan, D. L., Scott, W. G., Yeh, J., Jancarik, J., Koshland, D. E., Jr., and Kim, S. H. (1991) Three-dimensional structures of the ligand-binding domain of the bacterial aspartate receptor with and without a ligand, *Science 254*, 1342-1347.

42. Scott, W. G., Milligan, D. L., Milburn, M. V., Prive, G. G., Yeh, J., Koshland, D. E., Jr., and Kim, S. H. (1993) Refined structures of the ligand-binding domain of the aspartate receptor from *Salmonella typhimurium*, *Journal of Molecular Biology 232*, 555-573.

43. Hegde, M., Englert, D. L., Schrock, S., Cohn, W. B., Vogt, C., Wood, T. K., Manson, M. D., and Jayaraman, A. (2011) Chemotaxis to the quorum-sensing signal AI-2 requires the Tsr chemoreceptor and the periplasmic LsrB AI-2-binding protein, *Journal of Bacteriology 193*, 768-773.

44. Aravind, L., and Ponting, C. P. (1999) The cytoplasmic helical linker domain of receptor histidine kinase and methyl-accepting proteins is common to many prokaryotic signalling proteins, *FEMS Microbiology Letters 176*, 111-116.

45. Butler, S. L., and Falke, J. J. (1998) Cysteine and disulfide scanning reveals two amphiphilic helices in the linker region of the aspartate chemoreceptor, *Biochemistry 37*, 10746-10756.

46. Russo, A. F., and Koshland, D. E., Jr. (1983) Separation of signal transduction and adaptation functions of the aspartate receptor in bacterial sensing, *Science 220*, 1016-1020.

47. Williams, S. B., and Stewart, V. (1999) Functional similarities among two-component sensors and methyl-accepting chemotaxis proteins suggest a role for linker region amphipathic helices in transmembrane signal transduction, *Molecular Microbiology 33*, 1093-1102.

48. Djordjevic, S., and Stock, A. M. (1998) Chemotaxis receptor recognition by protein methyltransferase CheR, *Nature Structural Biology 5*, 446-450.

49. Hazelbauer, G. L., Park, C., and Nowlin, D. M. (1989) Adaptational "crosstalk" and the crucial role of methylation in chemotactic migration by *Escherichia coli*, *Proceedings of the National Academy of Sciences of the United States of America 86*, 1448-1452.

50. Mello, B. A., and Tu, Y. (2007) Effects of adaptation in maintaining high sensitivity over a wide range of backgrounds for *Escherichia coli* chemotaxis, *Biophysical Journal 92*, 2329-2337.

51. Liu, J. D., and Parkinson, J. S. (1991) Genetic evidence for interaction between the CheW and Tsr proteins during chemoreceptor signaling by *Escherichia coli*, *Journal of Bacteriology 173*, 4941-4951.

52. Levit, M. N., Liu, Y., and Stock, J. B. (1999) Mechanism of CheA protein kinase activation in receptor signaling complexes, *Biochemistry 38*, 6651-6658.

53. Tawa, P., and Stewart, R. C. (1994) Kinetics of CheA autophosphorylation and dephosphorylation reactions, *Biochemistry 33*, 7917-7924.

54. Bilwes, A. M., Alex, L. A., Crane, B. R., and Simon, M. I. (1999) Structure of CheA, a signal-transducing histidine kinase, *Cell 96*, 131-141.

55. Bourret, R. B., Hess, J. F., and Simon, M. I. (1990) Conserved aspartate residues and phosphorylation in signal transduction by the chemotaxis protein CheY, *Proceedings of the National Academy of Sciences of the United States of America 87*, 41-45.

56. Roman, S. J., Meyers, M., Volz, K., and Matsumura, P. (1992) A chemotactic signaling surface on CheY defined by suppressors of flagellar switch mutations, *Journal of Bacteriology 174*, 6247-6255.

57. Welch, M., Oosawa, K., Aizawa, S., and Eisenbach, M. (1993) Phosphorylation-dependent binding of a signal molecule to the flagellar switch of bacteria, *Proceedings of the National Academy of Sciences of the United States of America 90*, 8787-8791.

58. Alon, U., Camarena, L., Surette, M. G., Aguera y Arcas, B., Liu, Y., Leibler, S., and Stock, J. B. (1998) Response regulator output in bacterial chemotaxis, *The EMBO Journal 17*, 4238-4248.

59. Barak, R., and Eisenbach, M. (1992) Correlation between phosphorylation of the chemotaxis protein CheY and its activity at the flagellar motor, *Biochemistry 31*, 1821-1826.

60. Shukla, D., Zhu, X. Y., and Matsumura, P. (1998) Flagellar motor-switch binding face of CheY and the biochemical basis of suppression by CheY mutants that compensate for motor-switch defects in *Escherichia coli*, *The Journal of Biological Chemistry 273*, 23993-23999.

61. Sourjik, V., and Berg, H. C. (2002) Binding of the *Escherichia coli* response regulator CheY to its target measured in vivo by fluorescence resonance energy transfer, *Proceedings of the National Academy of Sciences of the United States of America 99*, 12669-12674.

62. Kehry, M. R., Bond, M. W., Hunkapiller, M. W., and Dahlquist, F. W. (1983) Enzymatic deamidation of methyl-accepting chemotaxis proteins in *Escherichia coli* catalyzed by the *cheB* gene product, *Proceedings of the National Academy of Sciences of the United States of America 80*, 3599-3603.

63. Biemann, H. P., and Koshland, D. E., Jr. (1994) Aspartate receptors of *Escherichia coli* and *Salmonella typhimurium* bind ligand with negative and half-of-the-sites cooperativity, *Biochemistry 33*, 629-634.

64. Yeh, J. I., Biemann, H. P., Prive, G. G., Pandit, J., Koshland, D. E., Jr., and Kim, S. H. (1996) High-resolution structures of the ligand binding domain of the wild-type bacterial aspartate receptor, *Journal of Molecular Biology 262*, 186-201.

65. Chi, Y. I., Yokota, H., and Kim, S. H. (1997) Apo structure of the ligand-binding domain of aspartate receptor from *Escherichia coli* and its comparison with ligand-bound or pseudoligand-bound structures, *FEBS Letters 414*, 327-332.

66. Hughson, A. G., and Hazelbauer, G. L. (1996) Detecting the conformational change of transmembrane signaling in a bacterial chemoreceptor by measuring effects on disulfide cross-linking in vivo, *Proceedings of the National Academy of Sciences of the United States of America 93*, 11546-11551.

67. Chervitz, S. A., and Falke, J. J. (1995) Lock on/off disulfides identify the transmembrane signaling helix of the aspartate receptor, *The Journal of Biological Chemistry 270*, 24043-24053.

68. Lai, W. C., Peach, M. L., Lybrand, T. P., and Hazelbauer, G. L. (2006) Diagnostic cross-linking of paired cysteine pairs demonstrates homologous structures for two chemoreceptor domains with low sequence identity, *Protein Science 15*, 94-101.

69. Zhou, Q., Ames, P., and Parkinson, J. S. (2009) Mutational analyses of HAMP helices suggest a dynamic bundle model of input-output signalling in chemoreceptors, *Molecular Microbiology 73*, 801-814.

70. Swain, K. E., Gonzalez, M. A., and Falke, J. J. (2009) Engineered socket study of signaling through a four-helix bundle: evidence for a yin-yang mechanism in the kinase control module of the aspartate receptor, *Biochemistry 48*, 9266-9277.

71. Samanta, D., Borbat, P. P., Dzikovski, B., Freed, J. H., and Crane, B. R. (2014) Bacterial chemoreceptor dynamics correlate with activity state and are coupled over long distances, *Proceedings of the Nationl Academy of Sciences of the United States of America 112*, 2455-2460.

72. Cluzel, P., Surette, M., and Leibler, S. (2000) An ultrasensitive bacterial motor revealed by monitoring signaling proteins in single cells, *Science 287*, 1652-1655.

73. Hess, J. F., Oosawa, K., Matsumura, P., and Simon, M. I. (1987) Protein phosphorylation is involved in bacterial chemotaxis, *Proceedings of the National Academy of Sciences of the United States of America 84*, 7609-7613.

74. Segall, J. E., Manson, M. D., and Berg, H. C. (1982) Signal processing times in bacterial chemotaxis, *Nature 296*, 855-857.

75. Sourjik, V., and Wingreen, N. S. (2012) Responding to chemical gradients: bacterial chemotaxis, *Current Opinion in Cell Biology 24*, 262-268.

76. Springer, M. S., Goy, M. F., and Adler, J. (1979) Protein methylation in behavioural control mechanisms and in signal transduction, *Nature 280*, 279-284.

77. Wu, J., Li, J., Li, G., Long, D. G., and Weis, R. M. (1996) The receptor binding site for the methyltransferase of bacterial chemotaxis is distinct from the sites of methylation, *Biochemistry 35*, 4984-4993.

78. Li, M., and Hazelbauer, G. L. (2005) Adaptational assistance in clusters of bacterial chemoreceptors, *Molecular Microbiology 56*, 1617-1626.

79. Muppirala, U. K., Desensi, S., Lybrand, T. P., Hazelbauer, G. L., and Li, Z. (2009) Molecular modeling of flexible arm-mediated interactions between bacterial chemoreceptors and their modification enzyme, *Protein Science 18*, 1702-1714.

80. Goy, M. F., Springer, M. S., and Adler, J. (1977) Sensory transduction in *Escherichia coli*: role of a protein methylation reaction in sensory adaptation, *Proceedings of the National Academy of Sciences of the United States of America 74*, 4964-4968.

81. Bassler, B. L. (2002) Small talk. Cell-to-cell communication in bacteria, *Cell 109*, 421-424.

82. Bansal, T., Jesudhasan, P., Pillai, S., Wood, T. K., and Jayaraman, A. (2008) Temporal regulation of enterohemorrhagic *Escherichia coli* virulence mediated by autoinducer-2, *Applied Microbiology and Biotechnology 78*, 811-819.

83. Surette, M. G., Miller, M. B., and Bassler, B. L. (1999) Quorum sensing in *Escherichia coli*, *Salmonella typhimurium*, and *Vibrio harveyi*: a new family of genes responsible for autoinducer production, *Proceedings of the National Academy of Sciences of the United States of America 96*, 1639-1644.

84. Xavier, K. B., and Bassler, B. L. (2003) LuxS quorum sensing: more than just a numbers game, *Current Opinion in Microbiology 6*, 191-197.

85. Mok, K. C., Wingreen, N. S., and Bassler, B. L. (2003) *Vibrio harveyi* quorum sensing: a coincidence detector for two autoinducers controls gene expression, *The EMBO Journal 22*, 870-881.

86. Kendall, M. M., and Sperandio, V. (2014) Cell-to-Cell Signaling in *Escherichia coli* and *Salmonella*, *EcoSal Plus 6*.

87. Bassler, B. L., Wright, M., and Silverman, M. R. (1994) Multiple signalling systems controlling expression of luminescence in *Vibrio harveyi*: sequence and

function of genes encoding a second sensory pathway, *Molecular Microbiology 13*, 273-286.

88. Federle, M. J., and Bassler, B. L. (2003) Interspecies communication in bacteria, *The Journal of Clinical Investigation 112*, 1291-1299.

89. Hilgers, M. T., and Ludwig, M. L. (2001) Crystal structure of the quorum-sensing protein LuxS reveals a catalytic metal site, *Proceedings of the National Academy of Sciences of the United States of America 98*, 11169-11174.

90. Pei, D., and Zhu, J. (2004) Mechanism of action of S-ribosylhomocysteinase (LuxS), *Current Opinion in Chemical Biology 8*, 492-497.

91. Zhu, J., Dizin, E., Hu, X., Wavreille, A. S., Park, J., and Pei, D. (2003) S-Ribosylhomocysteinase (LuxS) is a mononuclear iron protein, *Biochemistry 42*, 4717-4726.

92. Schauder, S., Shokat, K., Surette, M. G., and Bassler, B. L. (2001) The LuxS family of bacterial autoinducers: biosynthesis of a novel quorum-sensing signal molecule, *Molecular Microbiology 41*, 463-476.

93. Winzer, K., Hardie, K. R., Burgess, N., Doherty, N., Kirke, D., Holden, M. T., Linforth, R., Cornell, K. A., Taylor, A. J., Hill, P. J., and Williams, P. (2002) LuxS: its role in central metabolism and the in vitro synthesis of 4-hydroxy-5-methyl-3(2H)-furanone, *Microbiology 148*, 909-922.

94. Chen, X., Schauder, S., Potier, N., Van Dorsselaer, A., Pelczer, I., Bassler, B. L., and Hughson, F. M. (2002) Structural identification of a bacterial quorum-sensing signal containing boron, *Nature 415*, 545-549.

95. Miller, S. T., Xavier, K. B., Campagna, S. R., Taga, M. E., Semmelhack, M. F., Bassler, B. L., and Hughson, F. M. (2004) *Salmonella typhimurium* recognizes a chemically distinct form of the bacterial quorum-sensing signal AI-2, *Molecular Cell 15*, 677-687.

96. Taga, M. E., Miller, S. T., and Bassler, B. L. (2003) Lsr-mediated transport and processing of AI-2 in *Salmonella typhimurium*, *Molecular Microbiology 50*, 1411-1427.

97. Taga, M. E., Semmelhack, J. L., and Bassler, B. L. (2001) The LuxS-dependent autoinducer AI-2 controls the expression of an ABC transporter that functions in AI-2 uptake in *Salmonella typhimurium*, *Molecular Microbiology 42*, 777-793.

98. Xavier, K. B., and Bassler, B. L. (2005) Regulation of uptake and processing of the quorum-sensing autoinducer AI-2 in *Escherichia coli*, *Journal of Bacteriology 187*, 238-248.

99. Herzberg, M., Kaye, I. K., Peti, W., and Wood, T. K. (2006) YdgG (TqsA) controls biofilm formation in *Escherichia coli* K-12 through autoinducer 2 transport, *Journal of Bacteriology 188*, 587-598.

100. Englert, D. L., Manson, M. D., and Jayaraman, A. (2009) Flow-based microfluidic device for quantifying bacterial chemotaxis in stable, competing gradients, *Applied and Environmental Microbiology 75*, 4557-4564.

101. Pereira, C. S., de Regt, A. K., Brito, P. H., Miller, S. T., and Xavier, K. B. (2009) Identification of functional LsrB-like autoinducer-2 receptors, *Journal of Bacteriology 191*, 6975-6987.

102. Rajamani, S., Zhu, J., Pei, D., and Sayre, R. (2007) A LuxP-FRET-based reporter for the detection and quantification of AI-2 bacterial quorum-sensing signal compounds, *Biochemistry 46*, 3990-3997.

103. Zhu, J., and Pei, D. (2008) A LuxP-based fluorescent sensor for bacterial autoinducer II, *ACS Chemical Biology 3*, 110-119.

104. Spurlino, J. C., Lu, G. Y., and Quiocho, F. A. (1991) The 2.3-A resolution structure of the maltose- or maltodextrin-binding protein, a primary receptor of bacterial active transport and chemotaxis, *The Journal of Biological Chemistry 266*, 5202-5219.

105. Gardina, P., Conway, C., Kossman, M., and Manson, M. (1992) Aspartate and maltose-binding protein interact with adjacent sites in the Tar chemotactic signal transducer of *Escherichia coli*, *Journal of Bacteriology 174*, 1528-1536.

106. Hazelbauer, G. L. (1975) Maltose chemoreceptor of *Escherichia coli*, *Journal of Bacteriology 122*, 206-214.

107. Tajima, H., Imada, K., Sakuma, M., Hattori, F., Nara, T., Kamo, N., Homma, M., and Kawagishi, I. (2011) Ligand specificity determined by differentially arranged

common ligand-binding residues in bacterial amino acid chemoreceptors Tsr and Tar, *The Journal of Biological Chemistry 286*, 42200-42210.

108. Christopher, J. A. (1988) SPOCK, The structural properties observation and calculation kit (The Center for Macromolecular Design, Texas A&M University College Station, TX).

109. Quiocho, F. A., Spurlino, J. C., and Rodseth, L. E. (1997) Extensive features of tight oligosaccharide binding revealed in high-resolution structures of the maltodextrin transport/chemosensory receptor, *Structure 5*, 997-1015.

110. Parkinson, J. S., and Houts, S. E. (1982) Isolation and behavior of *Escherichia coli* deletion mutants lacking chemotaxis functions, *Journal of Bacteriology 151*, 106-113.

111. Guzman, L. M., Belin, D., Carson, M. J., and Beckwith, J. (1995) Tight regulation, modulation, and high-level expression by vectors containing the arabinose PBAD promoter, *Journal of Bacteriology 177*, 4121-4130.

112. Miller, J. H. (1972) Experiments in molecular genetics. Cold Spring Harbor Laboratory Press: Cold Spring Harbor, NY.

113. Taga, M. E. (2005) Methods for analysis of bacterial autoinducer-2 production, *Current Protocols in Microbiology Chapter 1*, Unit 1C 1.

114. Ascenso, O. S., Marques, J. C., Santos, A. R., Xavier, K. B., Ventura, M. R., and Maycock, C. D. (2011) An efficient synthesis of the precursor of AI-2, the signalling molecule for inter-species quorum sensing, *Bioorganic and Medicinal Chemistry 19*, 1236-1241.

115. Adler, J. (1973) A method for measuring chemotaxis and use of the method to determine optimum conditions for chemotaxis by *Escherichia coli*, *Journal of General Microbiology 74*, 77-91.

116. Long, T., Tu, K. C., Wang, Y., Mehta, P., Ong, N. P., Bassler, B. L., and Wingreen, N. S. (2009) Quantifying the integration of quorum-sensing signals with single-cell resolution, *PLoS Biology 7*, e68.

117. Datsenko, K. A., and Wanner, B. L. (2000) One-step inactivation of chromosomal genes in *Escherichia coli* K-12 using PCR products, *Proceedings*

of the National Academy of Sciences of the United States of America 97, 6640-6645.

118. Kitagawa, M., Ara, T., Arifuzzaman, M., Ioka-Nakamichi, T., Inamoto, E., Toyonaga, H., and Mori, H. (2005) Complete set of ORF clones of *Escherichia coli* ASKA library (a complete set of *E. coli* K-12 ORF archive): unique resources for biological research, *DNA Research 12*, 291-299.

119. Callahan, A. M., and Parkinson, J. S. (1985) Genetics of methyl-accepting chemotaxis proteins in *Escherichia coli*: *cheD* mutations affect the structure and function of the Tsr transducer, *Journal of Bacteriology 161*, 96-104.

120. Baba, T., Ara, T., Hasegawa, M., Takai, Y., Okumura, Y., Baba, M., Datsenko, K. A., Tomita, M., Wanner, B. L., and Mori, H. (2006) Construction of *Escherichia coli* K-12 in-frame, single-gene knockout mutants: the Keio collection, *Molecular Systems Biology 2*, 2006 0008.

121. Pasupuleti, S., Sule, N., Cohn, W. B., MacKenzie, D. S., Jayaraman, A., and Manson, M. D. (2014) Chemotaxis of *Escherichia coli* to norepinephrine (NE) requires conversion of NE to 3,4-dihydroxymandelic acid, *Journal of Bacteriology 196*, 3992-4000.

122. Zhang, Y., Gardina, P. J., Kuebler, A. S., Kang, H. S., Christopher, J. A., and Manson, M. D. (1999) Model of maltose-binding protein/chemoreceptor complex supports intrasubunit signaling mechanism, *Proceedings of the National Academy of Sciences of the United States of America 96*, 939-944.

123. Pearlman, D. A., Case, D. A., Caldwell, J. W., Ross, W. S., Cheatham, T. E., III. (1995) AMBER 4.1 (University of California, San Francisco).

124. Carter, P. (1986) Site-directed mutagenesis, *The Biochemical Journal 237*, 1-7.

125. Gardina, P. J., Bormans, A. F., Hawkins, M. A., Meeker, J. W., and Manson, M. D. (1997) Maltose-binding protein interacts simultaneously and asymmetrically with both subunits of the Tar chemoreceptor, *Molecular Microbiology 23*, 1181-1191.

126. Gardina, P. J., Bormans, A. F., and Manson, M. D. (1998) A mechanism for simultaneous sensing of aspartate and maltose by the Tar chemoreceptor of *Escherichia coli*, *Molecular Microbiology 29*, 1147-1154.

127. Zhang, Y., Conway, C., Rosato, M., Suh, Y., and Manson, M. D. (1992) Maltose chemotaxis involves residues in the N-terminal and C-terminal domains on the same face of maltose-binding protein, *The Journal of Biological Chemistry 267*, 22813-22820.

128. Adler, J., and Templeton, B. (1967) The effect of environmental conditions on the motility of *Escherichia coli*, *Journal of General Microbiology 46*, 175-184.

129. Mesibov, R., and Adler, J. (1972) Chemotaxis toward amino acids in *Escherichia coli*, *Journal of Bacteriology 112*, 315-326.

130. Amsler, C. D., Cho, M., and Matsumura, P. (1993) Multiple factors underlying the maximum motility of *Escherichia coli* as cultures enter post-exponential growth, *Journal of Bacteriology 175*, 6238-6244.

131. Staropoli, J. F., and Alon, U. (2000) Computerized analysis of chemotaxis at different stages of bacterial growth, *Biophysical Journal 78*, 513-519.

132. Iwama, T., Kawagishi, I., Gomi, S., Homma, M., and Imae, Y. (1995) In vivo sulfhydryl modification of the ligand-binding site of Tsr, the *Escherichia coli* serine chemoreceptor, *Journal of Bacteriology 177*, 2218-2221.

133. Jeffery, C. J., and Koshland, D. E., Jr. (1993) Three-dimensional structural model of the serine receptor ligand-binding domain, *Protein Science 2*, 559-566.

134. Bitbol, A. F., and Wingreen, N. S. (2015) Fundamental constraints on the abundances of chemotaxis proteins, *Biophysical Journal 108*, 1293-1305.

135. Buron-Barral, M. C., Gosink, K. K., and Parkinson, J. S. (2006) Loss- and gain-of-function mutations in the F1-HAMP region of the *Escherichia coli* aerotaxis transducer Aer, *Journal of Bacteriology 188*, 3477-3486.

136. Ames, P., Zhou, Q., and Parkinson, J. S. (2014) HAMP domain structural determinants for signalling and sensory adaptation in Tsr, the *Escherichia coli* serine chemoreceptor, *Molecular Microbiology 91*, 875-886.

137. Hedblom, M. L., and Adler, J. (1980) Genetic and biochemical properties of *Escherichia coli* mutants with defects in serine chemotaxis, *Journal of Bacteriology 144*, 1048-1060.

138. Wang, E. A., and Koshland, D. E., Jr. (1980) Receptor structure in the bacterial sensing system, *Proceedings of the National Academy of Sciences of the United States of America 77*, 7157-7161.

139. Lee, L., Mizuno, T., and Imae, Y. (1988) Thermosensing properties of *Escherichia coli tsr* mutants defective in serine chemoreception, *Journal of Bacteriology 170*, 4769-4774.

140. Zhang, Y., Mannering, D. E., Davidson, A. L., Yao, N., and Manson, M. D. (1996) Maltose-binding protein containing an interdomain disulfide bridge confers a dominant-negative phenotype for transport and chemotaxis, *The Journal of Biological Chemistry 271*, 17881-17889.

141. Kalinin, Y., Neumann, S., Sourjik, V., and Wu, M. (2010) Responses of *Escherichia coli* bacteria to two opposing chemoattractant gradients depend on the chemoreceptor ratio, *Journal of Bacteriology 192*, 1796-1800.